

DR. SONIA CAMPOS-SOTO (Orcid ID : 0000-0001-5418-7032)

DR. M. ISABEL BENITO (Orcid ID : 0000-0002-8711-0864)

PROF. NIGEL P MOUNTNEY (Orcid ID : 0000-0002-8356-9889)

DR. PABLO SUAREZ-GONZALEZ (Orcid ID : 0000-0002-2370-5017)

Article type : Original Article

Where humid and arid meet: Sedimentology of coastal siliciclastic successions deposited in apparently contrasting climates

Sonia Campos-Soto^{a*}, M. Isabel Benito^{b,c}, Nigel P. Mountney^d, Piret Plink-Björklund^e, I. Emma Quijada^f, Pablo Suarez-Gonzalez^b, Alberto Cobos^g

^a Laboratoire Morphodynamique Continentale et Côtière, Université de Caen Normandie, Caen, 14000, France.

^b Departamento de Geodinámica, Estratigrafía y Paleontología, Facultad de Ciencias Geológicas, Universidad Complutense de Madrid, Madrid, 28040, Spain.

^c Instituto de Geociencias IGEO (CSIC, UCM), Madrid, 28040, Spain

^d Fluvial & Eolian Research Group, School of Earth and Environment, University of Leeds, Leeds, LS2 9JT, United Kingdom.

^e Department of Geology and Geological Engineering, Colorado School of Mines, Golden, CO 80401, USA.

^f Departamento de Geología, Universidad de Oviedo, Oviedo, 33005, Spain.

^g Fundación Conjunto Paleontológico de Teruel-Dinópolis, Teruel, 44002, Spain

*Corresponding author. Email: sonia.campos-soto@unicaen.fr

This article has been accepted for publication and undergone full peer review but has not been through the copyediting, typesetting, pagination and proofreading process, which may lead to differences between this version and the [Version of Record](#). Please cite this article as [doi: 10.1111/SED.12958](https://doi.org/10.1111/SED.12958)

This article is protected by copyright. All rights reserved

Running title: Successions of apparently contrasting climates

Associate Editor: Gonzalo Veiga

ABSTRACT

Deciphering the palaeoenvironmental and palaeoclimatic setting of ancient successions that include deposits typical of different climates can be challenging. This is the case in the Late Jurassic succession cropping out in eastern Spain (South-Iberian and western Maestrazgo basins), where deposits characteristic of both arid to semiarid and humid to subhumid settings have been identified through a detailed analysis of eight stratigraphic sections. These sections comprise shallow marine carbonates changing upward and laterally to a predominantly siliciclastic coastal and alluvial succession, including abundant dinosaur remains. Deposition of coastal and alluvial sediments occurred in flood plains, ephemeral and perennial fluvial channels, aeolian dunes, deltas, distributary mouth-bars and associated distributary channels, and shallow water bodies influenced by both fresh and marine waters. Some of these deposits, notably those of aeolian and ephemeral fluvial origin, are characteristic of arid to semiarid climates. However, there are also abundant deposits that can be demonstrably shown to have a coeval origin, which are indicative of permanent water courses: (i) sediments of seasonal discharge fluvial channels with perennial to semi-perennial flow, displaying subcritical and supercritical flow sedimentary structures; (ii) deltaic sediments deposited in permanent freshwater bodies; and (iii) abundant plant and dinosaur remains, especially of herbivorous dinosaurs, which required the presence of permanent water sources and abundant vegetation. These apparently contrasting sedimentary features indicate that deposition occurred under a seasonal climate controlled by monsoonal-type precipitation. These deposits are analogous to those observed nowadays in the Lençóis Maranhenses National Park (north-east Brazil), where a subhumid tropical climate with a seasonal precipitation pattern prevails. Thus, this study shows that only through careful facies analysis and interpretation of depositional processes that can be shown to be occurring concurrently in neighbouring and related depositional systems can the detailed palaeoenvironmental and palaeoclimatic setting of complex coastal sedimentary successions be confidently reconstructed in detail.

KEYWORDS

Aeolian dunes, deltaic deposits, eastern Iberia, fluvial channels, Kimmeridgian–Tithonian, supercritical flow bedforms.

INTRODUCTION

Sedimentological analyses of ancient successions, supported by comparison to analogous modern environments, provide a valuable technique with which to reconstruct ancient environmental and climatic settings. The sedimentary analysis of modern environments has allowed the recognition of certain deposits that predominate in different climate regimes (*i.e.* climatically significant rocks, *sensu* Hallam, 1984; climate-indicative lithologies, *sensu* Holz & Scherer, 2000; or climate-sensitive sediments, *sensu* Gibbs *et*

al., 2002). The inferred significance of such deposits has been widely employed to interpret the palaeoclimatic setting of the fossil record. For example, the occurrence of evaporites, deposits of ephemeral channels (*i.e.* wadis), aeolian dunes and ephemeral lakes, among others, has been used to interpret arid to semiarid climates in the fossil record (*e.g.* Tucker & Benton, 1982; Stear, 1983; 1985; Hallam, 1984; 1985; Zharkov *et al.*, 1998; Holz and Scherer, 2000; Rees *et al.*, 2004; Rodríguez-López *et al.*, 2010; Priddy & Clarke, 2020). Nevertheless, in the case of aeolian dunes, it is also important to remark that they are also widely reported from modern humid to subhumid settings (*e.g.* Mountney & Russell, 2009; Al-Masrahy & Mountney, 2015; dos Santos & dos Santos, 2015). In contrast, the presence of abundant coal, plant remains and permanent water courses has been used as the basis for interpreting humid to subhumid climates (*e.g.* Tucker & Benton, 1982; Hallam, 1984; Collinson, 1996; Zharkov *et al.*, 1998; Rees *et al.*, 2004).

A significant challenge arises when trying to reconstruct the palaeoenvironmental and palaeoclimatic setting of sedimentary successions that include features typical of both arid and humid settings. This is the case of the Late Jurassic Villar del Arzobispo Formation, which crops out in eastern Spain (western Maestrazgo and South-Iberian basins; Teruel and Valencia provinces; Fig. 1). This succession comprises mixed siliciclastic–carbonate sediments deposited in shallow marine, coastal and alluvial settings (*e.g.* Meléndez *et al.*, 1979; Mas & Alonso, 1981; Mas *et al.*, 1984; Luque *et al.*, 2005; Campos-Soto *et al.*, 2016a, 2017a, 2019), and it is internationally renowned for its abundance of dinosaur remains of theropods, sauropods, thyreophoran and ornithopods (*e.g.* Suñer *et al.*, 2008; Alcalá *et al.*, 2009; 2018; Campos-Soto *et al.*, 2017a, and references therein; Cobos *et al.*, 2020; Royo-Torres *et al.*, 2020), including the fossils of the largest dinosaur found in Europe, *Turiasaurus riodevensis* Royo-Torres, Cobos & Alcalá, 2006. The stratal arrangement of siliciclastic coastal and alluvial deposits of this unit indicates the apparently contemporaneous development of a variety of subaqueous and subaerial depositional settings (Campos-Soto *et al.*, 2016a, 2017a, 2019). They include aeolian dune and ephemeral channel deposits, which are apparently indicative of arid to semiarid climates. However, the succession additionally comprises other coeval deposits that are apparently indicative of a humid to subhumid climate, such as those of deltas with abundant plant remains, as well as diverse and abundant large dinosaur faunas, which would require the availability of permanent water sources and abundant vegetation. Moreover, this succession includes deposits of perennial to semi-perennial fluvial channels with evidence of seasonal discharge, which commonly develop nowadays in monsoonal domains, but which could also conceivably occur in arid to semiarid settings if their catchment area is located in the monsoonal domain (Plink-Björklund, 2015). Thus, sedimentological features characteristic of both arid and humid climatic end-members are present in deposits of sub-environments that were apparently active contemporaneously; the palaeoenvironmental and palaeoclimatic interpretation of this succession is therefore challenging.

The aim of this study is to show how a detailed lithofacies analysis of a dominantly siliciclastic coastal and alluvial-plain succession can be applied to demonstrate the co-existence of a range of sub-environments that are variably indicative of both arid and humid climatic settings. Specific research objectives are to: (i) analyse the subaqueous and subaerial depositional settings and document their interactions; (ii) compare these deposits with modern analogues; (iii) reconstruct the palaeoenvironments, palaeogeography and palaeoclimate of eastern Iberia during deposition; and (iv) demonstrate how the deposits of coeval sub-environments with evidence for apparently contrasting climates can co-exist.

GEOLOGICAL SETTING

The South-Iberian and Maestrazgo basins are two of the extensional basins in the Mesozoic Iberian Extensional System (also referred to as the Iberian Basin) developed in eastern Iberia during the Late Oxfordian–Middle Albian (Fig. 1A to C), and inverted during the Cenozoic Alpine Orogeny (*e.g.* Salas *et al.*, 2001; Mas *et al.*, 2004; Martín-Chivelet *et al.*, 2019). During their extensional development, these basins were surrounded to the west and north-east by the Iberian and Ebro massifs, respectively, while marine areas were located to the east/south-east and north of Iberia (Tethys and Boreal realms, respectively; Fig. 1D; *e.g.* Salas *et al.*, 2001; Mas *et al.*, 2004). These basins were separated by the Valencian Massif, a north-west/south-east emergent area developed in the position where the Javalambre Range is now located (Fig. 1B and D; *e.g.* Mas & Alonso, 1981; Mas *et al.*, 2004; Campos-Soto *et al.*, 2019). The Maestrazgo Basin comprises several sub-basins separated by tectonic structures (*e.g.* Salas & Guimerà, 1996, 1997; Salas *et al.*, 2001; Martín-Chivelet *et al.*, 2019). The sedimentary record analysed in this paper crops out in the western Peñagolosa sub-basin, located to the south-west of the Maestrazgo basin (Fig. 1B).

The deposits documented herein belong to the Villar del Arzobispo Formation (*sensu* Campos-Soto *et al.*, 2019; Figs 1C, 2 and 3), a mixed siliciclastic–carbonate succession dated as Kimmeridgian–Tithonian (Campos-Soto *et al.*, 2016a; 2016b; 2017a, 2019). This succession was deposited in a shallow marine carbonate platform setting that evolved into essentially siliciclastic coastal and alluvial environments, expressed as an overall regressive trend (Figs 2 and 3; *e.g.* Meléndez *et al.*, 1979; Mas & Alonso, 1981; Mas *et al.*, 1984, 2004; Hernández *et al.*, 1985; Luque *et al.*, 2005; Campos-Soto *et al.*, 2016a, 2017a, 2019; Pacios *et al.*, 2018). However, Campos-Soto *et al.* (2016b, 2017a, 2019) documented evidence for a marine transgression in the Tithonian, during the deposition of the uppermost part of the unit (Figs 2 and 3). Additionally, marked thickness variations of the studied succession were largely controlled by the development of syn-sedimentary extensional faults (Figs 2 and 3; Fig. S1 of Supplementary Material; see Campos-Soto *et al.*, 2017a, 2019).

The Villar del Arzobispo Formation conformably overlies the Higuieruelas Formation (Figs 1C, 2 and 3), an oncolitic limestone unit dated as Kimmeridgian (Campos-Soto *et al.*, 2015a, 2016a, 2017a;

Pacios *et al.*, 2018) and deposited in a mid to inner carbonate platform setting (*e.g.* Gómez, 1979; Gómez & Goy, 1979; Aurell *et al.*, 1994; Campos-Soto *et al.*, 2015a, 2016a). The Villar del Arzobispo Formation is unconformably overlain by Lower Cretaceous siliciclastic and/or carbonate units (Figs 1C, 2 and 3), deposited in shallow marine to coastal and alluvial environments (*e.g.* Vilas *et al.*, 1982; Canerot *et al.*, 1982; Salas, 1987; Mas *et al.*, 2004; Fernandez-Labrador, 2016).

The Villar del Arzobispo Formation has been studied in different areas of the South-Iberian and western Maestrazgo basins (Figs 1C, 2 and 3). In all areas, its sedimentary record is equivalent and comprises two informal parts (Fig. 2; Campos-Soto *et al.*, 2016b, 2017a, 2019): (i) a Kimmeridgian, essentially carbonate lower part (CLP); and (ii) a Kimmeridgian–Tithonian, essentially siliciclastic upper part (SUP). The thickness and facies distribution differ in sections located to the east/south-east and sections located to the north and west (Campos-Soto *et al.*, 2017a, 2019; Figs 1C, 2 and 3). The eastern and south-eastern sections, located closer to the Tethys Ocean, occupied a part of the basin subject to relatively high subsidence rates during sedimentation; here, the accumulated succession is thicker and deposits display greater marine influence than in the northern and western sections, which themselves occupied more landward and slowly subsiding areas (Figs 1D, 2 and 3; Campos-Soto *et al.*, 2017a, 2019).

In all areas, the CLP comprises bioclastic and/or oolitic limestone with abundant marine fossils alternating with non-channelized sandstone, siliciclastic mudstone, marl and minor channelized sandstone and conglomerate (Figs 2 and 3); this part of the succession, Kimmeridgian in age, has been interpreted as deposited in a shallow marine carbonate platform that received siliciclastic sediments from nearby emergent areas (Campos-Soto *et al.*, 2016a, 2017a, 2019). Shallow marine deposits of the CLP change upward to deposits of the SUP, which mainly comprises reddish siliciclastic mudstone interbedded with non-channelized sandstone and channelized sandstone and conglomerate, interpreted as deposited in a coastal and alluvial plain during a regressive stage during the Kimmeridgian-Tithonian (Figs 1D, 2, 3 and 4; Campos-Soto *et al.*, 2015b, 2016a, 2017a, 2017b, 2019). Siliciclastic deposits are interbedded and laterally related with limestone and marl, mainly towards the upper part of the SUP, during which a marine transgression took place during the Tithonian (Figs 2, 3 and 5; Fig. S1 of Supplementary Material; Campos-Soto *et al.*, 2016b, 2017a, 2019). Some limestone beds are peloidal and/or micritic, include very scattered marine fossils, and display tidal structures and abundant subaerial exposure features (including abundant dinosaur tracks). Collectively, these features indicate sedimentation in intertidal to supratidal carbonate flats (Campos-Soto *et al.* 2017a, 2019). Other limestone beds are bioclastic and/or oolitic and include abundant marine fossils (Fig. 2). These limestone beds are progressively more abundant and include a higher proportion of fossils characteristic of normal marine salinities (such as echinoderms, dasyclads, red algae and corals) towards the east and south-eastern sections (Figs 2 and 5; Fig. S1 of

Supplementary Material), indicating that the coastal setting was laterally connected to the east/south-east to a shallow marine carbonate platform (Campos-Soto *et al.*, 2017a, 2019).

MATERIALS AND METHODS

This paper is based on the detailed stratigraphic and sedimentological study, and geological mapping, of the Villar del Arzobispo Formation (Figs 1C and 2). Geological mapping was performed by field observations, supported by analysis of aerial photographs and data (stratigraphic units and tectonic structures) provided by the Spanish Geological Survey (GEODE, scale 1:50,000; López-Olmedo *et al.*, 2018). The map shown in Fig. 1C was generated with the ArcGIS software.

Eight stratigraphic sections were measured and logged at centimetre to metre-scale in the areas with best outcrop exposures: the total cumulative length of measured sections is 5072 m (Fig. 2). Four sections were logged in the western Maestrazgo Basin (Cedrillas, El Castellar, Formiche Alto and Mora de Rubielos); the other four in the South-Iberian Basin (Riodeva, Losilla-Alpuente, Benagéber and Villar del Arzobispo). One-hundred-and-forty-six additional outcrops of the studied succession were also analysed to study the composition, texture, sedimentary structures, fossil content, facies relationships, geometry and lateral continuity of beds that make up larger-scale architectural elements (see details of the additional studied outcrops in Campos Soto, 2020). Three-hundred-and-forty-eight palaeocurrent measurements were obtained from the studied siliciclastic deposits, mainly from the dip azimuth of large-scale cross-strata and clinofolds, and also from small-scale ripple structures. Palaeocurrents obtained from supercritical flow sedimentary structures have not been taken into consideration for palaeocurrent analysis, as these bedforms could migrate downstream and upstream (*e.g.* Alexander *et al.*, 2001; Cartigny *et al.*, 2014; Ono *et al.*, 2020). Paleocurrent data were plotted as rose diagrams using the PAST software (Hammer *et al.*, 2001). Rose diagrams were constructed for architectural elements to show mean palaeocurrent directions and their variability, grouped in classes of 24°, in which the length of each sector represents the relative abundance of measurements. The number of readings has been indicated with the letter 'n'.

Four-hundred-and-fifty-five rock samples were systematically collected throughout the stratigraphic sections and from the additional studied outcrops. A 30 µm thick, polished and uncovered thin section was prepared for each sample to perform petrographic analysis under transmitted light microscopy. The terminology used for siliciclastic rocks follows the Udden-Wentworth grain-size scale classification (Udden, 1914; Wentworth, 1922) modified by Blair & McPherson (1999) and the classifications of Folk (1968) and Powers (1953) for sorting and roundness, respectively. Carbonate rocks were classified following the classification of Dunham (1962).

This research also includes the analysis of Google Earth's satellite images of modern coastal settings deemed to be analogous to the studied ancient succession, principally that located at the Lençóis Maranhenses National Park (north-east Brazil), in which the different subenvironments (aeolian dunes, interdunes, fluvial and tidal channels, shallow water bodies, deltas, flood plains) and the interactions observed between them have been analysed in detail in this study.

RESULTS

This research focuses on the sedimentological analysis of the siliciclastic deposits of the Villar del Arzobispo Formation, which form 65 to 85% of the succession, depending on the location (Figs 2 and 3). The other 15 to 35% are the shallow marine and tide-influenced limestone deposits (Figs 2 and 3). The siliciclastic deposits are more abundant in the SUP and towards the landward sections located to the north and west (Riodeva and Benagéber sections in the South-Iberian Basin; Cedrillas and El Castellar sections in the western Maestrazgo Basin) (Figs 2, 3 and 4). They are less abundant towards the seaward sections located to the east/south-east (Losilla-Alpuente and Villar del Arzobispo sections in the South-Iberian Basin; Formiche Alto and Mora de Rubielos sections in the western Maestrazgo Basin) (Figs 2, 3 and 5). Through sedimentological analysis, 11 siliciclastic architectural elements have been identified, each of them comprising a distinctive facies assemblage and geometric arrangement; these correspond to elements deposited in four primary depositional settings: (i) fluvial; (ii) deltaic; (iii) coastal to shallow marine; and (iv) aeolian (Table 1).

Fluvial depositional setting

Fluvial deposits are observed along the SUP and rarely in the CLP (Fig. 2). They are interbedded and laterally related with the aeolian and deltaic elements (Figs 2 and 4) and with the coastal to shallow marine elements (Fig. 2). Three fluvial architectural elements have been distinguished.

Ephemeral fluvial channel architectural element

Description. This element typically forms less than 1% of the studied unit, although in the landward areas of the South-Iberian Basin it forms up to 3% of the succession (Fig. 2). It is interbedded with the flood plain, aeolian dune and deltaic elements (Figs 2 and 6A to C). It comprises decimetre to metre-thick conglomerate lenses (up to 3 m thick) displaying erosive bases, sharp flat tops and short lateral extent (commonly <10 m; Fig. 6A to C). Erosive bases are commonly symmetrical and slightly incisive (1:7 height/width ratios; Fig. 6B) or, locally, they are asymmetrical, displaying one very steep margin and another less steep one, and incising up to 3 m into the underlying deposits (1:3 height/width ratios; Fig. 6C). Conglomerate lenses may be massive or may display a large-scale (up to 3 m thick) cross-strata set

(Fig. 6B and C). In the case of the asymmetrical lenses, strata are conformable to the less steep margin of the erosive surface (Fig. 6C). Conglomerate is very poorly sorted and mostly clast-supported, though locally matrix-supported, and comprises subangular to subrounded pebbles and cobbles within a medium to coarse-grained sandy matrix (Fig. 6D to F). Conglomerate clasts mainly consist of siliciclastic mudstone, carbonate and sandstone (Fig. 6E to F), ranging from 0.4 to 10 cm in diameter, although larger clasts up to 20 cm in diameter locally occur. Rounded quartzite pebbles, up to 6 cm in diameter, are rarely observed (Fig. 6D), although they become relatively abundant upward in the SUP in the South-Iberian Basin. In places, conglomerate includes fragments of tree trunks (up to 12 cm in length) and some incomplete dinosaur teeth and bones (up to 20 cm in length; Fig. 6G).

Palaeocurrents in the South-Iberian Basin indicate transport directions towards the south-west/north-west and the north-east/south-east, whereas the scarce palaeocurrents obtained in the western Maestrazgo Basin indicate a main transport towards the south/south-west and the south-east (Figs 2 and 6A).

Interpretation. Clast-supported or locally matrix-supported fabrics, sandy matrix and the very poor sorting of conglomerates, suggest deposition by flash flows, which transported high concentrations of sediment (sand and gravels) in suspension (Costa, 1988; DeCelles *et al.*, 1991; Pierson, 2005). The erosive bases and the short lateral extent of the conglomerates, and their relation to flood plain and aeolian deposits indicates their likely deposition in ephemeral channels under episodic and high velocity currents, similar to those observed in other ancient (*e.g.* Cain & Mountney, 2009; Banham & Mountney, 2014) and modern settings (*e.g.* Glennie, 1970; Picard & High, 1973). In present-day settings, ephemeral channels develop during seasonal rainfalls and are characterized by short periods of flow (Picard & High, 1973). The fact that these deposits are commonly characterized by a single set of cross-strata indicates that channel development may have occurred in a single scour and fill event. This is also interpreted for conglomerates displaying massive fabrics, as they do not show internal erosive surfaces, grain size variations or other evidence of flow fluctuation or interruption. The asymmetrical erosive bases with strata that are conformable to their less steep margin, and the upstream-dipping cross-strata are similar to experimentally produced hydraulic jump deposits in Froude supercritical flow conditions, where upstream dipping backset strata formed during upstream migration of hydraulic jumps, and the infilling of hydraulic jump scours resulted in conformable strata (Ono *et al.*, 2020). Similar strata have been documented in ancient fluvial deposits and interpreted as chute and pool and cyclic step deposits (*e.g.* Fielding, 2006; Plink-Björklund, 2015; Wang & Plink-Björklund, 2020).

Palaeocurrents directed to the north-east/south-east in the South-Iberian Basin and to the south/south-west and south-east in the western Maestrazgo Basin suggest that these deposits were derived

from erosion of the Iberian and Ebro massifs, located to the north-west/south-west and to the north/north-east, respectively (Fig. 1D), which were the main emergent areas in Iberia during the Late Jurassic (e.g. Salas *et al.*, 2001; Mas *et al.*, 2004). Nevertheless, palaeocurrents of the South-Iberian Basin also indicate transport directions to the south-west/north-west, which are more difficult to interpret. They could indicate that these deposits were also derived from the Valencian Massif, located to the north-east/south-east (Fig. 1D). Alternatively, they could correspond to palaeocurrents measured in the backsets produced by hydraulic jump migration (e.g. Alexander *et al.*, 2001; Cartigny *et al.*, 2014; Ono *et al.*, 2020).

The very poorly sorted siliciclastic mudstone, carbonate and sandstone pebbles and cobbles are interpreted as intraformational clasts derived from the erosion and reworking of compacted sediments located in nearby flood plain areas, as similarly interpreted in other ancient fluvial deposits (e.g. North & Taylor, 1996; Deluca & Eriksson, 1989; Hinds *et al.*, 2004; Cain & Mountney, 2006; Banham & Mountney, 2014). The fact that conglomerates contain a greater abundance of quartzite pebbles upward in the SUP in the South-Iberian Basin suggests that older rocks were successively eroded, i.e. Jurassic carbonate rocks in the earlier stages of erosion and Palaeozoic to Triassic rocks in the later stages. Nevertheless, further provenance studies are necessary to determine the specific source area of these clasts.

Multi-storey fluvial channel architectural element

Description. This element forms 10 to 25% of the studied succession in the South-Iberian Basin (Fig. 2) and 5 to 10% in the western Maestrazgo Basin (Fig. 2). It is more abundant in the landward sections of both basins. In all areas, this element is more abundant in the SUP, although rare examples are observed in the CLP (Fig. 2). It is interbedded with the flood plain element (Figs 4 and 7A to E) and with the aeolian dune elements (Fig. 4). It comprises sandstone or sandstone and conglomerate arranged in metre-thick multi-storey bodies (in some cases up to 15 m thick, Figs 4 and 7A to E) displaying erosive bases and a large lateral extent, in some exposures in excess of 250 m.

Sandstone is moderately to poorly sorted and displays medium to coarse grain sizes, although fine grain sizes are also observed in some bodies. Sandstone shows large-scale sets of cross-strata (rarely trough cross-strata) up to 1.5 m thick (Fig. 7B, C and E). Set thickness decreases upward in some bodies (Fig. 7B and C). Locally, millimetre to centimetre-thick layers of siliciclastic mudstone, which may contain abundant carbonaceous detritus, occur between cross-sets (Fig. 7E and F) and/or at the lower part of the foresets and bottomsets.

A distinctive feature of this element is the common occurrence of large internal erosive surfaces that locally incise downward up to 2.4 m (Fig. 7B to F). Another distinctive feature is the occurrence of sandstone displaying convex-up low-angle cross-strata (Fig. 8A and B) and scour-and-fill structures, which

are filled by backset or foreset strata that, in places, gradually flatten upward (Figs 7B, 7C, 8C and 8D). Locally, flattening-upward strata show wavelengths of several metres (Fig. 7B and C). In addition, sandstone locally includes fragments of fossilized wood and tree trunks up to a few metres long.

Conglomerate, where present, overlies the erosive base of bodies and/or the internal erosive surfaces (Fig. 7B to D) and may be up to 2 m thick. Conglomerate is very poorly sorted and comprises subangular to subrounded pebbles and cobbles (up to 8 cm in diameter), and fragments of fossilized wood up to 10 cm long in places. Composition of conglomerate is identical to that reported in the ephemeral channel element. Conglomerate is structureless or displays large-scale cross-strata with sets up to 1.5 m thick. In some bodies, conglomerate displays scour-and-fill structures comprising asymmetrical scours, with a steeper upstream margin, and are filled by backset strata that gradually flatten upward and fine upward to medium to coarse-grained sandstone (Fig. 7B and C).

Palaeocurrents measured in the South-Iberian Basin indicate main transport directions to the north-east/south and, less commonly, to the south-west/north, whereas in the western Maestrazgo Basin, data indicate main transport directions to the north-east and, less commonly, to the north and east/south (Fig. 7A).

Interpretation. The erosive bases and large lateral extent of these deposits and their interbedding with flood plain deposits, are features typical of fluvial channels that migrated across a flood plain. The internal erosive surfaces filled by very poorly-sorted conglomerate or sandstone, are interpreted to develop during episodes of intense precipitation that produced a rapid rise in flow discharge and velocity within the channels, causing the partial erosion of earlier deposits of the channels and the subsequent deposition of intraformational clasts (siliciclastic mudstone, carbonate and sandstone clasts) and fragments of tree trunks and other plant remains, which were eroded and transported from nearby flood plain areas. Similar sedimentary features have been reported in other ancient and modern fluvial channels characterized by a seasonally highly variable discharge (Abdullatif, 1989; Deluca & Eriksson, 1989; Browne & Plint, 1994; North & Taylor, 1996; McKie, 2011; Fielding *et al.*, 2009, 2011, 2018; Plink-Björklund, 2015). In these seasonal rivers, intraformational conglomerates are locally derived (*i.e.* from flood plains) and their deposits are associated with a rapid decrease of water level occurring during early phases of the waning stage of floods, when upper flow regime conditions occur (*e.g.* Singh *et al.*, 1993; North & Taylor, 1996; Gibling & Tandom, 1997; Plink-Björklund, 2015). Fragments of tree trunks and plant remains similar to those of the studied deposits have been described in other ancient and modern seasonal rivers, especially in those developed in subhumid subtropics (*e.g.* Fielding & Alexander, 1996; Alexander *et al.*, 1999; Fielding *et al.*, 1997, 2009, 2011; Allen *et al.*, 2014; Plink-Björklund, 2015, and references therein), and are derived from the destruction of trees or other plants, during floods, that grow in the channel margins or in areas of

channel bed that get exposed during periods of non-flood discharges (Fielding *et al.*, 1997; Alexander *et al.*, 1999).

The convex-up low-angle cross-strata resemble antidune structures formed under supercritical flow in flume experiments (e.g. Alexander *et al.*, 2001; Cartigny *et al.*, 2014), and in other ancient fluvial deposits (e.g. Fielding, 2006; Fielding *et al.*, 2009; Plink-Björklund, 2015; Wang & Plink-Björklund, 2020). The asymmetrical scour-and-fill structures with backset or foreset strata that in places flatten and fine upward are similar to the structures produced during the infilling of hydraulic jump scours under supercritical flow conditions in chutes and pools and cyclic steps in flume experiments (e.g. Alexander *et al.*, 2001; Cartigny *et al.*, 2014; Ono *et al.*, 2020), in numerical simulations (Vellinga *et al.*, 2018), and in other ancient seasonal fluvial channels (e.g. Fielding, 2006; Fielding *et al.*, 2009; Plink-Björklund, 2015; Wang & Plink-Björklund, 2020). Backset strata have also been reported in bar head deposits of some Pliocene alluvial sediments in south-east Spain (Viseras & Fernández, 1994, 1995). However, bar deposits have not been identified in the studied fluvial channel deposits. In fact, the occurrence of poorly developed barforms, or even their absence, is a common characteristic that has been reported in many ancient and modern examples of seasonal discharge rivers (e.g., Fielding *et al.*, 2009; Plink-Björklund, 2015, and references therein).

Regarding the recent experimental work performed on the study of supercritical flow bedforms, it has been observed that antidunes develop downstream of chutes and pools (Cartigny *et al.*, 2014), and convex-up low-angle strata and scour-and-fill structures have been observed developing coevally by the upstream migration of cyclic steps (Ono *et al.*, 2020). Thus, these authors highlight that, although these structures are produced under supercritical flows, caution must be used when trying to assign specific structures observed at the outcrop to specific supercritical flow bedforms.

During periods of non-flood discharges, sand would have been deposited through the migration of subaqueous dunes, as indicated by the occurrence of sandstone displaying large-scale cross-strata (occasionally trough cross-strata). This is similarly observed in some channels developed in settings with seasonal rainfall, such as in the Gash River in Sudan (Abdullatif, 1989), in which subaqueous dunes and ripples migrate during periods of non-flood discharges or during less intense flood phases (Plink-Björklund, 2015).

In addition, the local occurrence of thin layers of siliciclastic mudstone containing abundant carbonaceous detritus between sandstone cross-sets and/or at the lower part of the foresets and at the bottomsets has been similarly identified in other modern and ancient seasonal fluvial channels, where they are deposited during the rapid waning stage that occur after high magnitude floods (e.g. Williams, 1971;

Abdullatif, 1989; Singh *et al.*, 1993; Shukla *et al.*, 2001; Allen *et al.*, 2011; Plink-Björklund, 2015, and references therein).

Thus, this element is interpreted as deposited in fluvial channels occupied by perennial or semi-perennial flow and characterized by episodic and seasonal discharge. Palaeocurrents measured in the South-Iberian Basin indicate that these deposits were mainly derived from the Iberian Massif and, in minor proportion, from the Valencian Massif, located to the south-west/north and north-east/south, respectively (Fig. 1D). By contrast, in the western Maestrazgo Basin, these deposits were derived from the Valencian Massif and, in minor proportion, from the Iberian and Ebro massifs (Fig. 1D).

Flood plain architectural element

Description. This is the most abundant element of the succession, especially in the SUP (Fig. 2). Depending on the section, it forms 40 to 70% of the studied succession in both basins, although in the most seaward section of the western Maestrazgo Basin (Mora de Rubielos section) it only forms around 15% of the studied succession. It is interbedded with the ephemeral and multi-storey fluvial channel, deltaic, aeolian and coastal to shallow marine elements (Figs 2 and 4). Towards the seaward sections it is also interbedded with limestone of tidal and shallow marine origin (Fig. 2). It is composed of siliciclastic mudstone alternating with non-channelized sandstone and locally oncolitic and stromatolitic limestone (Fig. 9A). Siliciclastic mudstone is typically reddish in colour and displays greenish or greyish mottling, carbonate nodules and root traces (Fig. 9B). In places, it includes dinosaur bones, which are commonly associated, disarticulated and/or articulated (Royo-Torres *et al.*, 2009; Cobos *et al.*, 2010; Campos-Soto *et al.*, 2017a, and references therein).

Non-channelized sandstones comprise very fine to medium-grained sandstone, arranged in decimetre-thick strata (up to 60 cm thick), displaying tabular geometries (Fig. 9C and D) or, locally, flat bases and convex-up tops (Fig. 9E), and short lateral extent (up to 40 m). Tabular sandstone may be massive or display large-scale cross-strata or parallel lamination, followed upward by current ripple strata (commonly climbing ripple strata), which are rarely overlain by wave ripple strata (Fig. 9D). Tabular sandstone in places is arranged in thickening-upward and coarsening-upward bodies up to 1.5 m thick (Fig. 9C). Sigmoidal cross-strata have been also observed in sandstone (Fig. 9E).

Palaeocurrents indicate the main transport direction to the east/north-east in the western Maestrazgo Basin and in the South-Iberian Basin to the west/south-west, and less commonly to the north-east (Fig. 9A).

Sandstone locally includes plant remains and large fragments of dinosaur bones, which are associated and/or articulated in places (see Royo-Torres *et al.*, 2009, 2020; Cobos *et al.*, 2010). Dinosaur

tracks have locally been observed at the base of some sandstone bodies, preserved as convex hyporeliefs or natural track casts (Fig. 9F), and locally at the top, preserved as concave epirreliefs (see Campos-Soto *et al.*, 2017a). In places, sandstone shows vertical and horizontal burrowing traces at the top. Some of the vertical traces are observed as paired circular openings at the top of sandstone (Fig. 9G). Sandstone of this element may also display edaphic features at the top, such as reddish, orange, yellowish and/or greenish mottling and root traces.

Locally, limestone up to 30 cm thick and displaying very limited lateral extension (less than 100 m) is sparsely interbedded with deposits of this element (Fig. 9A and H). Limestone includes oncoids (Fig. 9I), stromatolites, variable amounts of quartz grains and may be associated with poorly sorted fragments of bivalves, including ostreids, up to 4 cm (Fig. 9J). Very rarely limestone includes benthic foraminifera, echinoid spines, gastropods, ostracods, charophytes and very scarce fragments of corals and ooids (Fig. 9K). Locally, limestone made up of oncoids is arranged in bodies with erosive bases and short lateral extent (up to 3 m).

Interpretation. This element is interpreted as deposited in a flood plain located in alluvial to coastal areas. Specifically, reddish siliciclastic mudstone displaying carbonate nodules, green mottling and root traces is interpreted as deposited on a flood plain (*e.g.* Miall, 1996; Selley, 2000; Viseras *et al.*, 2006) subject to subaerial exposure periods and palaeosol development (Freytet & Plaziat, 1982; Alonso-Zarza & Wright, 2010; Soares *et al.*, 2020; Yeste *et al.*, 2020). Non-channelized sandstone displaying parallel lamination at the base and current or, commonly, climbing ripple strata at the top is interpreted as splay lobe deposits (Burns *et al.*, 2017, 2019; Yeste *et al.*, 2020), which developed due to the spreading out of an unconfined flow as a result of the breaking of a levee of a fluvial channel during flood events (Coleman, 1969; Miall, 2010). During these flood events, ephemeral currents transported large dinosaur bone remains, as similarly reported in other ancient settings (*e.g.* González Riga & Astini, 2007; Vogt *et al.*, 2016; Coram *et al.*, 2017). Repeated flooding episodes produced the progradation of the splay deposits, giving rise to the coarsening-upward and thickening-upward bodies, which are common in this type of deposit (*e.g.* Farrell, 1987; Bridge, 2006; Yeste *et al.*, 2020). Moreover, the sigmoidal cross-strata observed in some bodies is interpreted as the result of progradation of splay lobes into standing water bodies (*cf.* Mutti, 1996; Turner & Tester, 2006).

Following deposition, the upper parts of splay lobes were reworked by waves and colonized by burrowers, as evidenced by the occurrence of wave ripple strata and burrows at the top of sandstone. Bioturbation observed as paired circular openings at the top of sandstone may correspond to U-shaped or Y-shaped burrows, which are common in marginal-marine environments (Buatois & Mangano, 2011), as similarly occurs in the deposits of the fluvial–tidal transition in the Upper Cretaceous Trempe Formation, in

the Pyrenees (Díez-Canseco *et al.*, 2014; 2016), for example. Splay lobes underwent subaerial exposure as indicated by the occurrence of edaphic features, as similarly reported in other ancient deposits (Yeste *et al.*, 2020), as well as by the local occurrence of dinosaur tracks at the top of sandstone. The occurrence of natural track casts at the base of sandstone indicates that dinosaurs passed across the flood plain, producing tracks in the underlying muddy sediment, as interpreted by Campos-Soto *et al.* (2017a) for the natural track casts present in sandstone in the western Maestrazgo Basin.

Limestone including oncoids and stromatolites and interbedded with siliciclastic deposits, is interpreted as deposited in shallow water bodies where benthic microbial communities interacted with detrital sediments and/or produced calcium carbonate precipitation (Burne & Moore, 1987; Riding, 1999; 2000). These shallow water bodies received siliciclastic and freshwater inputs, as limestone includes quartz grains, which may be abundant, and locally charophytes, and were also influenced by brackish and marine waters, as limestone locally includes poorly sorted brackish and marine bioclasts that were transported by storms and/or spring tides (Campos-Soto *et al.*, 2016a, 2019). Oncolitic limestone bodies displaying erosive bases and short lateral extent are interpreted as oncoid channels, similar to those reported in other ancient coastal (Suarez-Gonzalez *et al.*, 2015) and fluvio-lacustrine settings (Arenas-Abad *et al.*, 2010).

Deltaic depositional setting

Description. Deltaic deposits are mainly observed in the SUP of the South-Iberian Basin, where they form 2 to 6% of the studied succession. In the western Maestrazgo Basin, these deposits form less than 1% of the studied succession (Fig. 2). They are interbedded and laterally related with the fluvial and aeolian elements (Figs 2 and 4). Deltaic deposits comprise sandstone with minor proportions of carbonaceous detritus and carbonaceous-rich, dark grey siliciclastic mudstone, displaying a coarsening-upward and thickening-upward succession. Each succession displays decimetre to metre thicknesses (up to 2 m), an exposed lateral extent of up to 100 m (Figs 10 and 11) and includes, from base to top, three architectural elements that are intimately related: the *delta-toe*, *delta-front* and *delta distributary channel elements*. Several deltaic successions may be vertically stacked giving rise to composite bodies up to 10 m thick, with an exposed lateral extension of up to 200m (Fig. 10A to C).

The *delta-toe element* comprises carbonaceous-rich, dark grey siliciclastic mudstone, interbedded upward with millimetre to centimetre-thick layers of very fine-grained and rippled sandstone, which display a very low angle-inclination and a great lateral extent (Fig. 10A to D).

Deposits of the *delta-toe element* change laterally and upward to the *delta-front element*, comprising sandstone displaying clinofolds, which have a sigmoidal outline in a flow-parallel direction (Fig. 11A and B). The lower part of the *delta-front element* comprises the lower part of foresets of

clinoforms, which display a very low angle-inclination and pass laterally and downward, along the bottomsets, to the delta-toe deposits (Fig. 10B and C). The lower part of foresets comprise centimetre-thick, very fine to fine-grained, well-sorted sandstone layers that alternate with millimetre to centimetre-thick layers of carbonaceous detritus (Figs 10B, 10C, 10E and 11B). Locally, sandstone layers at the lowermost part of the delta-front element, along the bottomsets, display poorly preserved dinosaur tracks, recorded as convex hyporeliefs or natural track casts, which show elongated shapes with irregular and deformed outlines and penetrate downward into the underlying delta-toe deposits (Fig. 10F). The upper part of the *delta-front element* comprises the upper part of foresets and the topsets of clinoforms, which are made up of fine to medium-grained, well-sorted sandstone that locally displays bioturbation. Locally, drapes of carbonaceous detritus may extend up to the topsets (Figs 10A and 11B).

The upper part of the *delta-front element* deposits may be truncated by erosive surfaces (Figs 10B, 10C and 11C to E), which become progressively more abundant and more incisive upward and eventually are overlain by deposits of the *delta terminal distributary channel element* (Fig. 11C to E). The *delta terminal distributary channel element* comprises decimetre to metre-thick sandstone bodies (up to 1.5 m) displaying erosive bases and a lateral extent of up to 10 m (Figs 10A to C and 11C to E). Sandstone is well-sorted and displays fine to medium grain sizes (Fig. 11F). Sandstone displays large-scale cross-strata with sets up to 1 m thick (Figs 11C to E). In places, sandstone displays backset strata or upward flattening strata (Fig. 10B to C).

Palaeocurrents measured in the South-Iberian Basin, mainly in the clinoforms of delta-front element and, in less proportion, in the cross-bedded sets of the delta terminal distributary channel element, indicate main transport directions to the south, to the west/north-west and to the north-east (Fig. 10A).

Interpretation. The coarsening-upward and thickening-upward trend and the clinoforms observed in these deposits likely record the progradation of deltaic sediments into standing water bodies (*e.g.* Bhattacharya, 2006, 2010; Enge *et al.*, 2010a; Legler *et al.*, 2013; Gugliotta *et al.*, 2015, 2016; Kurcinka *et al.*, 2018).

Carbonaceous-rich, dark grey siliciclastic mudstone located in the lower part of the element, along the *delta-toe* (Fig. 10A to D), is interpreted to have been deposited by settling of suspension load during periods of low flow (Bhattacharya, 2010; Legler *et al.*, 2013; Enge *et al.*, 2010a). The thin layers of very fine-grained rippled sandstone interbedded with carbonaceous-rich, dark grey siliciclastic mudstone at the delta-toe indicate the episodic influx of siliciclastic discharges into the delta toes.

Delta-toe deposits change laterally and upward to *delta-front* sandstone displaying clinoforms characterized by low-angle and laterally-continuous foresets with drapes of carbonaceous detritus that may

extend up to the lower part of foresets, as similarly reported in other ancient and modern deltaic deposits (e.g. Bhattacharya, 2006, 2010; Enge *et al.*, 2010a, 2010b; Schomacker *et al.*, 2010; Bayet-Goll & de Carvalho, 2013; Legler *et al.*, 2013; Ahmed *et al.*, 2014; Kurcinka *et al.*, 2018). Sandstone is interpreted to be deposited by unconfined flows during flood episodes and carbonaceous detritus by settling down from suspension during periods of low flow (interflood periods, *sensu* Gugliotta *et al.*, 2015, 2016). During periods of low flow delta-front deposits were occasionally burrowed, as suggested by bioturbation present locally at the top of sandstone.

The large-scale cross-strata sandstone infilling the erosive surfaces that incise downward into the upper part of the *delta-front* sediments are interpreted as the infill of *deltaic terminal distributary channels* that migrated in a deltaic plain, as similarly observed in other ancient deltaic deposits (Olariu & Bhattacharya, 2006; Bhattacharya, 2010). In places, sandstone displays backset or flattening upward strata (Fig. 10B and C). Similar structures have been observed in experimentally produced deltaic deposits (Muto *et al.*, 2012) due to the development of hydraulic jumps at the channel mouth, and have also been identified in other ancient deltaic successions (e.g. Massari, 1996, Lang *et al.*, 2017). Thus, it is possible that, during episodes of intense rainfall, supercritical flow conditions were achieved in the *delta terminal distributary channels*, leading to the formation of hydraulic jumps and the infilling of associated scours.

Palaeocurrents obtained in the South-Iberian Basin indicate that deltaic deposits were mainly associated with fluvial channels flowing to the west/north-west, to the south and to the north-east, which coincides with some of the transport directions of the multi-storey fluvial channel deposits of this basin (see Figs 7A and 10A). The standing water bodies where deltaic sediments were deposited occupied positions on a flood plain, as the deltaic deposits are commonly interbedded with the flood plain element. These water bodies were shallow, as evidenced by the height of clinoforms (from decimetres to up to 2 m) and by the occurrence of dinosaur tracks at the base of thinly bedded sandstone layers overlying delta toe deposits (Fig. 10F). The poor preservation of dinosaur tracks, showing irregular and deformed outlines, suggests that the delta-toe sediments had a high-water content and a low yield strength at the moment when the tracks were made (Allen, 1997; Marty *et al.*, 2009). The scarcity of evidence for subaerial exposure and edaphic features, which are common in the flood plain and splay lobe deposits, but have been only observed locally at the top of the *delta-toe to delta-front element* (see *Flood plain architectural element* section), suggests that the water bodies were also relatively permanent.

The salinity of the water bodies is difficult to determine as no fossils or sedimentary structures indicative of salinity have been observed within the deltaic deposits. If these water bodies received some marine influence during their deposition, it would be expected to observe brackish or marine fossils, as they occur in the sediments deposited in the shallow marine to brackish-influenced water bodies located in the

flood plain (see limestone of *Flood plain architectural element* section). It would be also expected to observe tidal structures, such as the occurrence of a cyclical pattern in the distribution of carbonaceous detritus within the delta-front deposits, for instance. However, none of these sedimentary structures or fossils have been observed within the deltaic elements. It cannot be discarded that the studied deltaic sediments were deposited in freshwater bodies, as dinosaurs would require the presence of permanent water sources and abundant vegetation; in fact, freshwater fossils of turtles (Pérez-García *et al.*, 2014) and bivalves (Delvene *et al.*, 2013) have been reported in the fluvial deposits of the studied succession in the South-Iberian Basin. Nevertheless, given the coastal setting of the studied succession, mixing of fresh and marine waters or local tidal influence is conceivable for some water bodies.

In addition, the occurrence of vertically stacked coarsening and thickening upward deltaic successions, of up to 2 m thick, leading to composite bodies of up to 10 m thick, is interpreted as a result of the combination of subsidence and high sedimentation rates, which would have produced the vertical superposition of the deltaic deposits.

Coastal to shallow marine depositional setting

Coastal to shallow marine siliciclastic deposits are observed both in the CLP and SUP interbedded and laterally related with tidal or shallow marine limestone and with marl, which includes brackish to marine bioclasts (ostreids, trigonoids and other bivalves, and large benthic foraminifera) and charophytes and was deposited in shallow marine to brackish areas that received freshwater inputs (Figs 2 and 5; Campos-Soto *et al.*, 2016a, 2019). Coastal to shallow marine deposits form less than 3 to 6% of the studied succession in the landward sections of the South-Iberian and western Maestrazgo basins, respectively (Fig. 2). In the seaward sections, they form up to 15 and 20% of the studied succession in the South-Iberian and western Maestrazgo basins respectively (Figs 2 and 5). Two elements have been distinguished:

Coastal terminal distributary channel architectural element

Description. This element occurs interbedded with the distributary mouth-bar element and with marl (Figs 5, 12A and 12B). It comprises fine to medium-grained sandstone arranged in metre-thick bodies (up to 3 m thick), with erosive bases and an exposed lateral extent of 50 m (Figs 5 and 12A to C). Sandstone displays large-scale cross-strata (Fig. 12D and E) and rarely includes millimetre to centimetre-thick layers of carbonaceous-rich marl between cross-sets (Fig. 12D to F). These thin layers of carbonaceous-rich marl may be also present at the bottomsets and the lower part of the foresets of large-scale cross-strata (Fig. 12E). In addition, some sandstone bodies may show internal erosive surfaces (Fig. 12C and F), similar to those described in the multi-storey fluvial channel element.

Locally, poorly sorted conglomerate is observed overlying the basal erosive surface of sandstone bodies or the internal erosive surfaces (Fig. 12F and G). It is made up by subangular to subrounded mudstone pebbles (up to 2.5 cm in diameter), within a coarse-grained sandy matrix, similar to those described in the multi-storey fluvial channel element, although in this case, it also includes scarce fragments of bivalves (Fig. 12G).

The scarce palaeocurrent data obtained in the west Maestrazgo Basin indicate main transport directions to the east/south-east (Fig. 12B).

Interpretation. Channelized sandstone of this element, interbedded with distributary mouth-bar element and marl, represents the infill of terminal distributary channels flowing into coastal and shallow marine areas and feeding distributary mouth-bar deposits, as similarly reported in other ancient examples (e.g. Olariu & Bhattacharya, 2006; Bhattacharya, 2010). The palaeocurrent data obtained in the west Maestrazgo Basin also support this interpretation, as they indicate that these distributary channels were flowing to the east/south-east, which coincides with the location of the Tethys Ocean during the Late Jurassic (Fig. 1D), as well as with the transport directions obtained in some of the distributary mouth-bar deposits of this basin (Figs 12B and 13A). The thin layers of carbonaceous-rich marl occurring between large-scale cross-sets and at the lower part of foresets and bottomsets are interpreted to be deposited by settling down from suspension during periods of low river discharge. Nevertheless, tidal influence could not be discarded, as these deposits were debouching into shallow marine areas. Moreover, the internal erosion surfaces observed within sandstone are interpreted to develop during periods of intense precipitation, which led to an increase of flow velocity and the erosion of the sediments of the channels, as similarly occurs in the multi-storey fluvial channel architectural element. This process was followed by deposition of poorly sorted mudstone conglomerates eroded and transported from upstream flood plain areas, as well as of fragments of bivalves, which were transported from nearby shallow marine areas.

Distributary mouth-bar architectural element

Description. This element occurs commonly interbedded with the coastal terminal distributary channel element and marl or with tidal limestone, including tidal sedimentary structures or with shallow marine limestone, which contains marine fossils, including locally corals in life position (Figs 12A and 13A to F). It is made up of fine to medium-grained sandstone commonly arranged in decimetre to metre-thick bodies (from 10 cm to 2.50 m), which display flat bases and flat or convex-up tops, commonly show short lateral extent (<20 m; Figs 12A and 13A to D) and rare thickening-upward and coarsening-upward trend (Fig. 13B). Sandstone may be massive or display large-scale cross-strata, which may be sigmoidal (Fig. 13C and D), and rare current and/or wave ripple strata at the top. Cross-bedded sandstone bodies pass

seaward to centimetre-thick bodies displaying current and/or wave ripple strata at the top, which alternate with marl, giving rise to wavy bedding (Fig. 13G). Sandstone may include carbonate intraclasts, ooids, brackish and marine bioclasts (Fig. 13H, Table 1) and plant remains. In places, sandstone displays bioturbation at the top (Fig. 13I).

Palaeocurrents measured in the South-Iberian Basin indicate main transport directions to the east, and less commonly to the north and south-east, and palaeocurrents measured in the western Maestrazgo Basin indicate main transport directions to the north-east and east and less commonly to the north and south (Fig. 13A).

Interpretation. These sandstone bodies are interpreted as distributary mouth-bars (*sensu* Wright, 1977; Bhattacharya, 2010) that were formed by the dispersal of unconfined flows at the mouth of terminal distributary channels debouching into coastal to shallow marine areas (*e.g.* Roberts, 1998; DuMars, 2002; Bhattacharya, 2010; Li *et al.*, 2013; Allgöver & Lignum, 2019). This interpretation is supported by palaeocurrent data, indicating that sediment was mainly transported to the north-east/south-east (Fig. 13A), where the Tethys Ocean was located at the time (Fig. 1D). These sediments were deposited in shallow marine areas where even coral reefs developed (Fig. 13C to F). This has been similarly observed in some Upper Miocene deposits of south-east Spain, interpreted as the result of distributary mouth-bars flowing into an interdistributary bay where coral reef patches developed (García-García *et al.*, 2006). Another example of this relationship is observed in the Indonesian Mahakam River Delta, although at a much larger scale, where large siliciclastic lobes of sediment are debouching into shallow marine areas where Halimeda bioherms are present (Storms *et al.*, 2005; Roberts & Sydow, 2010).

At the mouth of terminal distributary channels, sediment was deposited through the migration of subaqueous dunes and, progressively seaward, through the migration of ripples, as a consequence of the decrease of flow velocity. This is indicated by the occurrence of decimetre to metre-thick sandstone bodies displaying large-scale cross-strata, which passes seaward to centimetre-thick rippled sandstone bodies. The repeated arrival of sand at the distributary mouth would have produced the progradation of these unconfined sediment bodies, giving rise to the coarsening-upward and thickening upward trend observed in this element. After deposition, these sediment bodies were prone to reworking by waves, as indicated by the occurrence of wave ripple strata at the top of sandstone, and by tidal currents, as indicated by the occurrence of wavy bedding and the fact that these deposits occur interbedded with intertidal to supratidal limestone including tidal sedimentary structures also indicates that they were deposited in a setting influenced by tides. Locally, these deposits were also reworked by storms, as interpreted by Campos-Soto *et al.* (2016a) in the Benagéber area (Fig. 1C).

Aeolian depositional setting

Aeolian deposits are observed in the SUP of the South-Iberian Basin, being more abundant in the landward sections (Figs 2 and 4), where they form up to 5% of the studied succession. They occur interbedded and laterally related with the fluvial and deltaic elements (Figs 2 and 4). Three types of architectural elements have been distinguished:

Simple aeolian dune architectural element

Description. This element occurs interbedded with the flood plain element or locally overlies the ephemeral fluvial channel or deltaic elements (Figs 2 and 14). This element is composed of fine to medium-grained, sub-angular to rounded and well-sorted sandstone, which is arranged in bodies up to 6 m thick (Fig. 14A to E, G and H), with flat bases and tops, and exposed lateral extents up to 100 m. Sandstone bodies characteristically comprise a single large-scale cross-stratified set up to 6 m thick, whose foresets are inclined up to 36° (Fig. 14A to E). A distinctive feature of this element is that, in some sandstone bodies, foresets display a convex-up outline and pass upward to low-angle inclined topsets (Fig. 14B and C). In detail, foreset deposits are made up of successive millimetre to centimetre-thick stratal packages (Fig. 14F). Each stratum may show inverse grain-size grading (from very fine to fine grain sizes at the bottom to medium grain sizes at the top, Fig. 14H). The contact between each stratum is sharp. Very rarely, scattered rounded to subrounded muddy-soft pebbles and rounded quartzite pebbles (up to 1.4 cm in diameter) have been observed but are confined exclusively to the lower part of foresets (in the lowermost 70 cm of sets). Palaeocurrents indicate transport directions towards the south-east, west/south-west, or the north-west, depending on the sandstone body measured (Fig. 14A).

Interpretation. Features of this element, notably the well-sorted nature of the sandstone, the characteristic occurrence of very large-scale cross-stratified sets up to 6 m-thick with foresets inclined at angles up to 36°, its geometry (flat bases and tops) and exposed lateral extent of up to 100 m, lead most logically to the interpretation of migratory aeolian dunes (Ahlbrandt & Fryberger, 1982; McKee, 1966; Mountney, 2006).

The internal structure of foresets, made up of millimetre to centimetre-thick strata displaying inverse grain size grading, is interpreted as the result of accumulation of grainflow deposits, as similarly reported from other ancient and modern aeolian dunes (McKee *et al.*, 1971; Hunter, 1977; Kocurek & Dott, 1981; Fryberger & Schenk, 1988), in which they are explained as the result of the repeated avalanching of sand in the lee side of dunes exceeding the angle of repose (Hunter, 1977; Ahlbrandt & Fryberger, 1982; Kocurek, 1991; Mountney, 2006). Palaeocurrents indicate transport of sand towards the west/south-west, the north-west or the south-east, depending on the sandstone body measured (Fig. 14A; see interpretation of

wind palaeocurrents in *Discussion*). This suggests that aeolian dunes migrated under the influence of prevailing unidirectional winds, which is characteristic of transverse aeolian dunes (*sensu* Fryberger & Dean, 1979; Mountney 2006). The style of the cross-strata observed in some bodies, characterized by convex-up foresets with preserved topsets, together with their vertical scale (Fig. 14B and C), is very similar to the features described in recent dome-shaped aeolian dunes by McKee (1966, 1979) in the White Sand National Monument (USA). According to this author, dome-shaped aeolian dunes initially begin as transverse or other type of dunes that are controlled by one dominant wind direction and are subsequently affected by episodes of strong winds. Therefore, the studied aeolian sandstone likely represents one of the few examples of well-preserved dome-shaped aeolian dunes in the pre-Quaternary fossil record; the few other examples are those of the Proterozoic of Greenland (Clemmensen, 1988) and India (Chakraborty, 1991), the Devonian of Australia (Jones, 1972) and the Triassic of the Cheshire Basin, UK (Thompson, 1969). In addition, the fact that aeolian dune deposits of this element are formed by one single set of large-scale cross-strata, suggests that they were formed under relatively low rates of sediment supply that merely allowed the migration, but not the climb, of one single transverse or dome-shaped aeolian dunes (Kocurek & Havholm, 1993; Mountney, 2006).

Sandstone of this element is well-sorted and made up of sub-angular to rounded grains. The occurrence of sub-angular (rarely even angular) grains has been identified in modern and ancient aeolian dune deposits (*e.g.* Kiersch, 1950; Thompson, 1969; Glennie, 1970; McKee, 1979; Rodríguez-López *et al.*, 2008; Galán-Abellán *et al.*, 2013), and some authors have even reported aeolian dune deposits displaying moderate (Mountney *et al.*, 1998) to poor sorting (McKee, 1966; Ahlbrandt, 1979), due to the short time of reworking and the close proximity to the source of sand.

The occurrence of pebbles in the lower parts of aeolian dune sets has been described in ancient and modern aeolian deposits. Mader (1981) and Turner & Makhlof (2005) identified pebbles up to 1 cm long and chert pebbles up to 5 cm long along the foresets of Triassic and Quaternary aeolian dune deposits of Germany and Jordan, respectively. Kiersch (1950) reported small pebbles and coarse grains of quartz and chalcedony along several cross-strata planes in the Jurassic Navajo Sandstone (Utah, USA). Rodríguez-López *et al.* (2010) identified scattered quartzite pebbles in the tosets of mid-Cretaceous aeolian dune deposits of Spain and interpreted them as derived from adjacent deflated wadis. These authors cite the work Glennie (1970), who reported pebbles in the foresets of small recent aeolian dune deposits and interpreted them as derived from an adjacent wadi bank by rolling or sliding. Additionally, pebbles of up to 1.5 cm and 2.3 cm in diameter have been recorded lodged in telephone poles at 1.6 m and 0.8 m heights, respectively; these were interpreted as having been transported by saltation during an intense windstorm in California, USA (Sakamoto-Arnold, 1981).

Massive and indistinctly stratified aeolian dune architectural element

Description. This element overlies the flood plain element and is overlain by the multi-storey fluvial channel element (Fig. 15A to C). This element may occur interbedded with ephemeral fluvial channelized conglomerate bodies, which display 90 cm to 3 m of thickness and up to 20 m of lateral extent (Fig. 15C and D; see *Ephemeral fluvial channel architectural element* section).

This element is made up of fine to medium-grained, sub-angular to rounded, well-sorted sandstone arranged in up to 25 m thick bodies, displaying flat bases and tops and an exposed lateral extent of up to 80 m (Fig. 15B to E). Sandstone mostly shows a massive appearance, although locally displays poorly preserved large-scale cross-strata with sets of up to 7 m thick (Fig. 15C and D), and with foresets inclined up to 30° (Fig. 15D, G and H). In some cross-stratified sets, foresets pass downward to laterally continuous bottomsets (Fig. 15B, E, G and H). Locally, the bottomsets and, less commonly, the lowermost part of foresets are draped by millimetre to centimetre-thick layers of carbonaceous detritus and mica flakes (Fig. 15G and H). Palaeocurrents indicate main transport directions to the west/north-west and, in minor proportion, to the south-west (Fig. 15A).

Interpretation. The homogeneous and well-sorted sandstone of this element, together with its massive appearance, its large thickness (up to 25 m thick), its flat base and great exposed lateral extent (up to 80 m), suggest an aeolian origin. The homogeneity of grain size and the good sorting are features typically described in aeolian deposits, such as in the Lower Jurassic Navajo Sandstone (*e.g.* Kiersch, 1950; Prothero & Schab, 1996; McKee, 1979), which, in places, characteristically exhibits a massive appearance (*e.g.* Ekdale *et al.*, 2007). Moreover, the occurrence of poorly preserved, large-scale cross-strata with sets of up to 7 m thick, displaying foresets inclined up to 30°, further supports an aeolian dune origin. Palaeocurrents indicate aeolian dune migration to the north-west/south-west (Fig. 15A; see more details of wind palaeocurrents in *Discussion*).

The drapes of carbonaceous detritus and mica flakes locally observed in the bottomsets and in the lowermost part of foresets are interpreted to have settled from suspension in wet interdunes subject to episodic floods (Ahlbrandt & Fryberger, 1981; 1982; Mountney, 2006). The occurrence of drapes in the lower part of the foresets indicates that the water level reached the lower part of aeolian dune flanks, and likely fluctuated. A similar process has been reported in the Great Sand Dunes (USA) and in the Namib Desert (Skeleton Coast), where episodic fluvial floods cause the inundation of interdune areas, where clays and/or wood detritus settle down and drape the interdune floor and the lower part of dune flanks (Langford, 1989, and Stanistreet & Stollhofen, 2002, respectively). Repeated interdune flooding and aeolian dune migration produced the successive interfingering of drapes and grainflows within the same cross-strata set

(Langford & Chan, 1989; Langford, 1989; Cain & Mountney, 2011). This type of draping (*i.e.* mud layers, carbonaceous/wood detritus and mica flakes) has been reported in other ancient (*e.g.* Thompson, 1969; Gradziński *et al.*, 1979; Pulvertaft, 1985; Langford & Chan, 1988; Veiga & Spalletti, 2007; Rodríguez-López *et al.*, 2008, 2012) and modern aeolian dune deposits (*e.g.* Ahlbrandt & Fryberger, 1981; Fryberger *et al.*, 1990; García-Hidalgo *et al.*, 2002; Mountney & Russell, 2006; 2009; Kocurek *et al.*, 2020).

The occurrence of ephemeral fluvial deposits interbedded with massive and indistinctly stratified aeolian dune deposits (Fig. 15C and D) is interpreted as the result of development of ephemeral channels between aeolian dunes during periods of intense precipitation, which would have led to the erosion of aeolian dune deposits. This type of fluvial–aeolian interaction has similarly been documented in other arid to semiarid modern (*e.g.* Glennie, 1970; Al-Masrahy & Mountney, 2015) and ancient settings (*e.g.* Herries, 1992; de Witt, 1999; Mountney *et al.*, 1998; Veiga *et al.*, 2002; Mountney & Jagger, 2004; Jordan & Mountney, 2010, 2012; Rodríguez-López *et al.*, 2010; 2014, and references therein; Soria *et al.*, 2011; Tripaldi *et al.*, 2011), as a result of development of wadis between aeolian dunes during flash-flood events. In the studied succession, aeolian dune deposits overlie those of ephemeral fluvial channels, indicating that, once the flood episode had finished, aeolian dunes would have migrated over the deposits of the once-again dry ephemeral channels, a process that similarly occurs in modern desert settings (Al-Masrahy & Mountney, 2015; Liu & Coulthard, 2015).

Climbing aeolian dune architectural element

Description. This element is interbedded with the deltaic and fluvial channel elements, and is overlain by the flood plain element (Figs 4 and 16). It comprises sub-angular to rounded, fine to medium-grained, well-sorted sandstone, which is arranged in metre-thick bodies (up to 5 m thick) with an exposed lateral extent of around 100 m (Fig. 16A to D). Sandstone displays large-scale cross-strata with sets up to 2 m thick (Fig. 16B), which are stacked in cosets (Fig. 16C and D). A characteristic feature of this element is the occurrence of bounding surfaces delimiting individual sets of cross-strata, which are inclined at low angles ($<10^\circ$) relative to the master coset bedding surface and dip in the opposite direction to the foreset dip (Fig. 16C and D). In some outcrops parallel to transport direction, these surfaces can be laterally traced at least for 50 m. Large-scale cross-strata comprises tangential foresets inclined at angles up to 32° (Fig. 16B to E), which occasionally are slightly deformed (Fig. 16E). In detail, foreset deposits comprise millimetre to centimetre-thick strata, made up of fine to medium-grained well-sorted sandstone, which pinch out towards the bottomsets (Fig. 16F to H). Towards the bottomsets, these strata are interbedded with other millimetre to centimetre-thick strata comprised of very fine to fine-grained and well-sorted sandstone, which pinch out upward (Fig. 16G and H).

Pseudomorphs after gypsum crystals, forming desert roses (Fig. 16I), have been locally observed within the sandstone. Additionally, very scattered subrounded muddy pebbles and rounded quartzite pebbles (up to 1.5 cm in diameter) are locally observed towards the lower part of sandstone bodies that overlie fluvial channelized elements, similar to those described in the *Simple aeolian dune architectural element* section. These pebbles mostly occur along the tangential foresets, preferentially towards the bottomsets.

Palaeocurrents measured in the tangential cross-strata sets indicate main transport directions towards the south-east in some sandstone bodies and towards the north-west in other sandstone bodies located in different stratigraphic positions (Fig. 16A).

Interpretation. Features of these deposits, such as the well-sorted grain texture, the occurrence of large-scale cross-strata sets comprising tangential foresets, which might be locally slightly deformed, and the occurrence of low-angle inclined bounding surfaces delimiting sets of cross-strata, indicate that this element records the downwind migration and accumulation of aeolian dunes, as has been similarly described in other ancient aeolian dune deposits (*e.g.* Kocurek, 1981; Ahlbrant & Fryberger, 1982; Spalletti & Colombo Piñol, 2005; Scherer & Lavina, 2005; Mountney, 2006; Spalletti *et al.*, 2010).

The internal structure of tangential cross-strata sandstone, comprising millimetre to centimetre-thick strata pinching out downward, is very similar to the sandflow cross-strata described by Hunter (1977) in modern aeolian dunes (here referred to as grainflow cross-strata, *sensu* Kocurek & Dott, 1981, and Kocurek, 1991, 1996), which develop due to the successive avalanching of sand in aeolian dune slipfaces. The very fine to fine-grained sandstone strata located at the bottomsets pinching out upward are interpreted as wind ripples that migrated over the plinth of aeolian dunes and dry interdunes (Hunter, 1977; Ahlbrant & Fryberger, 1982; Kocurek, 1991). The occurrence of slightly deformed foresets is interpreted as the result of slumping of cohesive, semi-consolidated sand in the lee side of dunes wetted by rains or dews (*e.g.* McKee *et al.*, 1971; Due & Dott, 1980; Loope *et al.*, 2001). Similar to what occurs in the simple aeolian dune architectural element, palaeocurrents show a unidirectional transport pattern for each sandstone body measured in different stratigraphic positions, indicating aeolian dune migration to the south-east for some bodies or the north-west for others (Fig. 16A; see interpretation of wind palaeocurrents in *Discussion*) and suggesting that deposition occurred in transverse aeolian dunes (*sensu* Fryberger & Dean, 1979; Mountney 2006).

The low-angle-inclined bounding surfaces that delimit individual sets of cross-strata are very similar to the interdune surfaces defined by Kocurek (1981, 1996) and described in many ancient aeolian deposits (*e.g.* Mountney & Thompson, 2002; Scherer & Lavina, 2005; Mountney & Jagger, 2004; Rodríguez-López *et al.*, 2008; Bállico *et al.*, 2017). Interdune surfaces result from the downwind migration

of an interdune trough over the stoss side of the preceding aeolian dune, producing the partial erosion and truncation of its upper part (Rubin & Hunter, 1982; Kocurek, 1981; 1991; 1996; Mountney, 2006).

Climbing transverse aeolian dune bedforms migrated over these surfaces, as they are overlain by tangential cross-strata sandstone. The fact that these deposits were formed by the accumulation of climbing aeolian bedforms indicates that the sediment supply during their deposition was high (Kocurek & Havholm, 1993; Mountney, 2006).

The occurrence of pseudomorphs after gypsum crystals, forming desert roses, similar to those locally observed within this element, have been reported in other aeolian deposits (*e.g.* Loope, 1988; Simpson & Erikson, 1993; Tripaldi *et al.*, 2011; Rodríguez-López *et al.*, 2013) and are interpreted as intrasediment gypsum crystals that grew in the pore spaces of aeolian sand located close to the water table (Warren, 2016).

DISCUSSION

Palaeoenvironmental setting of eastern Iberia during the Late Jurassic

Siliciclastic sediments of the Villar del Arzobispo Formation were deposited in fluvial, deltaic, aeolian and coastal to shallow marine depositional environments that developed in eastern Iberia during the Late Jurassic (Figs 1D and 17). These deposits are interbedded and laterally related with one another and possess stratal relationships to indicate that they developed coevally (Figs 2, 3, 4, 5 and 17; Fig. S1 of Supplementary Material). During the first steps of evolution of the studied succession (during sedimentation of the CLP), deposition of siliciclastic sediments was scarce and mainly occurred in coastal to shallow marine marly and carbonate areas (Figs 2 and 3; Campos-Soto *et al.*, 2016a, 2017a, 2019). Upward, during sedimentation of the SUP, a large abundance of siliciclastic sediments was deposited in a coastal and alluvial plain (Figs 2, 3 and 17; Campos-Soto *et al.*, 2016a, 2017a, 2019; Campos-Soto *et al.*, 2016a, 2017a, 2019). Landward, deposition mainly took place in fluvial, deltaic and aeolian environments that were laterally and vertically related (Figs 3, 4 and 17), while seaward, it progressively occurred in coastal to shallow marine environments located in areas with high subsidence rates, where siliciclastics are interbedded to the east/south-east with shallow water marl, with intertidal to supratidal peloidal and/or micritic limestone and with shallow marine bioclastic and oolitic limestone (Figs 2, 3, 5 and 17; Fig. S1 of Supplementary Material; Campos-Soto *et al.*, 2016a, 2017a, 2019).

The coastal and alluvial plain was formed by broad and vegetated flood plains (*see Flood plain architectural element* section), which were crossed by ephemeral and perennial to semi-perennial fluvial channels that had a highly seasonal discharge (*see Ephemeral and Multi-storey fluvial channel architectural elements*, respectively; Fig. 17). During flood events, flood plain areas underwent deposition

of splay lobes as a result of the breaking of channel levées (see *Flood plain architectural element* section). Fluvial channels flowed into shallow water bodies located in the flood plain that were probably freshwater, leading to deposition of small deltas (see *Deltaic architectural elements*). Some fluvial channels ultimately flowed into coastal to shallow marine areas (see *Coastal terminal distributary channel architectural element*), resulting in the deposition of distributary mouth-bars (see *Distributary mouth-bar architectural element*; Figs 5 and 17). Some of the shallow water bodies located in the flood plain underwent carbonate precipitation and development of oncoids and stromatolites (see *Flood plain architectural element*). Some of these water bodies were influenced by freshwater and received siliciclastic input, as limestone includes abundant quartz grains and locally charophytes. Other water bodies were also influenced by brackish and marine waters, as limestone locally includes brackish and marine fossils that were probably transported from shallow marine areas by storms and/or spring tides (see *Flood plain architectural element*; Fig. 17).

During periods of non-flood discharges, subaqueous siliciclastic deposits likely underwent periods of subaerial exposure. Subsequently, sand of these deposits was reworked by wind and deposited in aeolian dunes that migrated over the coastal and alluvial plain, as reported in modern (*e.g.* Glennie, 1970; Langford, 1989; Singh *et al.*, 1993; Collinson, 1996) and ancient settings (*e.g.* Thompson, 1969; Mountney *et al.*, 1998). Aeolian dunes developed next to deltas and eventually migrated over their deltaic plain, as evidenced by the occurrence of aeolian deposits overlying the deltaic elements (Figs 2, 4, 10A, 16C, 16D and 17). Aeolian dunes could also migrate over deposits of fluvial channels that became subaerially exposed during periods of non-flood discharges, as indicated by the occurrence of aeolian dune deposits overlying fluvial channel sediments (Figs 4, 15C and 15D). Aeolian deposits are only preserved in the landward sections of the South-Iberian Basin (Riodeva and Benagéber sections; Figs 1C, 1D, 2 and 4), which contain a greater proportion of subaqueous siliciclastic deposits than sections of the western Maestrazgo Basin. The South-Iberian Basin was largely surrounded by emergent areas (Iberian and Valencian massifs), whereas the western Maestrazgo Basin only had emergent areas towards the south-west (Fig. 1D). In this way, the South-Iberian Basin received greater input of siliciclastic detritus. Subaerial exposure was common, and deposits were repeatedly reworked by the wind. In contrast, broader coastal plains developed in the western Maestrazgo Basin and received relatively less siliciclastic input.

Palaeocurrents of the aeolian dune deposits indicate predominant wind transport directions to the west (ranging between north-west/south-west) and rarely to the south-east (Figs 14A, 15A and 16A). This is based on the interpretation of perfectly transverse dune types migrating under the influence of a unidirectional wind (*cf.* Rubin, 1987). Palaeocurrents pointing to the west (north-west/south-west) are in agreement with palaeowind directions shown in the palaeogeographic models of eastern Iberia during the Late Jurassic (Fig. 1D), which interpret winds approaching eastern Iberia from the east and south (from the Tethys Ocean; Fig. 1D) during the winter and summer, respectively (Sellwood & Valdes, 2008), as well as

hurricanes and storms also coming from the Tethys Ocean (Marsaglia & Klein, 1983). Winds approaching the South-Iberian Basin from the Tethys Ocean might have been deflected by the surrounding Iberian and Valencian massifs, resulting in them blowing parallel to the north-west/south-east oriented Valencian Massif, thereby producing winds blowing to the south-east in the basin and, thus, leading to the migration of aeolian dunes to the south-east. This similarly occurs in some present-day mountain ranges, which act as barriers to prevailing wind currents, causing their deflection, so they blow parallel to the trend of the mountain ranges (*e.g.* O'Connor *et al.*, 1994; McCauley & Sturman, 1999; Neiman *et al.*, 2010). Moreover, other investigations interpret that winds also approached Iberia from the north (from the Boreal realm; Fig. 1D) during the Kimmeridgian (Benito *et al.*, 2005). These northerly winds could have penetrated along the Iberian Basin and increased their velocity, as a consequence of its southward narrowing (Fig. 1D), leading to the occurrence of south-eastward winds in the south-east Iberian Basin.

Deciphering the palaeoclimate of eastern Iberia during the Late Jurassic

Palaeoclimatic and palaeogeographic reconstructions for the Late Jurassic show that Iberia was located in the subtropics (Fig. 1D) and that its climate was warm (Valdes, 1993; Valdes & Sellwood, 1992), seasonal (Rees *et al.*, 2000; Diéguez *et al.*, 2010) and subject to seasonal rainfalls (Valdes & Sellwood, 1992) and hurricanes coming from the Tethys Ocean (Marsaglia & Klein, 1983). Models also show a trend of increasing aridity during the Late Jurassic (Hallam, 1984, 1985; Hallam *et al.*, 1993). However, recent studies place the limit between the arid and the tropical-subtropical belts at the eastern margin of Iberia, from where more humid conditions prevailed (Sellwood & Valdes, 2008; Boucot *et al.*, 2013). In this context, the fact that the siliciclastic sediments of the studied succession include coeval deposits that are common of both arid to semiarid and humid to subhumid settings makes it difficult to discern the specific palaeoclimatic setting that prevailed during deposition.

The studied succession includes ephemeral fluvial channels and aeolian dune deposits, locally containing desert roses, which are features commonly linked to arid to semiarid settings (*e.g.* Tucker & Benton, 1982; Holz & Scherer, 2000; Spalletti & Colombo Piñol, 2005; Boucot *et al.*, 2013; Priddy & Clarke, 2020). In fact, the fluvial–aeolian interactions recorded in the studied deposits, such as the development of ephemeral fluvial channels between aeolian dunes and the presence of standing water bodies in interdunes during periods of rainfall, are similar to those reported in many present-day and ancient arid to semiarid environments (*e.g.* Glennie, 1970; Langford, 1989; Stanistreet & Stollhofen, 2002; Veiga *et al.*, 2002; Veiga & Spalletti, 2007; Rodríguez-López *et al.*, 2014, and references therein; Al-Masrahy & Mountney, 2015; Liu & Coulthard, 2015; Kocurek *et al.*, 2020; see *Massive and indistinctly stratified aeolian dune architectural element*; Fig. 15). Nevertheless, similar fluvial–aeolian interactions can also occur in humid to subhumid climates in present-day settings (*e.g.* Mountney & Russell, 2009; Al-

Masrahy & Mountney, 2015; dos Santos & dos Santos, 2015). Aeolian dunes, accumulated through the process of bedform climbing, have been widely documented in many ancient examples developed in arid to semiarid settings (e.g. Kocurek, 1981; Clemmensen, 1989; Mountney *et al.*, 1999; Mountney & Thompson, 2002), but they also occur nowadays in modern humid to subhumid climates, such as in the coastal plains of Oregon (USA; Cooper, 1958; Hunter *et al.*, 1983; Peterson *et al.*, 2007). In these coastal plains of Oregon, aeolian dune fields of relatively modest size (from 7 to 15 km² approximately) develop next to coastal lakes and vegetated areas, which are crossed by rivers (Cooper, 1958; Hunter *et al.*, 1983; Peterson *et al.*, 2007). These aeolian dunes develop in areas with high sediment supply, where aeolian sand comes from wind reworking of a local source of subaerial exposed sand; this is similar to the interpreted setting for the climbing aeolian dune deposits of the studied succession. In the case of the coastal aeolian dunes of Oregon, aeolian sand comes predominantly from the reworking of sandy beach sediments (Peterson *et al.*, 2007), whereas in the case of the Late Jurassic succession it was predominantly derived from the sandy fluvial and deltaic sediments that underwent subaerial exposure after periods seasonal rainfalls (see *Palaeoenvironmental setting of eastern Iberia during the Late Jurassic* section).

The studied unit also includes abundant deposits indicative of permanent water courses that occur laterally and vertically related with those of the aeolian and ephemeral fluvial channels (Figs 2 and 4). Some of them correspond to those deposited in perennial to semi-perennial fluvial channels that had a seasonal discharge. Variable discharge rivers nowadays occur in areas controlled by monsoonal-type precipitation (e.g. Fielding *et al.*, 2011; Plink-Björklund, 2015), which is coherent with the interpretation of common development of seasonal storms and hurricanes in Iberia during the Late Jurassic (Marsaglia & Klein, 1983; Valdes & Sellwood, 1992). In present-day settings, seasonal rivers transmit a perennial discharge in monsoonal domains, whereas in subtropical arid to semiarid settings they typically only transmit flow during the monsoonal season and could even be dry the rest of time, unless their catchment area is located in the monsoonal domain (for example, the Nile River; Plink-Björklund, 2015). Other deposits indicative of permanent water courses correspond to the deltaic sediments, which were deposited in permanent to semi-permanent water bodies, as well as the abundant vegetation. Although vegetation can locally develop in arid to semiarid settings in low-lying areas with a high water table, the occurrence of plant remains (carbonaceous detritus, fragments of fossil trunks and other remains) and/or edaphic features occurs widespread in all the studied deposits (fluvial channels, distributary mouth-bars, deltaic, flood plain, splay lobes, wet interdunes of the *Massive and indistinctly stratified aeolian element*) in both basins (Fig. 2; Table 1). Furthermore, the studied deposits include a great abundance of dinosaur remains and, especially, of herbivorous dinosaurs (sauropods, stegosaurs and scarce ornithopods; e.g. Casanovas-Cladellas *et al.*, 1999, 2001; Cobos *et al.*, 2010, 2020; Royo-Torres *et al.*, 2006, 2009, 2020; Alcalá *et al.*, 2009, 2018; Company *et al.*, 2010; Suñer *et al.*, 2014). These observations reinforce the interpretation of a setting with

availability of abundant vegetation and permanent freshwater sources. Therefore, collectively these features indicate a more humid and seasonal setting that was controlled by monsoonal-type precipitation during deposition of the studied succession. This interpretation is coherent with that recently made for the coeval Late Jurassic Lourinhã Formation in Portugal, which points to a warm subhumid climate with a strongly seasonal precipitation pattern (Myers *et al.*, 2012).

Comparison with modern analogous systems

A modern coastal setting that includes a wide variety of depositional subenvironments characteristic of arid to semiarid and humid to subhumid settings, similar to what occurs in the Villar del Arzobispo Formation, is developed in the Lençóis Maranhenses National Park in north-east Brazil (Fig. 18). It comprises an aeolian dune field located next to an estuary (Fig. 18A), where flood plains, intermittent interdune ponds, perennial and ephemeral rivers, tidal plains (*e.g.* Gonçalves *et al.*, 2003; Parteli *et al.*, 2006; dos Santos & dos Santos, 2015; Ielpi, 2017) and deltas develop. This system forms in a tropical subhumid climate in which 90% of annual rainfall occurs during the wet season (Parteli *et al.*, 2006; dos Santos & dos Santos, 2015). During seasonal rainfall, interdune ponds are flooded by rainwater or by the upwelling of groundwater (dos Santos & dos Santos, 2015), giving rise to standing water bodies in the interdune areas (Fig. 18B), as similarly interpreted for the studied aeolian deposits (see *Massive and indistinctly stratified aeolian dune architectural element*). In Lençóis Maranhenses, sand of aeolian dunes developing next to tidal channels is reworked by tides (Fig. 18C). This process cannot be discarded in the studied deposits, as aeolian interdunes might have been flooded by storms and/or spring tides, since they developed in a coastal setting.

In Lençóis Maranhenses, semi-perennial rivers cross the flood plain areas and flow into shallow water bodies where deltaic sediments are deposited (Fig. 18D), as similarly interpreted for the studied deposits (see *Deltaic architectural elements*). In this system, rivers also transect the aeolian dune field (Fig. 18E to G; Ielpi, 2017). In some cases, rivers erode aeolian dune flanks (Fig. 18F) and, in other cases, aeolian dunes migrate over fluvial channels that are dried out or transmit a very low discharge (Fig. 18G), as similarly interpreted for the studied succession (see *Massive and indistinctly stratified aeolian dune architectural element*). Furthermore, in Lençóis Maranhenses, aeolian dunes migrate over small shallow deltas (Fig. 18E, H and I). Similarly, the studied fossil aeolian dunes locally overlie deltaic deposits (Figs 4, 10A, 16C and 16D), indicating that aeolian dunes developed next to a delta and migrated over the deltaic plain. In Lençóis Maranhenses, aeolian dunes are reworked by distributary channels (Fig. 18I). A similar process would explain the generally well-sorted texture of sandstone deposited in the delta terminal distributary channels and the delta fronts of the studied deposits (Fig. 11F).

Nevertheless, although the Late Jurassic and the Brazilian systems have numerous similarities, they also show differences regarding their geotectonic setting, which influence the sedimentary features of their fluvial deposits. The presently active Brazilian system is developed in a stable tectonic setting. By contrast, the Late Jurassic succession was deposited in a tectonically-active extensional basin, which would have led to the development of steeper topographic gradients. This would have favoured the incision of streams, as occurs in nowadays tectonically-active settings (*e.g.* Bull, 2007; Allen & Allen, 2013), which could transport very poorly sorted conglomerates displaying clasts of large sizes and subangular shapes and deposit them in the ephemeral and perennial to semi-perennial fluvial channels during periods of intense rainfall (Figs 1D, 2 and 17), as those observed in the studied succession. Another difference is that, in the Late Jurassic system, aeolian dunes did not form an extensive dune field like in Lençóis Maranhenses. The ancient system was likely similar to the transition zone located between the tidal flats of the estuary and the aeolian field of the Brazilian analogue (Fig. 18A). Aeolian dunes were apparently more abundant towards the landward areas of the South-Iberian Basin (Fig. 1D).

Moreover, the studied succession locally includes desert roses in the aeolian deposits (see *Climbing aeolian dune architectural element*), which, to our knowledge, have not been reported in the Brazilian aeolian dunes. Nevertheless, although the occurrence of evaporites has traditionally been linked to arid or semiarid settings (*e.g.* Hallam, 1984; Warren, 2016), they have also been locally identified in humid (see Argentinean Rio de la Plata estuary in Carol *et al.*, 2016) and subhumid settings (see Australian Burdekin River Delta in Fielding *et al.*, 2006).

Thus, the comparison made between deposits of the Villar del Arzobispo Formation and those of present-day settings highlights that deposits that characteristically develop under the influence of contrasting climate regimes (arid and humid) could appear laterally and vertically interbedded in the fossil record as a result of deposition in intermediate climates. This study highlights the importance of carrying out a careful and thorough sedimentological analysis when interpreting the palaeoclimatic significance of ancient successions, taking into account all available evidence from deposits that represent multiple coeval sub-environments in the rock record.

CONCLUSIONS

This work presents the sedimentological analysis of the siliciclastic deposits of the Late Jurassic Villar del Arzobispo Formation cropping out in the South-Iberian and western Maestrazgo basins. Detailed lithofacies analysis has enabled establishment of the palaeoenvironmental, palaeogeographical and palaeoclimatic setting of eastern Iberia during the Late Jurassic.

The siliciclastic studied succession was deposited in a coastal and alluvial plain crossed by ephemeral and perennial to semi-perennial fluvial channels that had a seasonal discharge and underwent deposition of splay lobes during flood events. Fluvial channels flowed into shallow freshwater bodies located in the flood plain, leading to the accumulation of small deltas. Seaward, fluvial channels bifurcated in distributary channels, which flowed into coastal and shallow marine areas, leading to the development of distributary mouth-bars. Some water bodies located in the flood plain were connected to the sea, allowing transport of brackish and marine bioclasts from shallow marine areas during storms and/or spring tides. Siliciclastic sediments underwent periods of subaerial exposure, causing the wind-reworking of sand to form aeolian dunes; this led to the preservation of one of the few known examples of dome-shaped aeolian dunes in the fossil record. The coastal and alluvial plain was laterally connected to the east/south-east to tidal flats and shallow marine areas, which underwent deposition of peloidal and/or micritic limestone and bioclastic and/or oolitic limestone, respectively.

The studied coastal and alluvial succession includes deposits that are typical of arid to semiarid settings, such as aeolian dunes and ephemeral channel deposits. However, the coeval occurrence of deposits indicative of permanent water courses, such as perennial to semi-perennial fluvial channel deposits and deltaic sediments deposited in permanent water bodies, as well as abundant plant remains and large dinosaur faunas, suggests a more humid and seasonal setting controlled by monsoonal-type precipitation.

A comparison performed between these Late Jurassic deposits and those developing nowadays in the Lençóis Maranhenses National Park (north-east Brazil) – a coastal system located in a subhumid tropical setting with a seasonal precipitation pattern that includes very similar aeolian, fluvial and deltaic environments to those interpreted in the studied succession – has revealed that deposits characteristic of contrasting climate regimes (arid and humid) could be laterally and vertically related in ancient successions as a result of deposition in complex coevally active coastal environments present in intermediate climates.

ACKNOWLEDGEMENTS

This research was funded by the Spanish projects PGC2018-094034-B-C21 and PGC2018-094034-B-C22 of the Ministry of Science, Innovation and Universities and the project CGL2014-52670-P of the Ministry of Economy and Competitiveness, by the Department of Education, Culture and Sport of the Government of Aragón, by the Research Group E04_20R FOCONTUR (financed by the Department of Science, University and Society of Knowledge of the Government of Aragón and FEDER funds 'Construyendo Europa desde Aragón'), by the Instituto Aragonés de Fomento and Dinópolis. The authors also thank the "Sedimentary Geology, Paleoclimate and Environmental Change" UCM Research Group (Ref. 910198). We are grateful to reviewers Claiton Scherer, Valentina Rossi and César Viseras, and to the associate editor Gonzalo Veiga for their suggestions, which have improved the paper. We are thankful to

Beatriz Moral, Juan Carlos Salamanca and Aitor Antón for thin-section preparation and laboratory support and to Valle López for helping with ArcGIS.

DATA AVAILABILITY STATEMENT

The data that support the findings of this study are available from the corresponding author upon reasonable request.

REFERENCES

- Abdullatif, O.M.** (1989) Channel-fill and sheet-flood facies sequence in the ephemeral terminal River Gash (Kassala, Sudan). *Sedimentary Geology*, **63**, 171-184.
- Ahlbrandt, T.S.** (1979) Textural parameters of eolian deposits. In: *A Study of Global Sand Seas*. (Ed. E.D. McKee), pp. 21-52. U.S. Government Printing Office, Washington.
- Ahlbrandt, T.S. and Fryberger, S.G.** (1981) Sedimentary features and significance of interdunes deposits. *SEPM Special Publication*, **31**, 293-314.
- Ahlbrandt, T.S. and Fryberger, S.G.** (1982) Introduction to aeolian deposits. In: *Sandstone Depositional Environments* (Eds. P.A. Scholle and D.R. Spearing), *AAPG Memoir*, **31**, 11-47.
- Ahmed, S., Bhattacharya, J.P., Garza, D.E. and Li, Y.** (2014) Facies architecture and stratigraphic evolution of a river-dominated delta front, Turonian Ferron Sandstone, Utah, U.S.A. *Journal of Sedimentary Research*, **84**, 97-121.
- Alcalá, L., Cobos, A., Delclòs, X., Luque, L., Mampel, L., Royo-Torres, R. and Soriano, C.** (2009) Mesozoic terrestrial ecosystems in Teruel. In: *Mesozoic Terrestrial ecosystems in Eastern Spain* (Coords. L. Alcalá., R. Royo-Torres), *¡Fundamental!*, **14**, 93-130.
- Alcalá, L., Cobos, A. and Royo-Torres, R.** (2018) Dinosaurios de la Península Ibérica. *PH: Boletín del Instituto Andaluz del Patrimonio Histórico*, **26**, 116-153.
- Alexander, J., Fielding, C.R. and Jenkins, G.** (1999) Plant-material deposition in the tropical Burdekin River, Australia: implications for ancient fluvial sediments. *Palaeogeography, Palaeoclimatology, Palaeoecology*, **153**, 105-125.
- Alexander, J., Bridge, J.S., Cheel, R.J. and LeClair, S.F.** (2001) Bedforms and associated sedimentary structures formed under supercritical water flows over aggrading sand beds. *Sedimentology*, **48**, 133-152.
- Allen, J.R.L.** (1997) Subfossil mammalian tracks (Flandrian) in the Severn Estuary, S.W. Britain: mechanics of formation, preservation and distribution. *Philosophical Transactions of the Royal Society B*, **352**, 481-518.
- Allen, P.A. and Allen, J.R.** (2013) *Basin Analysis. Principles and Application*. Third Edition. Wiley-Blackwell, Chichester, 619 pp.

- Allen, P.A., Fielding, C.R., Gibling, M.R. and Rygel, M.C.** (2011) Fluvial response to paleo-equatorial climate fluctuations during the late Paleozoic ice age. *Geological Society of America Bulletin*, **123**, 1524-1538.
- Allen, J.P., Fielding, C.R., Gibling, M.R. and Rygel, M.C.** (2014) Recognizing products of palaeoclimate fluctuation in the fluvial stratigraphic record: An example from the Pennsylvanian to Lower Permian of Cape Breton Island, Nova Scotia. *Sedimentology*, **61**, 1332-1381.
- Allgöwer, A.M. and Lignum, J.S.** (2019) Fine-scale variations in distributary mouth-bar morphology in the Middle Triassic Caley Member of the Bedout Sub-basin, Western Australia. In: *Sedimentary Basins of Western Australia V: Proceedings of the Petroleum Exploration Society of Australia Symposium* (Eds. M. Keep and S.J. Moss), pp. 1-23.
- Al-Masrahy, M.A. and Mountney, N.P.** (2015) A classification scheme for fluvial-aeolian system interaction in desert-margin settings. *Aeolian Research*, **17**, 67-88.
- Alonso-Zarza, A.M. and Wright, V.P.** (2010) Palustrine carbonates. In: *Carbonates in Continental Settings: Geochemistry, Diagenesis and Applications* (Eds. A.M. Alonso-Zarza and L.H. Tanner), *Developments in Sedimentology* 61, pp. 103-132. Elsevier, Amsterdam.
- Arenas-Abad, C., Vázquez-Urbez, M., Pardo-Tirapu, G. and Sancho-Marcén, C.** (2010) Fluvial and associated carbonate deposits. In: *Carbonates in Continental Settings: Geochemistry, Diagenesis and Applications* (Eds. A.M. Alonso-Zarza and L.H. Tanner), *Developments in Sedimentology* 61, pp. 133-175. Elsevier, Amsterdam.
- Aurell, M., Mas, R., Meléndez, A. and Salas, R.** (1994) El tránsito Jurásico-Cretácico en la Cordillera Ibérica: relación tectónica-sedimentación y evolución paleogeográfica. *Cuadernos de Geología Ibérica*, **18**, 369-396.
- Bagnold, R.A.** (1971) *The physics of blown sand and desert dunes*. Methuen & Co, London, 265pp.
- Banham, S.G. and Mountney, N.P.** (2014) Climatic versus halokinetic control on sedimentation in a dryland fluvial succession. *Sedimentology*, **61**, 570-608.
- Bállico, M.B., Scherer, C.M.S., Mountney, N.P., Souza, E.G., Peis, A.D., Raja Gabaglia, G.P. and Magalhães, A.J.C.** (2017) Sedimentary cycles in a Mesoproterozoic aeolian erg-margin succession: Mangabeira Formation, Espinhaço Supergroup, Brazil. *Sedimentary Geology*, **349**, 1-14.
- Bayet-Goll, A. and Neto de Carvalho, C.** (2016) Ichnology and sedimentology of a tide-influenced delta in the Ordovician from the northeastern Alborz range of Iran (Kopet Dagh region). *Lethaia*, **49**, 327-350.

- Benito, M.I., Lohmann, K.C. and Mas, R.** (2005) Late Jurassic paleogeography and paleoclimate in the Northern Iberian Basin of Spain: constraints from diagenetic records in reefal and continental carbonates. *Journal of Sedimentary Research*, **75**, 82-96.
- Bhattacharya, J.P.** (2006) Deltas. In: *Facies Models Revisited*. (Eds. H. Posamentier and R.G. Walker), *SEPM Spec. Publ.*, 84, 237-292.
- Bhattacharya, J.P.** (2010) Deltas. In: *Facies Models 4* (Eds. N.P. James and R.W. Dalrymple), pp. 233-264. Geological Association of Canada, Newfoundland.
- Blair, T.C. and McPherson, J.G.** (1999) Grain-size and textural classification of coarse sedimentary particles. *Journal of Sedimentary Research*, **69**, 6-19.
- Bridge, J.S.** (2006) Fluvial facies models: recent developments. In: *Facies Models Revisited*. (Eds. H.W. Posamentier and R.G. Walker), *SEPM Spec. Publ.*, 84, 85-170.
- Bridges, N.T., Spagnuolo, M.G., de Silva, S.L., Zimmerland, J.R. and Neely, E.M.** (2015) Formation of gravel-mantled megaripples on Earth and Mars: Insights from the Argentinean Puna and wind tunnel experiments. *Aeolian Research*, **17**, 49-60.
- Boucot, A.J., Xu, C., Scotese, C.R. and Morley, R.J.** (2013) *Phanerozoic Palaeoclimate: an atlas of lithologic indicators of climate*. Concepts in Sedimentology and Paleontology 11, SEPM, Darlington, 478 pp.
- Bover-Arnal, T. and Salas, R.** (2019) Geology of the 'Senia stone' from Ulldecona, Catalonia (Aptian, Maestrat Basin, Iberian Chain) and its implications for regional stratigraphy. *Cretaceous Research*, **96**, 38-58.
- Browne, G.H. and Plint, G.** (1994) Alternating braidplain and lacustrine deposition in a strike-slip setting: the Pennsylvanian Boss Point Formation of the Cumberland Basin, Maritime Canada. *Journal of Sedimentary Research*, **B64**, 40-59.
- Buatois, L.A. and Mángano, M.G.** (2011) *Ichnology: Organism-substrate interactions in space and time*. Cambridge University Press, New York, 358 pp.
- Bull, W.B.** (2007) *Tectonic Geomorphology of Mountains: A New Approach to Paleoseismology*. Blackwell Publishing, Malden, 316 pp.
- Burne, R.V. and Moore, L.S.** (1987) Microbialites: organosedimentary deposits of benthic microbial communities. *Palaios*, **2**, 241-254.

Burns, C.E., Mountney, N.P., Hodgson, D.M. and Colombera, L. (2017) Anatomy and dimensions of fluvial crevasse-splay deposits: examples from the Cretaceous Mesaverde Group, Utah. *Sedimentary Geology*, **351**, 21-35.

Burns, C.E., Mountney, N.P., Hodgson, D.M. and Colombera, L. (2019) Stratigraphic architecture and hierarchy of fluvial overbank crevasse-splay deposits. *Journal of the Geological Society of London*, **176**, 629-649.

Campos Soto, S. (2020) *Stratigraphy, sedimentology and age of the Kimmeridgian-Tithonian coastal systems of the Se Iberian Basin: implications of the new results on the correlation of units and on Iberian palaeogeography*. Unpublished PhD Thesis. Universidad Complutense de Madrid, Madrid, 342 pp.

Campos-Soto, S., Caus, E., Benito, M. I. and Mas, R. (2015a) Nuevas aportaciones sedimentológicas y cronoestratigráficas sobre las Fms. Higuieruelas y Villar del Arzobispo en Benagéber (NO de Valencia). In: *Abstracts XXXI Jornadas de Paleontología*, pp. 83-85. Baeza, Spain.

Campos-Soto, S., Benito, M. I., Mas, R., Quijada, I. E. and Suarez-Gonzalez, P. (2015b) Between tides, winds and rivers: deciphering challenging sandstone bodies in a multifaceted coastal system (Late Jurassic-Early Cretaceous, South Iberian Basin, SE Spain). In: *Abstracts 9th International Conference on Tidal Sedimentology*, pp. 46-49. Puerto Madryn, Argentina.

Campos-Soto, S., Benito, M. I., Mas, R., Caus, E., Cobos, A., Suarez-Gonzalez, P. and Quijada, I.E. (2016a) Revisiting the Late Jurassic-Early Cretaceous of the NW South Iberian Basin: new ages and sedimentary environments. *Journal of Iberian Geology*, **42**, 69-94.

Campos-Soto, S., Caus, E., Bucur, I.I., Bentio, M.I., Suarez-Gonzalez, P., Quijada, I.E., Fernandez, L. and Mas, R. (2016b) Registro de una transgresión marina en torno al tránsito Jurásico-Cretácico al oeste de la sub-cuenca de Peñagolosa (Teruel). *Geo-Temas*, **16**, 121-124.

Campos-Soto, S., Cobos, A., Caus, E., Benito, M.I., Fernández-Labrador, L., Suarez-Gonzalez, P., Quijada, I.E., Mas, R., Royo-Torres, R. and Alcalá, L. (2017a) Jurassic Coastal Park: A great diversity of palaeoenvironments for the dinosaurs of the Villar del Arzobispo Formation (Teruel, eastern Spain). *Palaeogeography, Palaeoclimatology, Palaeoecology*, **485**, 154-177.

Campos-Soto, S., Benito, M.I., Mountney, N.P., Quijada, I.E., Suarez-Gonzalez, P., Cobos, A. and Mas, R. (2017b) Unveiling coastal aeolian facies in the Upper Jurassic record of eastern Iberia: new insights from the dinosaur fossil-bearing Villar del Arzobispo Fm (Teruel, E Spain). In: *Abstracts 33rd International Meeting of Sedimentology*, pp. 151. Toulouse, France.

- Campos-Soto, S., Benito, M.I., Cobos, A., Caus, E., Quijada, I.E., Suarez-Gonzalez, P., Mas, R., Royo-Torres, R. and Alcalá, L.** (2019) Revisiting the age and palaeoenvironments of the Upper Jurassic-Lower Cretaceous? dinosaur-bearing sedimentary record of eastern Spain: implications for Iberian palaeogeography. *Journal of Iberian Geology*, **45**, 471-510.
- Cain, S.A. and Mountney, N.P.** (2009) Spatial and temporal evolution of a terminal fluvial fan system: the Permian Organ Rock Formation, South-east Utah, USA. *Sedimentology*, **56**, 1774-1800.
- Cain, S.A. and Mountney, N.P.** (2011) Downstream changes and associated fluvial-aeolian interactions in an ancient terminal fluvial fan system: the Permian Organ Rock Formation, SE Utah. In: *From River to Rock Record* (Eds. S. Davidson, S. Leleu and C. North), *SEPM Spec. Publ.*, **97**, 165-187.
- Canérot, J., Cugny, P., Pardo, G., Salas, R. and Villena, J.** (1982) Ibérica Central-Maestrazgo. In: *El Cretácico de España* (Ed. A. García), pp. 273- 344. Universidad Complutense de Madrid, Madrid.
- Caride de Liñán, C.** (1994) Mapa geológico de la península Ibérica, Baleares y Canaerías. Mapa Geológico de España E. 1:1.1.000.000. Edición 1995. IGME, Madrid.
- Carol, E.S., Alvarez, M.P. and Borzi, G.E.** (2016) Assessment of factors enabling halite formation in a marsh in a humid temperate climate (Ajó Marsh, Argentina). *Marine Pollution Bulletin*, **106**, 323-328.
- Cartigny, M.J.B., Ventra, D., Postma, G. and Van den Berg, J.** (2014) Morphodynamics and sedimentary structures of bedforms under supercritical-flow conditions: New insights from flume experiments. *Sedimentology*, **61**, 712-748.
- Casnovas-Cladellas, M.L., Santafé-Llopis, J.V., Santisteban, C. and Pereda-Suberbiola, X.** (1999) Estegosaurios (Dinosauria) del Jurásico Superior-Cretácico Inferior de la Comarca de los Serranos (Valencia, España). *Revista Española de Paleontología*, nºextr. Homenaje al Prof. J. Truyols, 57-63.
- Casnovas-Cladellas, M.L., Santafé-Llopis, J.V. and Sanz, J.L.** (2001) *Losillasaurus giganteus*, un nuevo saurópodo del tránsito Jurásico-Cretácico de la cuenca de “Los Serranos” (Valencia, España). *Paleontología i Evolució*, **32-33**, 99-122.
- Chakraborty, T.** (1991) Sedimentology of a Proterozoic erg: the Venkatpur Sandstone, Pranhita-Godavari Valley, south India. *Sedimentology*, **38**, 301-332.
- Clemmensen, L.B.** (1988) Aeolian morphology preserved by lava cover, the Precambrian Mussartut Member, Eriksfjord Formation, South Greenland. *Bulletin of the Geological Society of Denmark*, **37**, 105-116.

- Cobos, A., Royo-Torres, R., Luque, L., Alcalá, L. and Mampel, L.** (2010) An Iberian stegosaurus paradise: the Villar del Arzobispo Formation (Tithonian-Berriasian) in Teruel (Spain). *Palaeogeography, Palaeoclimatology, Palaeoecology*, **293**, 223-236.
- Cobos, A., Gascó, F., Royo-Torres, R. and Lockley, M.G.** (2016) Dinosaur Tracks as “Four-Dimensional Phenomena” Reveal How Different Species Moved. In: *Dinosaur Tracks: The Next Steps* (Eds. P.L. Falkingham, D. Marty, D. and A. Richter), pp. 244-256. Indiana University Press, Bloomington.
- Cobos, A., Alcalá, L. and Royo-Torres, R.** (2020) The Dinosaur Route in El Castellar (Teruel, Spain): Palaeontology as a factor of territorial development and scientific education in a sparsely inhabited area. *Geoheritage*, **12**, 52.
- Coleman, J.M.** (1969) Brahmaputra river: Channel processes and sedimentation. *Sedimentary Geology*, **3**, 129-239.
- Collinson, J.D.** (1996) Alluvial sediments. In: *Sedimentary Environments. Processes, Facies and Stratigraphy* (Ed. H.G. Reading), 3rd edn, pp. 37-82. Blackwell Science, Oxford.
- Company, J., Pereda-Suberbiola, X. and Ruiz-Omeñaca, J.I.** (2010) New stegosaurian (Ornithischia, Thyreophora) remains from Jurassic-Cretaceous transition beds of Valencia province (Southwestern Iberian Range, Spain). *Journal of Iberian Geology*, **36**, 243-252.
- Cooper, W. S.** (1958) *Coastal sand dunes of Oregon and Washington*. Geological Society of America Memoir 72, 169 pp.
- Coram, R.A., Radley, J.D. and Martill, D.M.** (2017) A Cretaceous calamity? The Hypsilophodon Bed of the Isle of Wight, southern England. *Geology Today*, **33**, 66-70.
- Costa, J.E.** (1988) Rheologic, geomorphic, and sedimentologic differentiation of water floods, hyperconcentrated flows, and debris flows. In: *Flood Geomorphology* (Eds. V.R. Baker, R.C. Kochel and P.C. Patton), pp. 113-122. Wiley, New York.
- de Wit, M.C.J.** (1999) Post-Gondwana drainage and the Development of Diamond Placers in Western South Africa. *Economic Geology*, **94**, 721-740.
- DeCelles, P.G., Gray, M.B., Ridgway, K.D., Cole, R.B., Pivnik, D.A., Pequer, A.N. and Srivastava, P.** (1991) Controls on synorogenic alluvial-fan architecture, Beartooth Conglomerate (Palaeocene), Wyoming and Montana. *Sedimentology*, **38**, 567-590.
- Deluca, J.L. and Eriksson, K.A.** (1989) Controls on synchronous ephemeral- and perennial-river sedimentation in the middle sandstone member of the Triassic Chinle Formation, northeastern New Mexico, U.S.A. *Sedimentary Geology*, **61**, 155-175.

- Delvene, G. Munt, M., Royo-Torres, R., Cobos, A. and Alcalá, L.** (2013) Late Jurassic-Early Cretaceous freshwater bivalves from Turiasaurus riodevensis bearing strata of Teruel (Spain). *Spanish Journal of Palaeontology*, **28**, 161-172.
- Diéguez, C., Peyrot, D. and Barrón, E.** (2010) Floristic and vegetational changes in the Iberian Peninsula during Jurassic and Cretaceous. *Review of Palaeobotany and Palynology*, **162**, 325-340.
- Díez-Canseco, D., Arz, J.A., Benito, M.I., Díaz-Molina M. and Arenillas, I.** (2014): Tidal influence in redbeds: A palaeoenvironmental and biochronostratigraphic reconstruction of the Lower Tresp Formation (South-Central Pyrenees, Spain) around the Cretaceous/Paleogene boundary. *Sedimentary Geology*, **312**, 31-49.
- Díez-Canseco, D., Buatois, L.A., Mángano, M.G., Díaz-Molina, M. and Benito, M.I.** (2016) Ichnofauna from coastal meandering channel systems (Upper Cretaceous Tresp Formation, South-Central Pyrenees, Spain): delineating the fluvial-tidal transition. *Journal of Paleontology*, **90**, 250-268.
- dos Santos, J.H.S and dos Santos, N.F.B.** (2015) The Lençóis Maranhenses: A Paradise of Dunes and Ponds. In: *Landscapes and Landforms of Brazil* (Eds. B.C. Vieira, A.A.R. Salgado and L.J.C. Santos), pp. 79-90. Springer, Dordrecht.
- Due, T.W. and Dott, H.** (1980) Genetic significance of deformed cross-bedding with examples from the Navajo and Webber Sandstones of Utah. *Journal of Sedimentary Petrology*, **50**, 793-812.
- DuMars, A.J.** (2002) *Distributary mouth bar formation and channel bifurcation in the Wax Lake Delta, Atchafalaya Bay, Louisiana*. LSU Master's Thesis, Louisiana State University, 88 pp.
- Dunham, R.J.** (1962) Classification of carbonate rocks according to depositional texture. In: *Classification of Carbonate Rocks* (Ed. W.E. Ham), *AAPG Mem.*, **1**, 108- 121.
- Ekdale, A.A., Bromley, R.G. and Loope, D.B.** (2007) Ichnofacies of an Ancient Erg: A Climatically Influenced Trace Fossil Association in the Jurassic Navajo Sandstone, Southern Utah, USA. In: *Trace Fossils: Concepts, Problems, Prospects* (Ed. W. Miller), pp. 562-574. Elsevier, Amsterdam.
- Enge, H.D., Howell, J.A. and Buckley, S.J.** (2010a) Quantifying clinofacet geometry in a forced-regressive riverdominated delta, Panther Tongue Member, Utah, USA. *Sedimentology*, **57**, 1750-1770.
- Enge, H.D., Howell, J.A. and Buckley, S.J.** (2010b) The geometry and internal architecture of stream mouth bars in the Panther Tongue and the Ferron Sandstone Members, Utah, U.S.A. *Journal of Sedimentary Research*, **80**, 1018-1031.
- Farrel, K.M.** (1987) Sedimentology and facies architecture of overbank deposits of the Mississippi River, False River Region, Louisiana. In: *Recent Developments in Fluvial Sedimentology* 39 (Eds. F.G.

Ethridge, R.M. Flores and M.D. Harvey), pp. 111-120. Society of Economic Paleontologists and Mineralogists, Tulsa.

Fernández-Labrador, L. (2016) *Estratigrafía y sedimentología de la Formación El Castellar en el oeste de la sub-cuenca de Penyalgosa (Cretácico Inferior, Cuenca del Maestrazgo, Teruel)*. Unpublished Master's Thesis, Universidad Complutense de Madrid, 50 pp.

Fielding, C.R. (2006) Upper flow regime sheets, lenses and scour fills: extending the range of architectural elements for fluvial sediment bodies. *Sedimentary Geology*, **190**, 227-240.

Fielding, C.R. and **Alexander, J.** (1996) Sedimentology of the Upper Burdekin River of North Queensland, Australia-an example of a tropical, variable discharge river. *Terra Nova*, **8**, 447-457.

Fielding, C.R., Alexander, J. and **Newman-Sutherland, E.** (1997) Preservation of in situ, arborescent vegetation and fluvial bar construction in the Burdekin River of north Queensland, Australia. *Palaeogeography, Palaeoclimatology, Palaeoecology*, **135**, 123-144.

Fielding, C.R., Trueman, J.J. and **Alexander, J.** (2006) Holocene depositional history of the Burdekin River Delta of northeastern Australia: a model for a low-accommodation, highstand delta. *Journal of Sedimentary Research*, **76**, 411-428.

Fielding, C.R., Allen, J.P., Alexander, J. and **Gibling, M.R.** (2009) A facies model for fluvial systems in the seasonal tropics and subtropics. *Geology*, **37**, 623-626.

Fielding, C.R., Allen, J.P., Alexander, J., Gibling, M.R., Rygel, M.C. and **Calder, H.H.** (2011) Fluvial Systems and Their Deposits in Hot, Seasonal Semiarid and Subhumid Settings: Modern and Ancient Examples. In: *From River to Rock Record. The Preservation of Fluvial Sediments and Their Subsequent Interpretation* (Eds. S.K. Davidson, S. Leleu and C.P. North), *SEPM Spec. Publ.*, **97**, 89-112.

Fielding, C.R., Alexander, J. and **Allen, J.P.** (2018) The role of discharge variability in the formation and preservation of alluvial sediment bodies. *Sedimentary Geology*, **365**, 1-20.

Folk, R.L. (1968) *Petrology of sedimentary rocks*. Hemphill Publishing Company, Austin, 182 pp.

Freytet, P. and **Plaziat, J.C.** (1982) *Continental Carbonate Sedimentation and Pedogenesis: Late Cretaceous and Early Tertiary of Southern France*. Contributions to Sedimentology 12. E. Schweizerbart'sche Verlagsbuchhandlung (Nägele u. Obermiller), Stuttgart, 213 pp.

Fryberger, S.G. and **Dean, G.** (1979) Dune forms and wind regime. In: *A Study of Global Sand Seas* (Ed. E.D. McKee, E.D.), Geological Survey Professional Paper 1052, pp. 137-170. U.S. Government Printing Office, Washington.

- Fryberger, S.G. and Schenk, C.J.** (1988) Pin stripe lamination: a distinctive feature of modern and ancient eolian sediments. *Sedimentary Geology*, **55**, 1-15.
- Fryberger, S.G., Krystinik, L.F. and Schenk, C.J.** (1990) Tidally flooded back-barrier dunefield, Guerrero Negro area, Baja California, Mexico. *Sedimentology*, **37**, 23-43.
- Galán-Abellán, B., López-Gómez, J., Barrenechea, J.F., Marzo, M., de la Horra, R. and Arche, R.** (2013) The beginning of the Buntsandstein cycle (Early–Middle Triassic) in the Catalan Ranges, NE Spain: Sedimentary and palaeogeographic implications. *Sedimentary Geology*, **296**, 86-102.
- García-García, F., Fernández, J., Viseras, C. and Soria, J.M.** (2006) High frequency cyclicity in a vertical alternation of Gilbert-type deltas and carbonate bioconstructions in late the Tortonian, Tabernas Basin, Southern Spain. *Sedimentary Geology*, **192**, 123-139
- García-Hidalgo, J.F., Temiño, J. and Segura, M.** (2002) Holocene eolian sediments on the southern border of the Duero Basin (Spain): origin and development of an eolian system in a temperate zone. *Journal of Sedimentary Research*, **72**, 30-39.
- Gatesy, S.M.** (2001) Skin impressions of Triassic theropods as records of foot movement. *Bulletin of the Museum of Comparative Zoology*, **156**, 137-149.
- Gerety, K.M. and Slingerland, R.** (1982) Nature of the saltating population in wind tunnel experiments with heterogeneous size-density sands. In: *Eolian sediments and processes* (Eds. M.E. Brookfield and T.S. Ahlbrandt), *Developments in Sedimentology*, **38**, 115-132.
- Gibbs, M.T., Rees, P.M., Kutzbach, J.E., Ziegler, A.M., Behling, P.J. and Rowley, D.B.** (2002) Simulations of Permian Climate and Comparisons with Climate-Sensitive Sediments. *The Journal of Geology*, **110**, 33-55.
- Gibling, M.R. and Tandon, S.K.** (1997) Erosional marks on consolidated banks and slump blocks in the Rupen River, north-west India. *Sedimentology*, **44**, 339-348.
- Gillies, J.A., Nickling, W.G., Tilson, M. and Furtak-Cole, E.** (2012) Wind-formed gravel bed forms, Wright Valley, Antarctica. *Journal of Geophysical Research*, **117**, F04017.
- Glennie, K.W.** (1970) *Desert Sedimentary Environments*. Elsevier, Amsterdam, 222 pp.
- Gómez, J.J.** (1979) *El Jurásico en facies carbonatadas del sector levantino de la Cordillera Ibérica*. Seminarios de Estratigrafía, Serie Monografías 4, 683 pp.
- Gómez, J.J. and Goy, J.A.** (1979) Las unidades litoestratigráficas del Jurásico medio y superior, en facies carbonatadas del sector levantino de la Cordillera Ibérica. *Estudios Geológicos*, **35**, 569-598.

Gonçalves, R.A., de Oliveira Lehugeur, L.G., de Alencar Castro, J.W. and Pedroto, A.E.S. (2003)

Classificação das feições eólicas dos Lençóis Maranhenses-Maranhão-Brasil. *Mercator*, **3**, 99-112.

González Riga, B.J. and Astini, R.A. (2007) Preservation of large titanosaur sauropods in overbank fluvial facies: A case study in the Cretaceous of Argentina. *Journal of South American Earth Sciences*, **23**, 290-303.

Gradziński, R., Gagol, J. and Slaczka, A. (1979) The Tumlin Sandstone (Holy Cross Mts, Central Poland): Lower Triassic deposits of aeolian dunes and interdune areas. *Acta Geologica Polonica*, **29**, 151-175.

Gugliotta, M., Flint, S.S., Hodgson, D.M. and Veiga, G.D. (2015) Stratigraphic record of river-dominated crevasse subdeltas with tidal influence (Lajas Formation, Argentina). *Journal of Sedimentary Research*, **85**, 265-284.

Gugliotta, M., Kurcinka, C.E., Dalrymple, R.W. Flint, S. and Hodgson, D.M. (2016) Decoupling seasonal fluctuations in fluvial discharge from the tidal signature in ancient deltaic deposits: an example from the Neuquén Basin, Argentina. *Journal of the Geological Society*, **173**, 94-107.

Hallam, A. (1984) Continental humid and arid zones during the Jurassic and Cretaceous. *Palaeogeography, Palaeoclimatology, Palaeoecology*, **47**, 195-223.

Hallam, A., Crame, J.A., Macenido, M.O., Francis, J. and Parrish, J.T. (1993) Jurassic Climates as Inferred from the Sedimentary and Fossil Record. *Philosophical Transactions of the Royal Society of London, Series B*, 341, 287-296.

Hammer, Ø., Harper, D.A.T. and Ryan, P.D. (2001) Past: Paleontological Statistics Software Package for Education and Data Analysis. *Palaeontologia electrónica*, **4**, 1-9.

Hernández, A., Godoy, A., Álvaro, M., Ramírez, J.I., Leal, M. C., Aguilar, M., Anadón, P., Moissenet, E., Meléndez, A., Gómez, J.J., Martín, J.M., García, J.C., Aramburu, C., Ortí, F. and Solé, N. (1985) Memoria de la Hoja nº 47 (Teruel), Mapa geológico de España E. 1:20.0000 (MAGNA). Primera edición. Madrid, I.G.M.E.

Herries, R.D. (1992) *Sedimentology of continental erg-margin interactions*. PhD Thesis. University of Aberdeen, Aberdeen, 228 pp.

Hinds, D.J., Aliyeva, E., Allen, M.B., Davies, C.E., Kroonenberg, S.B., Simmons, M.D. and Vincent, S.J. (2004) Sedimentation in a discharge dominated fluvial-lacustrine system: the Neogene Productive Series of the South Caspian Basin, Azerbaijan. *Marine and Petroleum Geology*, **21**, 613-638.

Holz, M. and Scherer, C.M.S. (2000) Sedimentological and paleontological evidence of paleoclimatic change during the Southbrazilian Triassic: the register of a global trend towards a humid paleoclimate. *Zentralblatt für Geologie und Paläontologie*, **11-12**, 1589-1609.

Hunter, R.E. (1977) Basic types of stratification in small eolian dunes. *Sedimentology*, **24**, 361-387.

Hunter, R.E., Richmond, B.M., and Alpha, T.R. (1983) Storm-controlled oblique dunes of the Oregon Coast. *Geological Society of America*, **94**, 1450-1465.

Ielpi, A. (2017) Lateral accretion of modern unvegetated rivers: remotely sensed fluvial-aeolian morphodynamics and perspectives on the Precambrian rock record. *Geological Magazine*, **154**, 609-624.

Iversen, J.D. (1982) Saltation threshold and deposition rate modelling. In: *Eolian sediments and processes* (Eds. M.E. Brookfield and T.S. Ahlbrandt), *Developments in Sedimentology*, **38**, 103-114.

Jones, B.G. (1972) Deformation structures in siltstone resulting from the migration of an Upper Devonian aeolian dune. *Journal of Sedimentary Petrology*, **42**, 935-940.

Jordan, O.D. and Mountney, N.P. (2010) Styles of interaction between aeolian, fluvial and shallow marine environments in the Pennsylvanian to Permian lower Cutler beds, south-east Utah, USA. *Sedimentology*, **57**, 1357-1385.

Jordan, O.D. and Mountney, N.P. (2012) Sequence stratigraphic evolution and cyclicity of an ancient coastal desert system: The Pennsylvanian-Permian lower Cutler beds, Paradox Basin, Utah, U.S.A. *Journal of Sedimentary Research*, **82**, 755-780.

Kiersch, G.A. (1950) Small-scale structures and other features of Navajo Sandstone, northern part of San Rafael Swell, Utah. *Bulletin of the American Association of Petroleum Geologists*, **34**, 923-942.

Kocurek, G. (1981) Significance of interdunes deposits and bounding surfaces in aeolian dune sands. *Sedimentology*, **28**, 753-780.

Kocurek, G. (1991) Interpretation of ancient eolian sand dunes. *Annual Review of Earth and Planetary Sciences*, **19**, 43-75.

Kocurek, G.A. (1996) Desert aeolian system. In: *Sedimentary Environments. Processes, Facies and Stratigraphy* (Ed. H.G. Reading), 3rd edn, pp. 125-153. Blackwell Science, Oxford.

Kocurek, G. and Dott, R.H. (1981) Distinctions and uses of stratification types in the interpretation of eolian sand. *Journal of Sedimentary Petrology*, **51**, 579-595.

Kocurek, G. and Havholm, K.G. (1993) Eolian sequence stratigraphy-a conceptual framework. In:

Siciliclastic Sequence Stratigraphy (Eds. P. Weimer and H.W. Posamentier), *American Association of Petroleum Geologists*, Memoir 58, 393–409.

Kocurek, G., Westerman, R., Hern, C., Tatum, D., Rajapara, H.M. and Singhvi, A.K. (2020) Aeolian

dune accommodation space for Holocene Wadi Channel Avulsion Strata, Wahiba Dune Field, Oman.

Sedimentary Geology, **399**, 105612.

Kurcinka, C., Dalrymple, R.W. and Gugliotta, M. (2018) Facies and architecture of river-dominated to

tide-influenced mouth bars in the lower Lajas Formation (Jurassic), Argentina. *AAPG Bulletin*, **102**,

885-912.

Lang, J., Sievers, J., Loewe, M., Igel, J. and Winsemann, J. (2017) 3D architecture of cyclic-step and

antidune deposits in glacial subaqueous fan and delta settings: Integrating outcrop and ground-

penetrating radar data. *Sedimentary Geology*, **362**, 83-100.

Langford, R.P. (1989) Fluvial-aeolian interactions: Part I, modern systems. *Sedimentology*, **36**, 1023-1035.

Langford, R.P. and Chan, M.A. (1989) Fluvial-aeolian interactions: Part II, ancient systems.

Sedimentology, **36**, 1037-1051.

Legler, B., Johnson, H.D., Hampson, G.J., Massart, B.Y.G., Jackson, C.A.L., Jackson, M.D., El-

Barkooky, A. and Ravnas, R. (2013) Facies model of a fine-grained, tide-dominated delta: Lower Dir

Abu Lifa Member (Eocene), Western Desert, Egypt. *Sedimentology*, **60**, 1313-1356.

Li, S., Yu, X., Li, S., Olariu, C. and Steel, R. (2013) Relationship between River-mouth Depositional

Processes and Delta Architectures, Huangqihai Lake, Inner Mongolia, North China. *AAPG Search and*

Discovery, 50832

Liu, B. and Coulthard, T.J. (2015) Mapping the interactions between rivers and sand dunes: Implications

for fluvial and aeolian geomorphology. *Geomorphology*, **231**, 246-257.

Loope, D.B. (1988) Rhizoliths in ancient eolianites. *Sedimentary Geology*, **56**, 301-314.

Loope, D.B., Rowe, C.M. and Joecke, R.M. (2001) Annual monsoon rains recorded by Jurassic dunes.

Nature, **412**, 64-66.

[dataset] **López Olmedo, F., Palacio Suárez, J.P., Dávila Ruiz, M.D.T., Luís López, F., García Rojo,**

E., Martínez Cano, M., Pérez-Ruiz, J., García-Brazales Gómez, R. and Monzón-Lara, O. (2018)

Mapa Geológico Digital Continuo E. 1:50.000, Zona Ibérica (Zona-1700). GEODE. Mapa Geológico

Digital Continuo de España, <http://info.igme.es/cartografiadigital/geologica/geodezona.aspx?Id=Z1700>. Accessed Feb. 2020.

Luque, L., Cobos, A., Royo-Torres, R., Espílez, E. and Alcalá, L. (2005) Caracterización de los depósitos sedimentarios con dinosaurios de Riodeva (Teruel). *Geogaceta*, **38**, 27-30.

Mader, D. (1981) Genesis of the Buntsandstein (Lower Triassic) in the western Eifel (Germany). *Sedimentary Geology*, **29**, 1-30.

Marsaglia, K.M. and Klein, G.D. (1983) The paleogeography of Paleozoic and Mesozoic storm depositional systems. *The Journal of Geology*, **91**, 117-142.

Martín-Chivelet, J., López-Gómez, J., Aguado, R., Arias, C., Arribas, J., Arribas, M.E., Aurell, M., Bádenas, M., Benito, M.I., Bover-Arnal, T., Casas-Sainz, A., Castro, J.M., Coruña, F., de Gea, G.A., Fornós, J.J., Fregenal-Martínez, M., García-Senz, J., Garófano, D., Gelabert, B., Giménez, J., González-Acebrón, L., Guimerà, J., Liesa, C.L., Mas, R., Meléndez, N., Molina, J.M., Muñoz, J.A., Navarrete, R., Nebot, M., Nieto, L.M., Omodeo-Salé, S., Pedrera, A., Carlos Peropadre, C., Quijada, I.E., Quijano, M.L., Reolid, M., Robador, A., Rodríguez-López, J.P., Rodríguez-Perea, A., Rosales, I., Ruiz-Ortiz, P.A., Sàbat, F., Salas, R., Soria, A.R., Suarez-Gonzalez, P. and Vilas, L. (2019) The Late Jurassic–Early Cretaceous Rifting. In: *The Geology of Iberia: A Geodynamic Approach. Volume 5: The Alpine Cycle*. (Eds. C. Quesada and J.T. Oliveira), pp. 169-249. Springer, Heidelberg.

Marty, D., Strasser, A. and Meyer, C.A. (2009) Formation and taphonomy of human footprints in microbial mats of present-day tidal-flat environments: implications for the study of fossil footprints. *Ichnos*, **16**, 127-142.

Mas, R. and Alonso, A. (1981) *Trabajo estratigráfico, sedimentológico y paleogeográfico de las facies Purbeck, Weald y Utrillas en el sector suroriental de la Cordillera Ibérica*. Memorias de las Hojas nº 55 (Lliria) y 43 (Valencia). Mapa Geológico de España E. 1:200.000 (MAGNA). Segunda serie. IGME, Madrid (Unpublished), 58 pp.

Mas, R., Alonso, A. and Meléndez, N. (1984) La Formación Villar del Arzobispo: un ejemplo de llanuras de mareas siliciclásticas asociadas a plataformas carbonatadas. Jurásico terminal. (NW de Valencia y E de Cuenca). *Publicaciones de Geología*, **20**, 175-188.

Mas, R., García, A., Salas, R., Meléndez, A., Alonso, A., Aurell, M., Bádenas, B., Benito, M.I., Carenas, B., García-Hidalgo, J.F., Gil, J. and Segura, M. (2004) Segunda fase de rifting: Jurásico Superior-Cretácico Inferior. In: *Geología de España* (Ed. J.A.), pp. 503-510. SGE-IGME, Madrid.

- Massari, F.** (1996) Upper-flow-regime stratification types on steep-face, coarse-grained, Gilbert-type progradational wedges (Pleistocene, Southern Italy). *Journal of Sedimentary Research*, **66**, 364-375.
- McCauley, M.P. and Sturman, A.P.** (1999) A Study of Orographic Blocking and Barrier Wind Development Upstream of the Southern Alps, New Zealand. *Meteorology and Atmospheric Physics*, **70**, 121-131.
- McKee, E.D.** (1966) Structures of dunes at White Sands National Monument, New Mexico (and a comparison with structures of dunes from other selected areas). *Sedimentology*, **7**, 1-69.
- McKee, E.D.** (1979) Ancient sandstones considered to be eolian. In: *A Study of Global Sand Seas*. (Ed. E.D. McKee), Geological Survey Professional Paper 1052, pp. 187-241. U.S. Government Printing Office, Washington.
- McKee, E.D., Douglass, J.R. and Rittenhouse, S.** (1971) Deformation of lee-side laminae in eolian dunes. *Geological Society of America Bulletin*, **32**, 359-378.
- McKie, T.** (2011) Architecture and behavior of dryland fluvial reservoirs, Triassic Skagerrak Formation, Central North Sea. In: *From River to Rock Record. The Preservation of Fluvial Sediments and Their Subsequent Interpretation* (Eds. S.K. Davidson, S. Leleu and C.P. North), *SEPM Spec. Publ.*, **97**, 189-214.
- Meléndez, A., Pardo, G., Pendón, J.G. and Villena, J.** (1979) Las facies terminales del Jurásico en el sector central de la Cordillera Ibérica. *Cuadernos de Geología*, **10**, 137-148.
- Miall, A.D.** (1996) *The Geology of Fluvial Deposits. Sedimentary Facies, Basin Analysis, and Petroleum Geology*. Springer, Berlin, 524 pp.
- Miall, A.D.** (2010) *The Geology of Stratigraphic Sequences*. Second Edition. Springer-Verlag, Berlin, 522pp.
- Mountney, N.P.** (2006) Aeolian Facies Models. In: *Facies Models Revisited* (Eds. H. Posamentier and R.G. Walker), *SEPM Spec. Publ.*, **84**, 19-83.
- Mountney, N.P. and Jagger, A.** (2004) Stratigraphic evolution of an aeolian erg margin system: the Permian Cedar Mesa Sandstone, SE Utah, USA. *Sedimentology*, **51**, 713-743.
- Mountney, N.P. and Russell, A.J.** (2006) Coastal aeolian dune development, Sólheimasandur, southern Iceland. *Sedimentary Geology*, **192**, 167-181.
- Mountney, N.P. and Russell, A.J.** (2009) Aeolian dune-field development in a water table-controlled system: Skeidarársandur, Southern Iceland. *Sedimentology*, **56**, 2107-2131.

Mountney, N.P. and Thompson, D.B. (2002) Stratigraphic evolution and preservation of aeolian dune and damp/wet interdune strata: an example from the Triassic Helsby Sandstone Formation, Cheshire Basin, UK. *Sedimentology*, **49**, 805-833.

Mountney, N.P., Howell, J. Flint, S. and Jerram, D. (1998) Aeolian and alluvial deposition within the Mesozoic Etjo Sandstone Formation, northwest Namibia. *Journal of African Earth Sciences*, **27**, 175-192.

Mountney, N.P., Howell, J. Flint, S. and Jerram, D. (1999) Climate, sediment supply and tectonics as controls on the deposition and preservation of the aeolian-fluvial Etjo Sandstone Formation, Namibia. *Journal of the Geological Society*, **156**, 771-777.

Muto, T., Yamagishi, C., Sekiguchi, T., Yokokawa, M. and Parker, G. (2012) The hydraulic autogenesis of distinct cyclicity in delta foreset bedding: flume experiments. *Journal of Sedimentary Research*, **82**, 545-558.

Mutti, E., Davoli, G., Tinterri, R. and Zavala, R. (1996) The Importance of Ancient Fluvio-Deltaic Systems Dominated by Catastrophic Flooding in Tectonically Active Basins. *Memorie di Scienze Geologiche*, **8**, 233-291.

Myers, T.S., Tabor, N.J., Jacobs, L.L. and Mateus, O. (2012) Palaeoclimate of the Late Jurassic of Portugal: comparison with the Western United States. *Sedimentology*, **59**, 1695-1717.

Neiman, P.J., Sukovich, E.M., Raff, F.M. and Hughes, M. (2010) A Seven-Year Wind Profiler-Based Climatology of the Windward Barrier Jet along California's Northern Sierra Nevada. *Monthly Weather Review*, **138**, 1206-1233.

North, C.P. and Taylor, K.S. (1996) Ephemeral-fluvial deposits: integrated outcrop and simulation studies reveal complexity. *AAPG Bulletin*, **80**, 811-830.

O'Connor, W.P., Bromwich, D.H. and Carrasco, J.F. (1994) Cyclonically Forced Barrier Winds along the Transantarctic Mountains near Ross Island. *Monthly Weather Review*, **122**, 137-150.

Olariu, C. and Bhattacharya, J.P. (2006) Terminal distributary channels and delta front architecture of river-dominated delta systems. *Journal of Sedimentary Research*, **76**, 212-233.

Ono, K., Plink-Björklund, P., Eggenhuisen, J.T. and Cartigny, M.J.B. (2020) Froude supercritical flow processes and sedimentary structures: New insights from experiments with a wide range of grain sizes. *Sedimentology*, (in press). DOI: 10.1111/sed.12682

Pacios, D., Campos-Soto, S., Suarez-Gonzalez, P., Benito, M.I., Cobos, A. and Caus, E. (2018)

Revisión cartográfica y estratigráfica del Jurásico Superior-Cretácico Inferior de Vilel (Teruel). *Geogaceta*, **63**, 19-22.

Parteli, E.J.R., Schwämmle, V., Herrmann, H.J., Monteiro, L.H.U. and Maia, L.P. (2006) Profile

measurement and simulation of a transverse dune field in the Lençóis Maranhenses. *Geomorphology*, **81**, 29-42.

Pérez-García, A., Royo-Torres, R. and Cobos, A. (2014) A new European Late Jurassic pleurosternid

(Testudines, Paracryptodira) and a new hypothesis of paracryptodiran phylogeny. *Journal of Systematic Palaeontology*, **13**, 351-369.

Peterson, C.D., Stock, E., Price, D.M., Hart, R., Reckendorf, F., Erlandson, J.M. and Hostetler, S.W.

(2007) Ages, distributions, and origins of upland coastal dune sheets in Oregon, USA. *Geomorphology*, **91**, 80-102

Picard, M.D. and High, L.R. (1973) *Sedimentary Structures of Ephemeral Streams*. Developments in

Sedimentology 17. Elsevier, Amsterdam, 223 pp.

Pierson, T.C. (2005) Hyperconcentrated flow: transitional process between water flow and debris flow. In:

Debris-Flow Hazards and Related Phenomena (Eds. M. Jakob and O. Hungr), pp. 159-202. Springer, Berlin.

Plink-Björklund, P. (2015) Morphodynamics of rivers strongly affected by monsoon precipitation:

Review of depositional style and forcing factors. *Sedimentary Geology*, **323**, 110-147.

Powers, M.C. (1953) A new roundness scale for sedimentary particles. *Journal of Sedimentary Petrology*,

23, 117-129.

Priddy, C.L. and Clarke, S.M. (2020) The sedimentology of an ephemeral fluvial-aeolian succession.

Sedimentology, **67**, 2392-2425.

Prothero, D. and Schwab, F. (1996) *Sedimentary geology: an introduction to sedimentary rocks and*

stratigraphy. Freeman cop, New York, 575 pp.

Pulvertaft, T.C.R. (1985) Aeolian dune and wet interdunes sedimentation in the Middle Proterozoic Dala

Sandstone, Sweden. *Sedimentary Geology*, **44**, 93-111.

Rees, P.M., Ziegler, A.M. and Valdes, P.J. (2000) Jurassic phytogeography and climates: new data and

model comparisons. In: *Warm climates in Earth History* (Eds. B.T. Huber, K.G. MacLeod and S.L. Wing), pp. 297-318. Cambridge University Press, Cambridge.

- Rees, P.M., Noto, C.R., Parrish, J.M. and Parrish, J.T.** (2004) Late Jurassic Climates, Vegetation, and Dinosaur Distributions. *The Journal of Geology*, **112**, 643-653.
- Riding, R.** (1999) The term stromatolite: towards an essential definition. *Lethaia*, **32**, 321-330.
- Riding, R.** (2000) Microbial carbonates: the geological record of calcified bacterial-algal mats and biofilms. *Sedimentology*, **47**, 179-214.
- Roberts, H.H.** (1998) Delta Switching: Early Responses to the Atchafalaya River Diversion. *Journal of Coastal Research*, **14**, 882-899.
- Roberts, H.R. and Sydow, J.** (2010) Late Quaternary stratigraphy and sedimentology of the offshore Mahakam Delta, east Kalimantan (Indonesia). In: *Tropical deltas of southeast Asia- Sedimentology, Stratigraphy, and Petroleum Geology* (Eds. F. Haasn Sidi, D. Nummedal, P. Imbert, H. Darman and H.W. Posamentier), *SEPM Spec.Publ.*, **76**, 125-145.
- Rodríguez-López, J.P., Meléndez, N., De Boer, P.L. and Soria, A.R.** (2008) Aeolian sand sea development along the mid-Cretaceous western Tethyan margin (Spain): erg sedimentology and palaeoclimate implications. *Sedimentology*, **55**, 1253-1292.
- Rodríguez-López, J.P., Meléndez, N., De Boer, P.L. and Soria, A.R.** (2010) The action of wind and water in a mid-Cretaceous subtropical erg-margin system close to the Variscan Iberian Massif, Spain. *Sedimentology*, **57**, 1315-1356.
- Rodríguez-López, J.P., Meléndez, N., De Boer, P.L. and Soria, A.R.** (2012) Controls on marine-erg margin cycle variability: aeolian-marine interaction in the mid-Cretaceous Iberian Desert System, Spain. *Sedimentology*, **59**, 466-501.
- Rodríguez-López, J.P., Meléndez, N., De Boer, P.L., Soria, A.R. and Liesa, C.L.** (2013) Spatial variability of multi-controlled aeolian supersurfaces in central-erg and marine-erg-margin systems. *Aeolian Research*, **11**, 141-154.
- Rodríguez-López, J.P., Clemmensen, L.B., Lancaster, N., Mountney, N.P. and Veiga, G.D.** (2014) Archean to Recent aeolian sand systems and their sedimentary record: Current understanding and future prospects. *Sedimentology*, **61**, 1487-1534.
- Royo-Torres, R., Cobos, A. and Alcalá, L.** (2006) A Giant European Dinosaur and a New Sauropod Clade. *Science*, **314**, 1925-1927.
- Royo-Torres, R., Cobos, A., Luque, L., Aberasturi, A., Espílez, E., Fierro, I., González, A., Mampel, L. and Alcalá, L.** (2009) High European sauropod dinosaur diversity during Jurassic-Cretaceous transition in Riodeva (Teruel, Spain). *Palaeontology*, **52**, 1009-1027.

Royo-Torres, R., Cobos, A., Mocho, P. and Alcalá, L. (2020) Origin and evolution of turiasaur dinosaurs set by means of a new “rosetta” specimen from Spain. *Zoological Journal of the Linnean Society*, **zlaa091**, 1-27.

Rubin, D.M. (1987) *Cross-bedding, bedforms and Paleocurrents*. SEPM Concepts in Sedimentology and Paleontology 1, Tulsa, 187 pp.

Rubin, D.M. and Hunter, R.E. (1982) Bedform climbing in theory and nature. *Sedimentology*, **29**, 121-138.

Sakamoto-Arnold, C.M. (1981) Eolian features produced by the December 1977 windstorm, southern San Joaquin Valley, California. *Journal of Geology*, **89**, 129-137.

Salas, R. (1987) *El Malm i el Cretaci inferior entre el Massís de Garrafi i la Serra D'Espada. Anàlisi de conca*. PhD Thesis. Universidad de Barcelona, Barcelona, 345 pp.

Salas, R. and Guimerà, J. (1996) Rasgos estructurales principales de la cuenca cretácica inferior del Maestrazgo (Cordillera Ibérica oriental). *Geogaceta*, **20**, 1704-1706.

Salas, R. and Guimerà, J. (1997) Estructura y estratigrafía secuencial de la cuenca del Maestrazgo durante la etapa de rift jurásica superior-cretácica inferior (Cordillera Ibérica oriental). *Boletín Geológico y Minero*, **108**, 393-402.

Salas, R., Guimerà, J., Mas, R., Martín-Closas, C., Meléndez, A. and Alonso, A. (2001) Evolution of the Mesozoic Central Iberian Rift System and its Cainozoic inversion (Iberian Chain). In: *Peri-Tethys Memoir 6: Peri- Tethyan Rift/Wrench Basins and Passive Margins* (Eds. P.A. Ziegler, W. Cavazza, A.F.H. Robertson, S. Crasquin-Soleau), *Mémoires du Muséum National d'Histoire Naturelle*, 186, 145-185.

Scherer, C.M.S. and Lavina, E.L. (2005) Sedimentary cycles and facies architecture of aeolian-fluvial strata of the Upper Jurassic Guara' Formation, southern Brazil. *Sedimentology*, **52**, 1323-1341.

Schomacker, E.R., Kjemperud, A.V., Nystuen, J.P. and Jahren, J.S. (2010) Recognition and significance of sharp-based mouth-bar deposits in the Eocene Green River Formation, Uinta Basin, Utah. *Sedimentology*, **57**, 1069-1087.

Selley, R.C. (2000) *Applied Sedimentology*. Academic Press, San Diego, 523 pp.

Sellwood, B.W. and Valdes, P.J. (2008) Jurassic climates. *Proceedings of the Geologists' Association*, **119**, 5-17.

- Shukla, U.K., Singh, I.B., Sharma, M. and Sharma, S.** (2001) A model of alluvial megafan sedimentation: Ganga megafan. *Sedimentary Geology*, **144**, 243-262.
- Simpson, E.L. and Eriksson, K.A.** (1993) Thin eolianites interbedded within a fluvial and marine succession: early Proterozoic Whitworth Formation, Mount Isa Inlier, Australia. *Sedimentary Geology*, **87**, 39-62.
- Singh, H., Parkash, B. and Gohain, K.** (1993) Facies analysis of the Kosi megafan deposits. *Sedimentary Geology*, **85**, 87-113.
- Soares, M.V.T., Basile, G., Lorenzoni, P., Colombera, L., Mountney, N.P., Martinelli, A.G., Mesquita, A.F., Marinho, T.S., Garcia, R.V. and Marconato, A.** (2020) Landscape and depositional controls on palaeosols of a distributive fluvial system (Upper Cretaceous, Brazil). *Sedimentary Geology*, **410**, 105774.
- Soria, A.R., Liesa, C.L., Rodríguez-López, J.P., Meléndez, N., de Boer, P.L. and Meléndez, A.** (2011) An Early Triassic evolving erg system (Iberian Chain, NE Spain): palaeoclimate implications. *Terra Nova*, **23**, 76-84.
- Spalletti, L.A. and Colombo Piñol, F.** (2005) From Alluvial Fan to Playa: An Upper Jurassic Ephemeral Fluvial System, Neuquen Basin, Argentina. *Gondwana Research*, **8**, 363-383.
- Spalletti, L.A., Limarino, C.O. and Colombo Piñol, F.** (2010) Internal anatomy of an erg sequence from the aeolian-fluvial system of the De La Cuesta Formation (Paganzo Basin, northwestern Argentina). *Geologica Acta*, **8**, 431-447.
- Stanistreet, I.G. and Stollhofen, H.** (2002) Hoanib River flood deposits of Namib Desert interdunes as analogues for thin permeability barrier mudstone layers in aeolianite reservoirs. *Sedimentology*, **49**, 719-736.
- Stear, W.M.** (1983) Morphological characteristics of ephemeral stream channel and overbank splay sandstone bodies in the Permian Lower Beaufort Group, Karoo Basin, South Africa. *Spec. Publ. Int. Ass. Sediment.*, **6**, 405-420.
- Stear, W.M.** (1985) Comparison of the bedform distribution and dynamics of modern and ancient sandy ephemeral flood deposits in the southwestern Karoo region, South Africa). *Sedimentary Geology*, **45**, 209-230.
- Storms, J.E.A., Hoogendoorn, R.M., Dam, R.A.C., Hoitink, A.J.F. and Kroonenberg, S.B.** (2005) Late-Holocene evolution of the Mahakam delta, East Kalimantan, Indonesia. *Sedimentary Geology*, **180**, 149-166.

Suarez-Gonzalez, P. Quijada, I.E., Benito, M.I. and Mas, R. (2015) Sedimentology of Ancient Coastal Wetlands: Insights From A Cretaceous Multifaceted Depositional System. *Journal of Sedimentary Research*, **85**, 95-117.

Suñer, M., Poza, B., Vila, B. and Santos-Cubedo, A. (2008) Síntesis del registro fósil de dinosaurios en el Este de la Península Ibérica. *Palaeontologica Nova*, **8**, 397-420.

Suñer, M., Santisteban, C. and Royo-Torres, R. (2014) Nuevas evidencias de dinosaurios saurópodos en el tránsito Jurásico-Cretácico de Alpuente (Los Serranos, Valencia). In: *XXX Jornadas de Paleontología de la Sociedad Española de Paleontología* (Coords. R. Royo-Torres, F.J. Verdú and L. Alcalá), *¡Fundamental!*, **24**, 233-236.

Thompson, D.B. (1969) Dome-shaped aeolian dunes in the Frodsham Member of the so-called "Keuper" Sandstone Formation (Scythian-?Anisian: Triassic) at Frodsham, Cheshire (England). *Sedimentary Geology*, **3**, 263-289.

Thierry, J., Barrier, E., Abbate, E., Alekseev, A.S., Ait-Ouali, R., Ait-Salem, H., Bouaziz, S., Canérot, J., Georgiev, G., Giraud, R., Hirsch, F., Ivanik, M., Le Metour, J., Le Nindre, Y.M., Medina, F., Mouty, M., Nazarevich, B., Nikishin, A.M., Page, K., Panov, D.L., Pique, A., Poisson, A., Voznezenski, A., Walley, C.D., Wong, T.E., Ziegler, M., Ait-Brahim, L., Bergerat, F., Bracene, R., Brunet, M.F., Cadet, J.P., Guezou, J.C., Jabaloy, A., Lepvrier, C. and Rimmelé, G. (2000) Early Tithonian. In: *Atlas peri-Tethys palaeogeographical maps* (Eds. J. Decorut, M. Gaetani, B. Vrielynck, E. Barrier, B. Biju-Duval, M.F. Brunet, J.P. Cadet, S. Crasquin, M. Sandulescu), Map-11. CCGM, Paris.

Tripaldi, A., Zárate, M.A., Brook, G.A. and Guo-Qiang, L. (2011) Late Quaternary paleoenvironments and paleoclimatic conditions in the distal Andean piedmont, southern Mendoza, Argentina. *Quaternary Research*, **76**, 253-263.

Tucker, M.E. and Benton, M.J. (1982) Triassic environments, climates and reptile evolution. *Palaeogeography, Palaeoclimatology, Palaeoecology*, **40**, 361-379.

Turner, B.R. and Makhlof, I. (2005) Quaternary sandstones, northeast Jordan: Age, depositional environments and climatic implications. *Palaeogeography, Palaeoclimatology, Palaeoecology*, **229**, 230-250.

Turner, B.R. and Tester, G.N. (2006) The Table Rock Sandstone: A fluvial, friction-dominated lobate mouth bar sandbody in the Westfalian B Coal Measures, NE England. *Sedimentary Geology*, **190**, 97-119.

Udden, J.A. (1914) Mechanical composition of clastic sediments. *Geological Society of America Bulletin*, 25, 655-744.

Valdes, P. (1993) Atmospheric General Circulation Models of the Jurassic. *Philosophical Transactions of the Royal Society of London. Series B: Biological Sciences*, 341, 317-326.

Valdes, P.J. and Sellwood, B.W. (1992) A palaeoclimate model for the Kimmeridgian. *Palaeogeography, Palaeoclimatology, Palaeoecology*, 95, 47-72.

Veiga, G. and Spalletti, L.A. (2007) The Upper Jurassic (Kimmeridgian) fluvial-aeolian systems of the southern Neuquen Basin, Argentina. *Gondwana Research*, 11, 286-302.

Veiga, G.D., Spalletti, L.A. and Flint, S. (2002) Aeolian/fluvial interactions and high-resolution sequence stratigraphy of a non-marine lowstand wedge: the Avile Member of the Agrio Formation (Lower Cretaceous), central Neuquen Basin, Argentina. *Sedimentology*, 49, 1001-1019.

Vellinga, A.J., Cartigny, M.J.B., Eggenhuisen, J.T. and Hansen, E.W.M. (2018) Morphodynamics and depositional signature of low-aggradation cyclic steps: New insights from a depth-resolved numerical model. *Sedimentology*, 65, 540-560.

Vilas, L., Mas, R., García, A., Arias, C., Alonso, A., Meléndez, N. and Rincón, R. (1982) Capítulo 8. Ibérica suroccidental. In: *El Cretácico de España* (Ed. A. García), pp. 457-514. Universidad Complutense de Madrid, Madrid.

Viseras, C. and Fernández, J. (1994) Channel migration patterns and related sequences in some alluvial fan systems. *Sedimentary Geology*, 88, 201-217.

Viseras, C. and Fernández, J. (1995) The role of erosion and deposition in the construction of alluvial fan sequences in the Guadix Formation (SE Spain). *Geologie en Mijnbouw*, 74, 21-33.

Viseras, C., Soria, J.M., Durán, J.J., Pla, S., Garrido, G., García-García, F. and Arribas, A. (2006). A large-mammal site in a meandering fluvial context (Fonelas P-1, Late Pliocene, Guadix Basin, Spain). Sedimentological keys for its paleoenvironmental reconstruction. *Palaeogeography, Palaeoclimatology, Palaeoecology*, 242, 139-168.

Vogt, M., Stinnesbeck, W., Zell, P., Kober, B., Kontny, J., Hezer, N., Frey, E., Rivera-Syla, H.E., Padilla Gutierrez, J.M., Amezcua, N. and Flores Huerta, D. (2016) Age and depositional environment of the “dinosaur graveyard” at Las Águilas, southern Coahuila, NE Mexico. *Palaeogeography, Palaeoclimatology, Palaeoecology*, 44, 758-769.

Wang, J. and Plink-Björklund, P. (2020) Variable-discharge-river macroforms in the Sunnyside Delta Interval of the Eocene Green River Formation, Uinta Basin, USA. *Sedimentology*, 67, 1914-1950.

Warren, J.K. (2016) *Evaporites. A geological Compendium*. Second Edition. Springer, Cham, 1813 pp.

Wentworth, C.K. (1922) A scale of grade and class terms for clastic sediments. *Journal of Geology*, **30**, 377-392.

Williams, G.E. (1971) Flood deposits of the sand-bed ephemeral streams of central Australia. *Sedimentology*, **17**, 1-40.

Wright, L.D. (1977) Sediment transport and deposition at river mouths: A synthesis. *Geological Society of America Bulletin*, **88**, 857-868

Yeste, L.M., Varela, A.N., Viseras, C., Mcdougall, N.D. and García-García, F. (2020) Reservoir architecture and heterogeneity distribution in floodplain sandstones: Key features in outcrop, core and wireline logs. *Sedimentology*, **67**, 3355-3388.

Zharkov, M.A., Murdmaa, I.O. and Filatova, N.I. (1998) Paleogeography of the Berriasian–Barremian Ages of the Early Cretaceous. *Stratigraphy and Geological Correlation*, **6**, 47-69.

FIGURE CAPTIONS

Fig. 1. (A) Simplified geological map of the Iberian Peninsula indicating the location of the South-Iberian and Maestrazgo basins within the Mesozoic Iberian Extensional System (modified from Mas *et al.*, 2004). The red square indicates the location of the map shown in Fig. 1B. (B) Geological map of eastern Spain showing the limits of the deposits of the Maestrazgo Basin and its sub-basins 'sb' (modified from Salas & Guimerà, 1996, 1997, Salas *et al.*, 2001; Bover-Arnal & Salas, 2019) and the South-Iberian Basin. The geological information of this map was obtained and modified from the geological map of the Iberian Peninsula and the Balearic and Canary Islands (1995 edition, scale 1:1,000,000, Caride de Liñan, 1995). (C) Geological map of the study area of the South-Iberian and the western Maestrazgo basins (modified from Campos-Soto *et al.*, 2019), showing the location of the stratigraphic sections, the main areas where additional outcrops have been studied for this work (for more details on the additional studied outcrops see Campos Soto, 2020) and the panels shown in Figs 4 and 5. The geological data were obtained and modified from the geological map Z1700 of the Geological Spanish Survey (GEODE, scale 1:50,000; López-Olmedo *et al.*, 2018). (D) Palaeogeographic reconstruction of eastern and northern Iberia during the Tithonian, to the left (palaeogeography and palaeocurrents obtained and modified from Thierry *et al.*, 2000 and Campos-Soto *et al.*, 2019, and references therein). To the right detailed palaeogeography of the South-Iberian and western Maestrazgo basins (data obtained and modified from Campos-Soto *et al.*, 2019). The line that represents the 30°N latitude in the palaeogeographic reconstruction of eastern and northern Iberia has been modified according to data published by Sellwood & Valdes (2008) and Boucot *et al.* (2013). Tracks of hurricanes and storms for the Late Jurassic are based on Marsaglia & Klein (1983) and wind tracks blowing from the Tethys and the Boreal realms are based on Sellwood & Valdes (2008) and Benito *et al.* (2005), respectively. Palaeocurrents obtained in this work from the subaquatic and aeolian deposits in the different studied areas of both basins have been represented in the palaeogeographic map with blue and orange arrows, respectively. The length of the arrows corresponds to the abundance of measurements. The palaeogeographic reconstruction of the South-Iberian and the western Maestrazgo Basin, to the right, shows the location of the specific areas studied here: CE (Cedrillas), CAS (El Castellar), FA (Formiche Alto) and MO (Mora de Rubielos) in the western Maestrazgo Basin, and RI (Riodeva), LO-AL (Losilla-Alpuente), BE (Benagéber) and VA (Villar del Arzobispo) in the South-Iberian Basin.

Fig. 2. Stratigraphic sections of the Villar del Arzobispo Formation logged in the western Maestrazgo (Cedrillas, El Castellar, Formiche Alto and Mora de Rubielos) and in the South-Iberian basins (Riodeva, Losilla-Alpuente, Benagéber and Villar del Arzobispo). Modified from Campos-Soto *et al.* (2019). This figure also includes a simplified map showing the location of the sections at the studied areas (see also Fig. 1C). All of the sections show, at their right part, the main sedimentary structures and palaeontological data, including the dinosaur remains (for more information on dinosaur fossil sites see figs 2 and 3 of Campos-

Soto *et al.*, 2017a and fig. 3A of Campos-Soto *et al.*, 2019). The Losilla-Alpuente section also shows, at its right part, some partial stratigraphic sections logged in laterally related outcrops.

Fig. 3. (A) Diagrams showing the different stages of system evolution during sedimentation of the Villar del Arzobispo Formation. These stages comprise: (i) the deposition of shallow marine deposits of the carbonate lower part (CLP) during the Kimmeridgian; (ii) deposition of the essentially siliciclastic deposits of the siliciclastic upper part (SUP) during a regressive stage during the Kimmeridgian–Tithonian; during this stage, fluvial, aeolian and deltaic depositional settings mainly developed landward; these settings passed gradually seaward to coastal to shallow marine settings; (iii) deposition of the upper part of the SUP during the Tithonian marine transgression. The reconstruction of the different stages of evolution is based on the data obtained from the stratigraphic sections (Fig. 2), the geological mapping (see Fig. 1C and Fig. S1 of Supplementary Material), and the ages obtained through the analysis of the larger benthic foraminifera – see Campos-Soto *et al.* (2016a; 2016b; 2017a; 2019). Deposits of each studied area are delimited by syn-sedimentary faults, which have been represented with vertical lines. In the Formiche Alto area, sedimentation took place in two different blocks delimited by syn-sedimentary faults (F1 and F2; see location on geological maps of Fig. 3C and Fig. S1 of Supplementary Material). Note that the block located to the south-east of F2 corresponds to the stratigraphic section shown in Fig. 2 for the Formiche Alto area. Areas with no outcrop control correspond to the areas where no Upper Jurassic deposits have been identified (see details in geological map of Fig. 1B). (B) Simplified palaeogeographic reconstruction of eastern Iberia during the Late Jurassic (see Fig. 1D for details), showing the location of the studied areas and the correlation line displayed in diagrams of Fig. 3A. The blue dashed line shows the position of the geological map of the Peñagolosa sub-basin shown in Fig. 3C. (C) Simplified geological map of the Peñagolosa sub-basin (western Maestrazgo basin) showing the location of the stratigraphic sections and the faults F1 and F2, which bound the two sedimentation blocks of the Formiche Alto area represented in Fig. 3A (modified from Campos-Soto *et al.*, 2017a). For more details of this geological map, see Fig. S1 of Supplementary Material.

Fig. 4. Panoramic field photograph (A) and line drawing (B) of deposits of the siliciclastic upper part (SUP) of the Villar del Arzobispo Formation at the most landward area of the South-Iberian Basin (see Fig. 1C for location). The SUP comprises flood plain, fluvial channel, aeolian dune and deltaic deposits that are interbedded and laterally related.

Fig. 5. Panoramic field photograph (A) and line drawing (B) of deposits of the uppermost part of the siliciclastic upper part (SUP) of the Villar del Arzobispo Formation at the most seaward area of the west Maestrazgo Basin (Mora de Rubielos area; see Fig. 1C and Fig. S1 of Supplementary Material for location). Note that siliciclastic deposits (coastal terminal distributary channel and distributary-mouth bar

deposits) and marl are interbedded and pass laterally to the south to shallow marine bioclastic and oolitic limestone, which, in turn, gets progressively thicker and more abundant southward.

Fig. 6. Ephemeral fluvial channel architectural element. (A) Schematic diagram and log of the ephemeral fluvial channel architectural element (bracket in the diagram shows the location of the log; see Fig. 2 for legend) and palaeocurrents. (B) Field photograph (Riodeva area) of channelized conglomerate displaying large-scale cross-strata and a slightly incisive erosive base. Hammer for scale is 32 cm long (white circle). (C) Field photograph (Riodeva area) of a conglomerate lens displaying an asymmetrical and incisive erosive base, with a very steep margin, to the right, and a less steep one, to the left. Conglomerate displays a unique set of cross-strata that is conformable to the less steep margin of the erosive base. (D) Field photograph (Riodeva area) of a very poorly-sorted and clast-supported conglomerate made by rounded quartzite (white arrows) and sandstone clasts (red arrow). (E) and (F) Field photographs (Cedrillas and Riodeva areas, respectively) of poorly-sorted and clast-supported conglomerates made up of subangular to subrounded, muddy and carbonate soft clasts. (G) Dinosaur bone (red arrow) observed within conglomerate in the Riodeva area.

Fig. 7. Multi-storey fluvial channel architectural element. (A) Schematic diagram and log of the multi-storey fluvial channel architectural element (bracket in the diagram shows the location of the log; see Fig. 2 for legend) and palaeocurrents. Field photograph (B) and line drawing (C) of channelized sandstone and conglomerate element at the Riodeva area. Sandstone displays large internal erosive surfaces filled by conglomerate or sandstone (red arrows). Sandstone displays scour and fill structures (blue arrows) filled by foresets and backsets (green arrows) strata that flatten upward in places. In the lower part of the body, sandstone displays upward flattening strata with long wavelength (blue bracket). Sandstone also displays sets of large-scale cross-strata at the upper part of the body (pink arrows), whose thickness decreases upward (red bracket). Conglomerate displays scour and fill structures filled by backset strata (white arrows). Note the asymmetrical scour filled by conglomerate in the lower part of the body, displaying backset strata that flatten upward and fine upward to sandstone (green bracket). (D) Field photograph (Riodeva area) of a multi-storey fluvial channel element composed of sandstone and conglomerate. Note that sandstone displays internal erosive surfaces (red dotted lines), which are filled by sandstone or conglomerate (white arrow and orange-shaded area). (E) Channelized sandstone (El Castellar area) displaying basal and internal erosive surfaces (red-dotted lines), which are filled by large-scale cross-strata sandstone. Locally there is a thin layer of siliciclastic mudstone containing abundant carbonaceous detritus interbedded with sandstone (yellow arrows). (F) Detail of the thin layers of siliciclastic mudstone containing carbonaceous detritus (yellow arrows) observed in Fig. 7E.

Fig. 8. Upper flow regime sedimentary structures observed within the multi-storey fluvial channel architectural element (El Castellar area). Field photograph (A) and line drawing (B) of a sandstone body displaying convex-up low-angle cross-strata (red bracket; blue arrows). Field photograph (C) and line drawing (D) of sandstone displaying scour and fill structures, which is directly overlying the convex-up low-angle cross-strata sandstone of Fig. 8A (red asterisk marks the same point in both pictures). Note that scours are filled by foreset and backset strata (yellow and red arrows, respectively) that flatten upward in places (blue bracket). In the upper part of the body, a large-scale cross-strata set is observed (white arrow), in which the inclination of foresets indicates the flow direction.

Fig. 9. Flood plain architectural element. (A) Schematic diagram and log of the flood plain architectural element (bracket in the diagram shows the location of the log; see Fig. 2 for legend) and palaeocurrents measured in the non-channelized sandstone deposits included in this element. (B) Field photograph (Formiche Alto area) of reddish siliciclastic mudstone displaying green mottling (red arrows). (C) Non-channelized sandstone body (El Castellar area) displaying a coarsening-upward and thickening-upward trend (yellow bracket). The lower part is made up of decimetre-thick sandstone beds, which include a fragment of a dinosaur bone (white arrow) and which are interbedded with greyish-greenish siliciclastic mudstone. (D) Non-channelized sandstone (Riodeva area) displaying parallel lamination followed upward by small-scale cross-strata. Wave ripple cross-strata are observed at the top. (E) Non-channelized sandstone displaying large-scale sigmoidal cross-strata (Benagéber area). (F) Dinosaur track observed at the base of a non-channelized sandstone bed (dotted yellow line) at the Riodeva area. The dinosaur track is preserved as a convex hyporelief (natural track cast) and shows slide marks (parallel striations, white arrow) made by skin scales. (G) Bioturbation observed as paired circular openings at the top of a non-channelized sandstone bed at the Riodeva area. (H) Field photograph of limestone (red arrow) interbedded with reddish siliciclastic mudstone (Riodeva area). (I) Limestone made up of oncoids (white arrows) that are up to 6 to 7 cm large at the Riodeva area. (J) Field photograph of bioclastic limestone containing poorly-sorted bivalve fragments (Losilla-Alpuente area). (K) Photomicrograph of poorly-sorted bioclastic limestone, which includes quartz grains, fragments of bivalves (green arrow), gastropods (yellow arrow), echinoderms (blue arrow), ostracods (white arrow), miliolids (red arrow) and ooids (orange arrows).

Fig. 10. Deltaic architectural elements. (A) Schematic diagram and log of the deltaic elements (bracket in the diagram shows the location of the log; see Fig. 2 for legend) and palaeocurrents obtained in clinofolds of the delta-front element and in cross-bedded sets of the delta terminal distributary channel element. Field photograph (B) and line drawing (C) of four coarsening-upward and thickening-upward deltaic successions (marked with blue brackets). Note that the lower and uppermost deltaic successions do not crop out completely. The first three deltaic successions, starting from the base, are made up of laterally-extensive centimetre-thick, very fine to fine-grained sandstone layers showing a very low angle inclination and

alternating with millimetre-thick carbonaceous detritus layers, which are interpreted as deposits of the delta front element (see text for details). In the two lowermost deltaic successions, the delta-front deposits are truncated at their uppermost part by the delta terminal distributary channel element (orange arrows). The delta terminal distributary channel element displays erosive surfaces and is filled by sandstone displaying upward flattening strata or backset strata (purple and green arrows, respectively). The uppermost deltaic succession is made up of carbonaceous-rich, dark-grey siliciclastic mudstone (delta-toe element, blue colour), which changes upward to alternating sandstone and carbonaceous detritus layers (delta front element). (D) Field photograph of the delta-toe element comprising carbonaceous-rich, dark-grey siliciclastic mudstone interbedded with very fine-grained rippled sandstone. (E) Field photograph of centimetre-thick sandstone layers alternating with millimetre to centimetre-thick carbonaceous detritus layers at the lower part of foresets of the delta-front element. (F) Field photograph of a sandstone layer at the lowermost part of the delta-front element displaying poorly-preserved dinosaur tracks at the base, which are preserved as convex hyporeliefs or natural casts (white arrows and black dotted line). The dinosaur tracks display elongated shapes, with irregular and deformed outlines and their infill is massive. They penetrate up to 70 cm into the underlying deposit, made up of alternating carbonaceous-rich, dark-grey siliciclastic mudstone and rippled sandstone layers, interpreted as delta toe deposits (see text for details). All photographs were taken at the Riodeva area.

Fig. 11. Deltaic architectural elements. (A) Field photograph of sandstone displaying clinoforms. (B) Detail of three coarsening-upward and thickening-upward deltaic successions (marked with blue brackets) displaying clinoforms. Note that the lower part of foresets are draped by carbonaceous detritus (red arrow) and, locally, these drapes extend upward to the topsets (white arrow). Field photograph (C) and line-drawing (D) of three coarsening-upward and thickening-upward deltaic successions (marked with blue brackets). Note that deposits of the lowermost succession are truncated by an erosive surface, which incises 1.30 m downward into the underlying sediments, made up of thinly-bedded sandstone and carbonaceous detritus layers (delta-front element), and it is filled by sandstone displaying large-scale cross-strata (delta terminal distributary channel element). The yellow star indicates the position of the sample shown in Fig. 11F. (E) Detail of deposits of the delta terminal distributary channel element observed in Fig. 11C and D, displaying an erosive base and formed by large-scale cross-strata sandstone. (F) Transmitted light photomicrograph of a well-sorted sandstone. The location of the sample is indicated in Fig. 11C and D with a yellow star. All photographs were taken at the Riodeva area.

Fig. 12. Coastal to shallow marine architectural elements. (A) Schematic diagram of the coastal to shallow marine architectural elements indicating the position of the logs shown in Figs 12B and 13A. (B) Log of the coastal terminal distributary channel architectural element (bracket in the diagram shows the location of the log in Fig. 12A; see Fig. 2 for legend) and palaeocurrents obtained in the western Maestrazgo Basin. (C)

and (D) Channelized sandstone (Formiche Alto area) displaying a basal erosive base (red dotted line) and large-scale cross-strata. This body is interbedded with marl (white arrows), which, in turn, is interbedded with shallow marine limestone (blue arrow) and distributary mouth-bar sandstone (orange arrows). Note that sandstone displays an internal erosive surface (pink dotted line) filled by poorly-sorted conglomerate and also includes thin layers of carbonaceous-rich marl between the large-scale cross-strata sets (yellow arrows). (E) Detail of the thin layers of carbonaceous-rich marl located between large-scale cross-strata sets (yellow arrow) and draping the bottomsets and the lower part of foresets (white arrows). See location in Fig. 12D. (F) Detail of the internal erosive surface (pink dotted line) filled by poorly-sorted conglomerate (see location in Fig. 12C). (G) Field photograph of poorly-sorted mudstone pebbles including fragments of bivalves overlaying the internal erosive surface (pink dotted line). See location in Fig. 12F. Coin for scale is 2.3 cm in diameter.

Fig. 13. Coastal to shallow marine architectural elements. (A) Log of the distributary mouth-bar element (bracket in the diagram shows the location of the log in Fig. 12A; see Fig. 2 for legend) and palaeocurrents. (B) Field photograph (Benagéber area) of a sandstone body displaying a coarsening-upward and thickening-upward trend (yellow bracket) and interbedded with shallow marine limestone (greyish strata below and above yellow bracket). Field photograph (C) and line drawing (D) of the distributary mouth-bar element (Mora de Rubielos area) comprising a non-channelized sandstone body interbedded with marl that includes corals in life position (black arrow indicates location of corals). Note that sandstone displays large-scale and sigmoidal cross-strata (white arrows). Hammer for scale is 32 cm long. (E) Field photograph of colonial corals observed in life position at the Mora de Rubielos area. Note that the white arrows point to its growth lines. See location of the coral at Fig. 13C and D. (F) Detail of the septa of the coral shown in Fig. 13E. (G) Field photograph (Mora de Rubielos area) of centimetre-thick sandstone displaying wave ripple strata at the top (white arrows) and interbedded with marl, giving rise to wavy bedding. (H) Trigonoids and ostreids observed within a sandstone body (white and blue arrows, respectively) at the Mora de Rubielos area. (I) Burrowing traces observed at the top of a sandstone body in the Formiche Alto area.

Fig. 14. Simple aeolian dune architectural element. (A) Schematic diagram and log of the simple aeolian dune architectural element (bracket in the diagram shows the location of the log, see Fig. 2 for legend) and palaeocurrents. Field photograph (B) and line drawing (C) of a sandstone body displaying a 6 m thick large-scale cross-strata set. Large-scale cross-strata set is made up of convex-up foresets passing upward to low-angle inclined topsets. (D) Field photograph of a metre-thick sandstone body displaying a single set of large-scale cross-strata. (E) Metre-thick sandstone body comprising a 4 m thick large-scale cross-strata set. Hammer for scale is 32 cm long (black circle). (F) Detail of large-scale cross-strata set observed in Fig. 14E. Large-scale cross-strata set is made up of successive centimetre-thick inversely graded strata. Note

that the contact between each stratum is sharp (red arrows). Hammer for scale is 32 cm long. (G) Transmitted light photomicrograph of simple dune aeolian sandstone displaying well-sorted subrounded to subangular grains. (H) Transmitted light photomicrograph of sandstone strata displaying inverse grain size grading. All photographs were taken at the Riodeva area.

Fig. 15. Massive and indistinctly stratified aeolian dune architectural element. (A) Schematic diagram and log of the massive and indistinctly stratified aeolian dune architectural element (bracket in the diagram shows the location of the log; see Fig. 2 for legend) and palaeocurrents. (B) Field photograph of massive and indistinctly stratified aeolian dune sandstone overlain by the multi-storey fluvial channel architectural element (its base is indicated with a yellow line). Black lines represent faults. (C) Field photograph of massive and indistinctly stratified aeolian dune sandstone, which is laterally interbedded with conglomerate bodies of the ephemeral fluvial channel architectural element (delimited by red lines). (D) Field photograph of massive and indistinctly stratified sandstone interbedded with conglomerate bodies (delimited by red lines). Sandstone displays poorly preserved large-scale cross-strata (foresets are outlined with black lines). Note that the blue circle shows a 2 m large pocket rule (white line). (E) Field photograph of massive and indistinctly stratified aeolian dune sandstone overlain by the multi-storey fluvial channel architectural element (its base is indicated with a yellow line). (F) Transmitted light photomicrograph of sandstone displaying subangular to subrounded and well-sorted grains. Field photograph (G) and line drawing (H) of sandstone displaying large-scale cross-strata in which foresets pass downward to laterally continuous bottomsets. Carbonaceous detritus and mica flakes drape some bottomsets and the lowermost part of some foresets. Note the high-angle foresets displayed by the cross-strata set to the right of the photograph (blue arrow). All photographs were taken at the Riodeva area.

Fig. 16. Climbing aeolian dune architectural element. (A) Schematic diagram and log of the climbing aeolian dune architectural element (bracket in the diagram shows the location of the log; see Fig. 2 for legend) and palaeocurrents. (B) Field photograph of sandstone displaying a large-scale cross-stratified set, at least 2 m thick (note that the person in the photograph is 1.65 m tall). Field photograph (C) and line drawing (D) of sandstone displaying large-scale tangential cross-strata sets. Individual sets are delimited by low-angle inclined bounding surfaces, which dip in the opposite direction to the foresets dip. (E) Field photograph of large-scale and high-angle cross-strata sandstone whose foresets are slightly deformed (yellow arrows). (F) Field photograph of tangential cross-strata sandstone. (G) Detail of the lower part of foresets and bottomsets of large-scale cross-strata sandstone. Foresets comprise centimetre-thick strata pinching out downward, which correspond to grainflow strata (gf). Grainflow strata are interbedded with centimetre-thick strata pinching out upward, corresponding to wind ripple strata (wr). (H) Detail of grainflow strata made up of fine to medium-grained sandstone (blue bracket) and wind ripple strata made

up of very fine to fine-grained sandstone (red brackets). (I) Sandstone pseudomorph after gypsum (desert rose formed by a rosette-like crystal aggregate). All photographs were taken at the Riodeva area.

Fig. 17. Reconstruction of the different palaeoenvironments inhabited by dinosaurs of the Villar del Arzobispo Formation and of the lateral relationships between them (not at scale).

Fig. 18. Interactions between fluvial, tidal, deltaic, and aeolian environments observed in the Lençóis Maranhenses National Park (north-east Brazil). Satellite images were taken from Google Earth© in 2019.

(A) The coastal dune field of the Lençóis Maranhenses National Park (to the right) is located next to the estuary of the Mearim River (to the left). (B) Aeolian dunes developing in a flooded area, at the end of the dune field. Note that stagnant water bodies develop in the interdune areas (blue arrows). (C) Aeolian dunes approaching a tidal channel (blue arrows). Note how the aeolian interdunes may get flooded (red arrows). (D) The coastal flood plain is crossed by the Grande River, which flows into a shallow water body in which deltaic sediments are deposited (red arrow). (E) The coastal dune field is penetrated by the Negro River (blue arrows) and in its margin small deltas develop in stagnant water bodies (red squares). (F) and (G) Interdune areas crossed by the Negro River. Note that the fluvial channel erodes the aeolian dune sediments in (F) (pink arrow) and that aeolian dunes migrate over the fluvial channel in (G) (blue arrow). Note that small deltas develop in the interdune areas (red arrows). (H) and (I) Deltas developing in the margins of the dune field. Note that the aeolian dunes migrate over the delta plain in (H) (blue arrows) and that the distributary channels rework the aeolian dune sediments in (I) (red arrow).

Table 1. Summary of the essentially siliciclastic coastal and alluvial architectural elements of the Villar del Arzobispo Formation in the South-Iberian and western Maestrazgo basins. See Fig. 2 for location of the architectural elements. The references are cited in the main text.

SUPPLEMENTARY MATERIAL

S1. (A) Geological map of western Maestrazgo and South-Iberian basins (modified from Campos-Soto *et al.*, 2019). The blue dotted rectangle indicates the location of the map shown in Fig. S1B. (B) Geological map of western Maestrazgo Basin (modified from Campos-Soto *et al.*, 2017a), showing the location of the stratigraphic sections of the Villar del Arzobispo Formation included in Fig. 2 and the position of the panel shown in Fig. 5. The map includes the detailed mapping of the shallow marine bioclastic and oolitic limestone (dark blue lines) and the inter- to supratidal peloidal and micritic limestone (light blue lines) of the studied succession, as well as the mapping of the syn-extensional faults that controlled its thickness variations. Note how shallow marine bioclastic and oolitic limestone gets progressively thinner and less abundant towards the north and gets thicker and more abundant towards the south-east of the study area, where the thickness of the studied succession significantly increases.

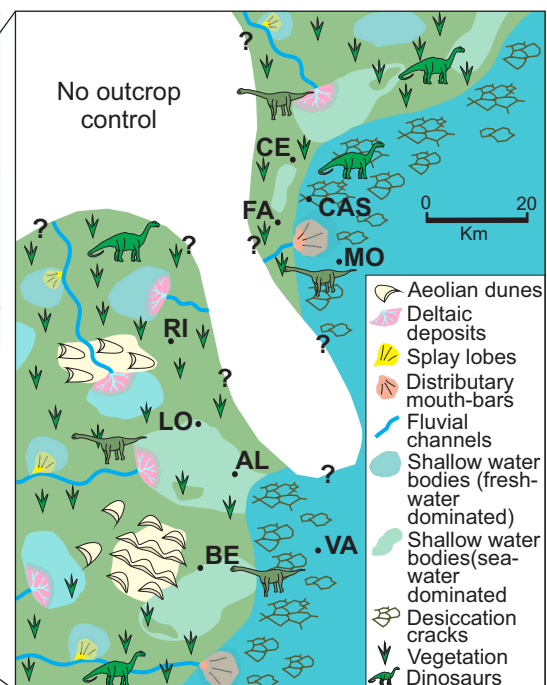
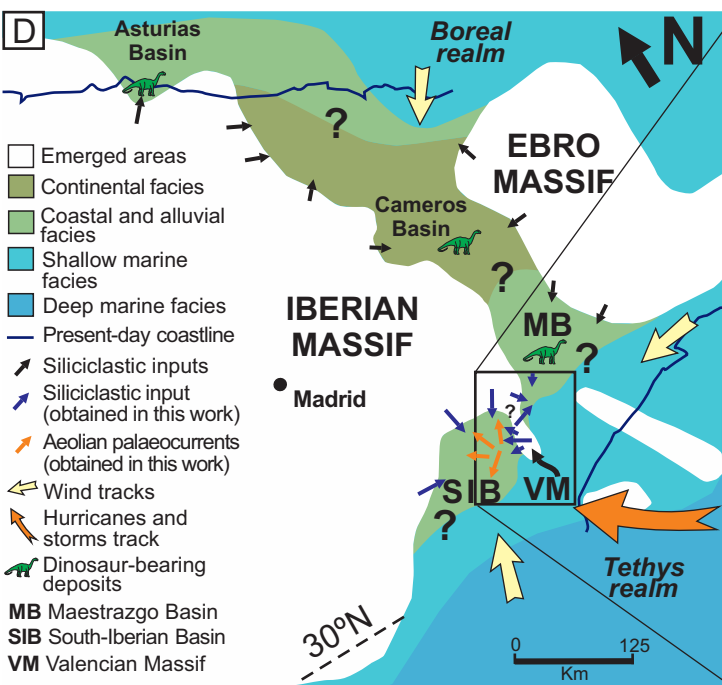
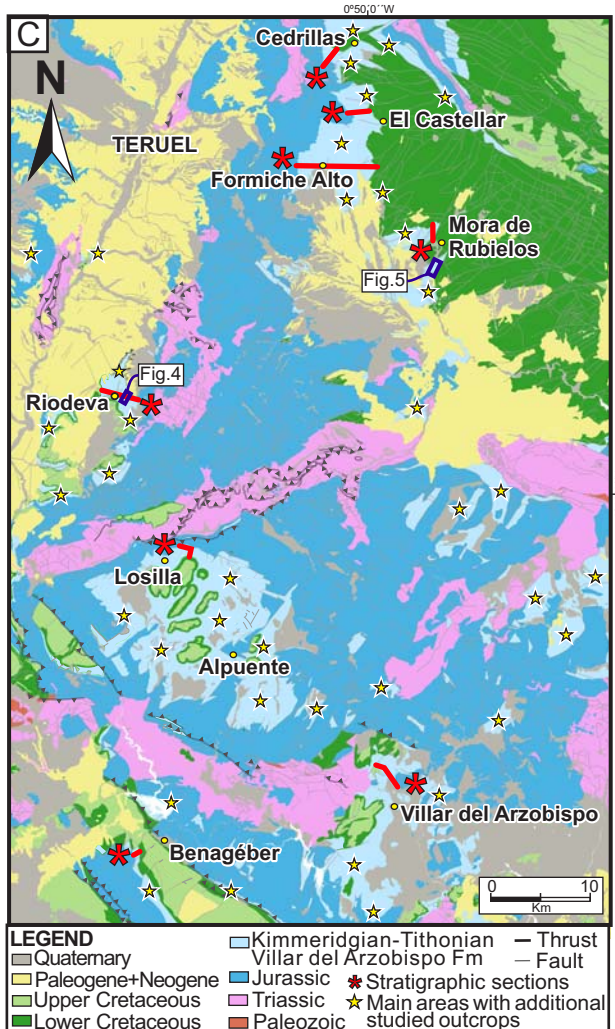
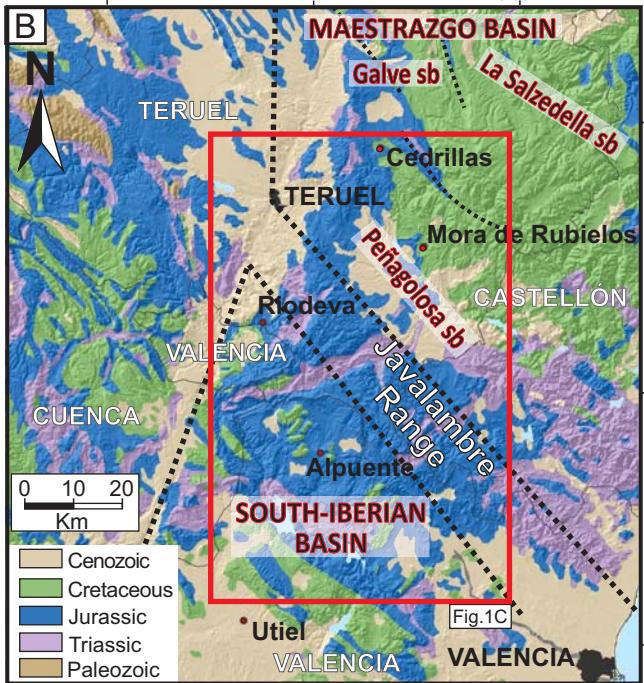
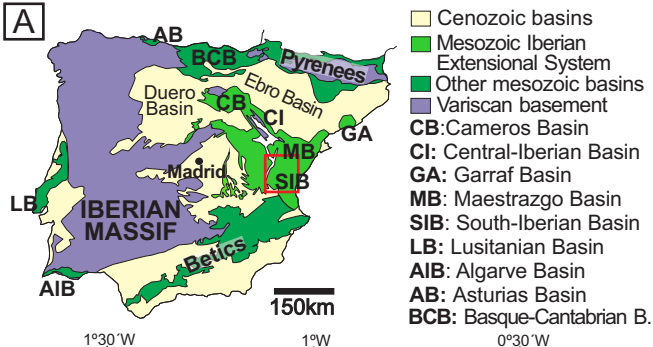
Table 1. Summary of the essentially siliciclastic coastal and alluvial architectural elements of the Villar del Arzobispo Formation in the South-Iberian and western Maestrazgo basins. See Fig. 2 for location of the architectural elements. The references are cited in the main text. CLP = carbonate lower part; SUP = siliciclastic upper part.

Depositional settings	Architectural elements	Sedimentary features and fossil content	Sedimentary structures	Stratigraphic position and occurrence in sections	Associated deposits	Environmental interpretation
Fluvial	Ephemeral fluvial channel	<p>Composition and sorting: Very poorly-sorted conglomerate. Commonly clast-supported. Subangular to subrounded mud, carbonate and sandstone clasts (<20 cm), locally rounded quartzite pebbles (<6 cm).</p> <p>Thickness and vertical arrangement: Decimetre to metre-thick bodies (<3 m) with erosive bases (commonly symmetrical and slightly incisive, locally asymmetrical and very incisive) and short lateral extent (<10 m).</p> <p>Fossil content: Fragments of tree trunks and dinosaur bones.</p> <p>Observations: More abundance of quartzite pebbles upward in the SUP of the South-Iberian Basin sections.</p>	<p>Tractive structures: Large-scale cross-strata (set thickness <3 m).</p> <p>Palaeocurrents: <i>South-Iberian Basin:</i> transport to the W–NW and the NE–SE. <i>Western Maestrazgo Basin:</i> transport to the S–SW and the SE.</p>	<p>South-Iberian Basin: <i>CLP:</i> Riodeva <i>SUP:</i> Riodeva, Benagéber and Villar del Arzobispo</p> <p>Western Maestrazgo Basin: <i>CLP:</i> Cedrillas <i>SUP:</i> Cedrillas, El Castellar and Formiche Alto</p>	<p>Interbedded with flood plain and massive and indistinctly stratified aeolian dune elements. Overlain by delta-toe and simple and climbing aeolian dune elements.</p>	<p>Ephemeral fluvial channels developed during periods of intense rainfall and in which conglomerates were deposited under episodic and flash flows.</p>
	Multi-storey fluvial channel	<p>Composition and sorting: <i>Sandstone:</i> medium to coarse-grained, occasionally fine-grained. Moderately to poorly-sorted. <i>Conglomerate:</i> very poorly-sorted, commonly clast-supported. Medium to coarse-grained sandy matrix. Minor pebbly sandstone. Subangular to subrounded mud, carbonate and sandstone clasts (<8 cm), locally rounded quartzite clasts (<5 cm). Conglomerate overlies erosive bases and internal erosive surfaces.</p> <p>Thickness and vertical and lateral arrangement: Metre-thick bodies (<15 m) with erosive bases and great exposed lateral extent (<250 m). Common fining-upward trend. Occurrence of large internal erosive surfaces.</p> <p>Fossil content: Fragments of tree trunks (up to few metres in size) and other plant remains (up to 30 cm in size).</p> <p>Observations: More abundance of quartzite pebbles upward in the SUP of the South-Iberian Basin sections.</p>	<p>Tractive structures: Large-scale cross-strata in sandstone and conglomerate (set thickness <1.5 m). Local upward decrease of set thickness. Locally thin layers of siliciclastic mudstone with abundant carbonaceous detritus are interbedded with cross-strata sandstone sets and/or at the lower part of foresets and bottomsets. Occasional supercritical flow sedimentary structures (convex-up low-angle cross-strata and scour and fill structures filled by backset and foreset strata that flatten upward in places).</p> <p>Palaeocurrents: <i>South-Iberian Basin:</i> main transport to the NE–S, minor to the W–N. <i>Western Maestrazgo Basin:</i> transport to the NE, minor to the N and E–SE.</p>	<p>South-Iberian Basin: <i>CLP:</i> Villar del Arzobispo <i>SUP:</i> All sections</p> <p>Western Maestrazgo Basin: <i>CLP:</i> El Castellar and Formiche Alto <i>SUP:</i> All sections</p>	<p>Interbedded with flood plain and simple, climbing and massive and indistinctly stratified aeolian dune elements. Overlying massive and indistinctly stratified aeolian element. Overlain by delta elements.</p>	<p>Perennial to semi-perennial fluvial channels characterized by episodic and seasonal discharge.</p>
	d	p	Composition, components, texture and/or sorting:	Tractive structures:	South-Iberian Basin:	Interbedded with

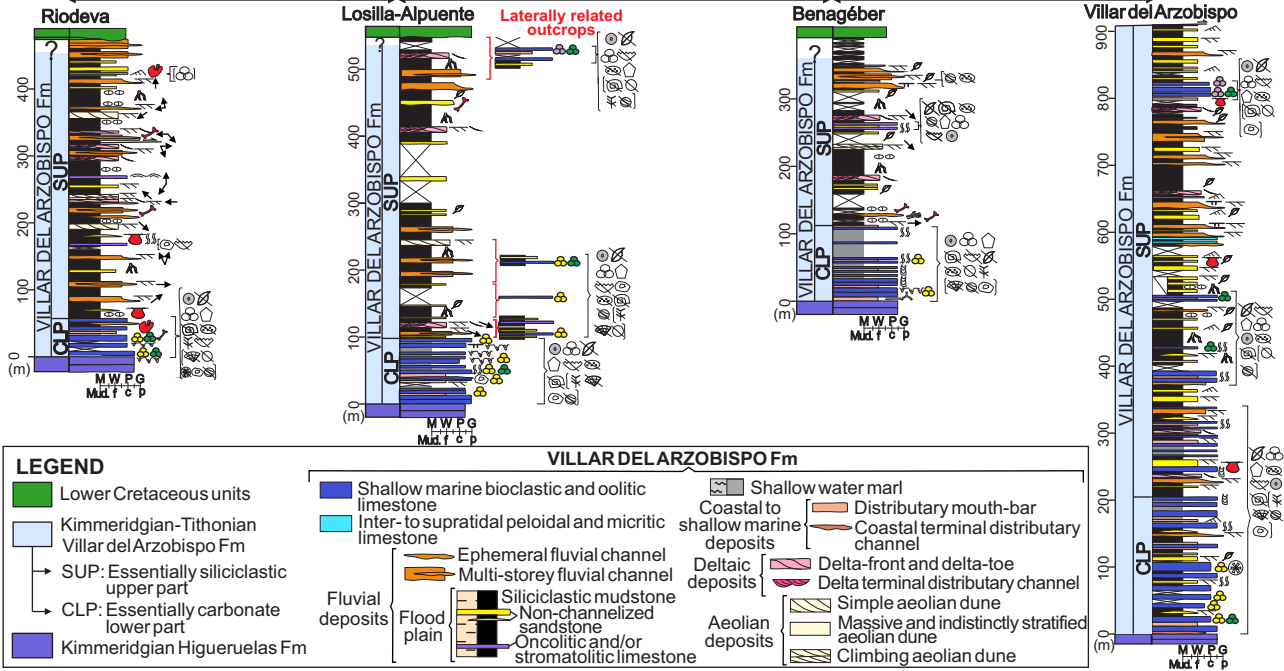
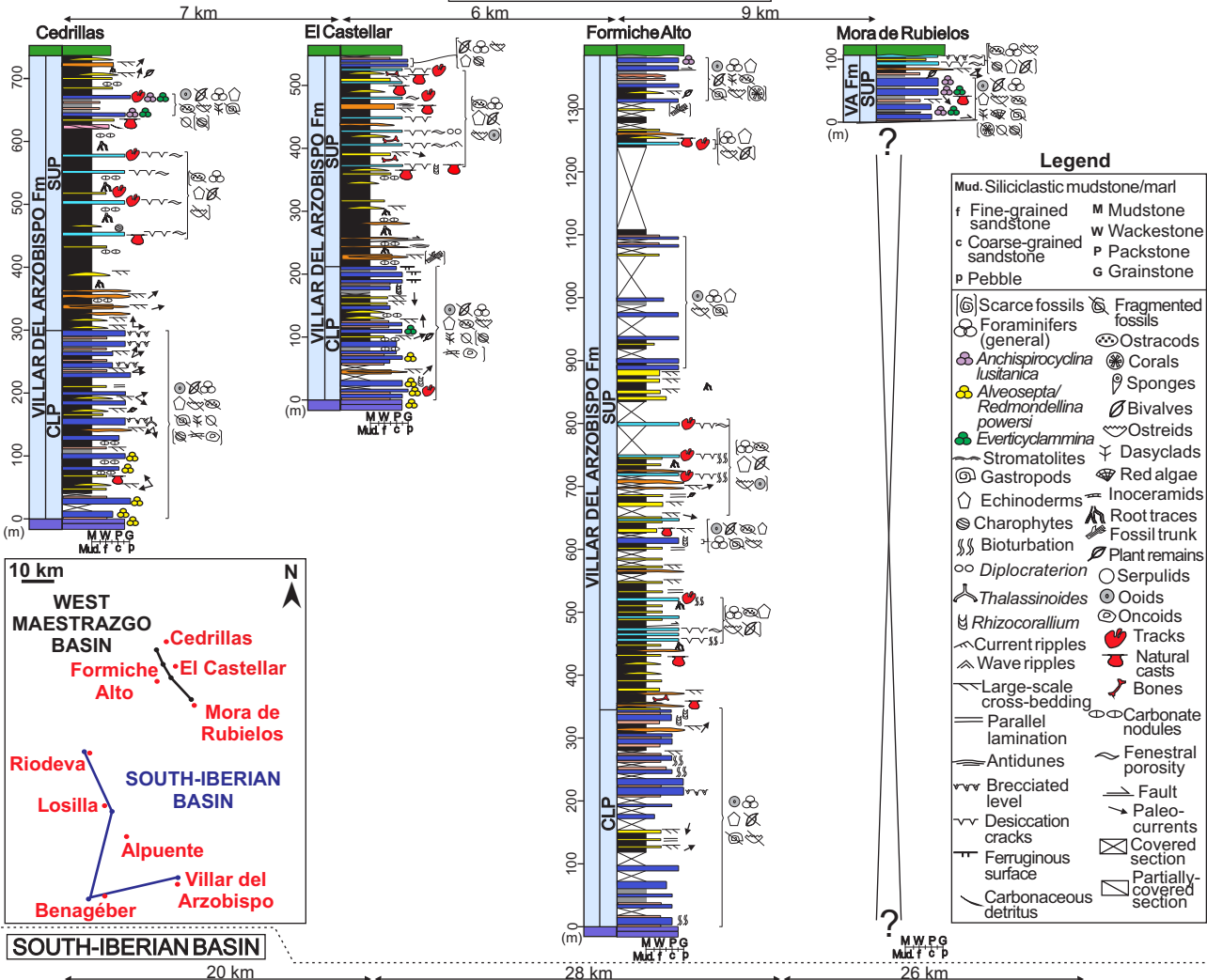
	<p><i>Siliciclastic mudstone</i>: typically reddish colour, and minor greyish and greenish colour.</p> <p><i>Sandstone</i>: very fine to medium-grained. Well to moderately-sorted.</p> <p><i>Limestone</i>: oncogenic and stromatolitic limestone, with variable amounts of quartz grains and local poorly-sorted bioclasts and ooids.</p> <p>Thickness and vertical and lateral arrangement:</p> <p><i>Sandstone</i>: Decimetre to metre-thick bodies (<60 cm) with tabular or flat-convex-up geometries and short lateral extent (<40 m). Tabular sandstone may be also arranged in coarsening and thickening-upward bodies (<1.5 m).</p> <p><i>Limestone</i>: Decimetre to metre-thick bodies (<30 cm), locally with erosive bases and short lateral extent (<3 m).</p> <p>Fossil content: dinosaur bones in siliciclastic mudstone and sandstone, plant remains in sandstone and bioclasts in limestone (fragments of bivalves, including ostreids, scarce benthic foraminifera, echinoid spines, gastropods, ostracods, charophytes and very scarce corals).</p>	<p><i>Sandstone</i>: parallel lamination followed upward by current ripples (climbing ripples) and locally by wave ripples. Large-scale cross-strata, sigmoidal cross-strata.</p> <p>Palaeocurrents:</p> <p><i>South-Iberian Basin</i>: main transport to the W–SW, minor to the NE.</p> <p><i>Western Maestrazgo Basin</i>: main transport to the E–NE.</p> <p>Bioturbation: Burrowing traces in sandstone and micritic limestone.</p> <p>Subaerial exposure features (top of beds): Edaphic features (carbonate nodules in siliciclastic mudstone, mottling and root traces in siliciclastic mudstone and sandstone), and dinosaur tracks in siliciclastic mudstone, sandstone and limestone.</p>	<p><i>CLP</i>: Riodeva and Villar del Arzobispo</p> <p><i>SUP</i>: All sections</p> <p>Western Maestrazgo Basin:</p> <p><i>CLP</i>: All sections</p> <p><i>SUP</i>: All sections</p>	<p>ephemeral and multi-storey fluvial channel, simple and climbing aeolian elements and tidal and shallow marine limestone.</p> <p>Overlying the delta terminal distributary channel, delta-front and distributary-mouth bar elements.</p> <p>Overlain by the delta-toe and the massive and indistinctly stratified aeolian dune elements.</p>	<p>alluvial to coastal areas that underwent periods of subaerial exposure and palaeosol development, as well as deposition of overbank splay lobes during flood events and in which shallow fresh, brackish and marine water bodies developed.</p>		
Deltaic	<p>Composition and sorting: Carbonaceous-rich, dark grey siliciclastic mudstone.</p> <p><i>Sandstone</i>: very fine-grained. Well-sorted.</p> <p>Thickness and vertical and lateral arrangement: Carbonaceous-rich, dark grey siliciclastic mudstone: <50 cm of thickness and great exposed lateral extent (<100 m).</p> <p><i>Sandstone</i>: Millimetre to centimetre-thick discontinuous layers.</p> <p>Fossil content: plant remains (carbonaceous detritus).</p>	<p>Overall thickness and vertical and lateral arrangement: Coarsening-upward and thickening-upward decimetre to metre-thick successions (<2 m) with <100 m of exposed lateral extension, composed,</p>	<p>Tractive structures: Current ripples in sandstone.</p> <p>Bioturbation: Dinosaur tracks.</p>	<p>South-Iberian Basin:</p> <p><i>SUP</i>: Riodeva, Losilla-Alpuente and Villar del Arzobispo</p> <p>Western Maestrazgo Basin:</p> <p><i>SUP</i>: Cedrillas</p>	<p>Overlying flood plain and ephemeral and multi-storey fluvial channel elements. Overlain by delta-front element.</p>	<p>Delta-toe sediments deposited by settling down from suspension of fine material. Siliciclastic input.</p>	<p>Deposition of deltaic sediments in shallow water bodies located in the flood plain. Probably freshwater; marine</p>

	<p>Delta-front</p> <p>Composition and sorting: Very fine to medium-grained, well-sorted sandstone.</p> <p>Thickness and vertical and lateral arrangement: Decimetre to metre-thick sandstone (<2 m) and great exposed lateral extent (<100 m).</p> <p>Fossil content: Plant remains (carbonaceous detritus).</p>	<p>from base to top, of delta-toe, delta-front and delta terminal distributary channel elements. Vertical stacking of individual deltaic successions producing composite bodies (<10 m) with great exposed lateral extent (<200 m).</p>	<p>Tractive structures: Clinofolds with low-angle and large laterally-continuous foresets. Drapes of carbonaceous detritus at the lower part of foresets, locally extend up to the topsets.</p> <p>Palaeocurrents: <i>South-Iberian Basin:</i> main transport to the W–NW and S, minor to the NE.</p> <p>Bioturbation: Local burrowing traces.</p>	<p>South-Iberian Basin: <i>SUP:</i> Riodeva, Losilla-Alpuente and Villar del Arzobispo</p> <p>Western Maestrazgo Basin: <i>SUP:</i> Cedrillas</p>	<p>Overlying delta-toe element. Overlain by delta terminal distributary channel, flood plain and simple or climbing aeolian dune elements.</p>	<p>Sandy delta-front sediments deposited by unconfined flows. Carbonaceous detritus deposited during periods of low flow.</p>	<p>influence is not discarded.</p>
	<p>Delta terminal distributary channel</p> <p>Composition and sorting: Fine to medium-grained, well-sorted sandstone.</p> <p>Thickness and vertical and lateral arrangement: Decimetre to metre-thick bodies (<1.5 m) with erosive bases and short lateral extent (<10 m).</p>		<p>Tractive structures: Large-scale cross-strata. Locally backset or upward flattening strata.</p> <p>Palaeocurrents: <i>South-Iberian Basin:</i> main transport to the NE and S, minor to the W and SSW.</p>	<p>South-Iberian Basin: <i>SUP:</i> Riodeva, Losilla-Alpuente and Villar del Arzobispo</p> <p>Western Maestrazgo Basin: <i>SUP:</i> Cedrillas</p>	<p>Overlying delta-front element. Overlain by flood plain and simple or climbing aeolian dune elements.</p>	<p>Delta terminal distributary channels migrating in a deltaic plain</p>	
<p>Coastal to shallow marine</p>	<p>Coastal terminal distributary channel</p> <p>Composition and sorting: Fine to medium-grained, well-sorted sandstone. Local poorly-sorted conglomerate (mudstone subangular to subrounded mudstone pebbles and scarce bioclasts) with medium to coarse-grained sandy matrix.</p> <p>Thickness and vertical and lateral arrangement: Metre-thick bodies (<3 m) with erosive bases and <50 m of exposed lateral extent. Occurrence of internal erosive surfaces.</p> <p>Fossil content: occasional fragments of bivalves in conglomerate.</p>		<p>Tractive structures: Large-scale cross-strata. Local thin layers of carbonaceous-rich marl interbedded with cross-strata sandstone sets and/or at the lower part of foresets and bottomsets.</p> <p>Palaeocurrents: <i>Western Maestrazgo Basin:</i> main transport to the E–SE.</p>	<p>South-Iberian Basin: <i>CLP:</i> Villar del Arzobispo</p> <p>Western Maestrazgo Basin: <i>SUP:</i> Formiche Alto and Mora de Rubielos</p>	<p>Interbedded with distributary mouth-bar element and marl.</p>	<p>Coastal terminal distributary channels flowing into coastal and shallow marine areas</p>	

Aeolian	Distributary mouth-bar	<p>Composition and sorting: Fine to medium-grained, well-sorted sandstone</p> <p>Thickness and vertical and lateral arrangement: Centimetre to metre-thick bodies (<2.5 m) with flat bases and flat or convex-up tops and short lateral extent (<20 m). Occasional coarsening and thickening upward trend.</p> <p>Fossil content: Occasional fragments of ostreids, trigonoids and other bivalves, corals, echinoderms, gastropods, large benthic foraminifera, miliolids, serpulids and plant remains.</p>	<p>Tractive structures:</p> <p><i>Decimetre to metre-thick bodies:</i> large-scale cross-strata, sigmoidal cross-strata, occasional wave and/or current ripples at the top.</p> <p><i>Centimetre-thick bodies:</i> wave and/or current ripples at the top, wavy bedding.</p> <p>Palaeocurrents:</p> <p><i>South-Iberian Basin:</i> main transport to the E, minor to the N and SE.</p> <p><i>Western Maestrazgo Basin:</i> main transport to the NE and E, minor to the N and S.</p> <p>Bioturbation: Burrowing traces at the top.</p>	<p>South-Iberian Basin:</p> <p><i>CLP:</i> all sections</p> <p><i>SUP:</i> Losilla-Alpuente and Villar del Arzobispo</p> <p>Western Maestrazgo Basin:</p> <p><i>CLP:</i> All sections</p> <p><i>SUP:</i> All sections</p>	<p>Interbedded with coastal terminal distributary channel element and marl or with tidal and shallow marine limestone.</p>	<p>Distributary mouth-bars formed by the spreading out of an unconfined flow at the terminus of distributary rivers in coastal and shallow marine areas.</p>
	Simple aeolian dune	<p>Composition and sorting: Fine to medium-grained, well-sorted sandstone. Locally very scattered rounded to subrounded muddy-soft pebbles and rounded quartzite pebbles (<1.4 cm).</p> <p>Thickness and vertical and lateral arrangement: Metre-thick bodies (<6 m) with flat bases and tops and great exposed lateral extent (<100 m).</p> <p>Fossil content: plant remains (carbonaceous detritus).</p>	<p>Tractive structures: Single large-scale cross-strata sets (<6 m). High angle foresets (<36°). Foresets locally pass upward to low-angle topsets.</p> <p>Palaeocurrents:</p> <p><i>South-Iberian Basin:</i> main transport to the SE, W–SW or the NW.</p>	<p>South-Iberian Basin:</p> <p><i>SUP:</i> Riodeva, Losilla-Alpuente and Benagéber</p>	<p>Interbedded with flood plain element. Locally overlies ephemeral fluvial channel, delta terminal distributary channel or delta-front elements.</p>	<p>Transverse and dome-shaped aeolian dunes migrating in the flood plain</p>
	Massive and indistinctly stratified aeolian dune	<p>Composition and sorting: Fine to medium-grained, well-sorted sandstone.</p> <p>Thickness and vertical and lateral arrangement: Metre-thick bodies (<25 m) with flat bases and tops and great exposed lateral extent (<80 m).</p> <p>Fossil content: Local plant remains (carbonaceous detritus).</p> <p>Observations: Massive appearance.</p>	<p>Tractive structures: Local poorly-preserved large-scale cross-strata (set thickness <7 m), high angle foresets (<30°). Local drapes of carbonaceous detritus and mica flakes at laterally continuous bottomsets and the lower part of foresets.</p> <p>Palaeocurrents:</p> <p><i>South-Iberian Basin:</i> main transport to the W–NW, minor to the SW.</p>	<p>South-Iberian Basin:</p> <p><i>SUP:</i> Riodeva</p>	<p>Interbedded with ephemeral fluvial channel element. Overlying coastal flood plain element. Overlain by multi-storey fluvial channel element.</p>	<p>Aeolian dunes subjected to episodic flooding, causing the inundation of interdune areas and the development of ephemeral channels between aeolian dunes.</p>

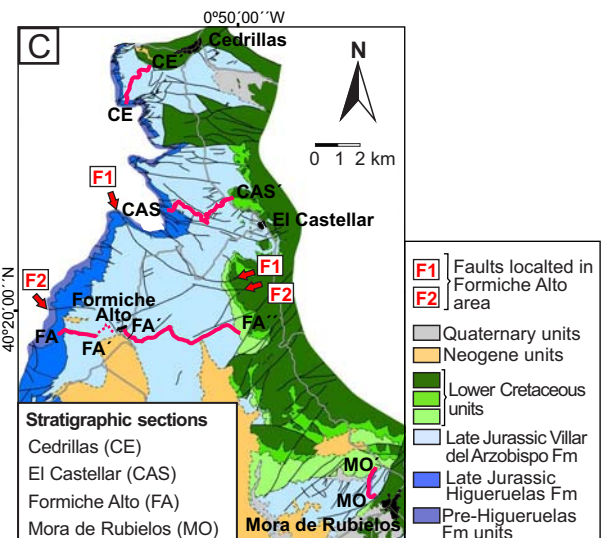
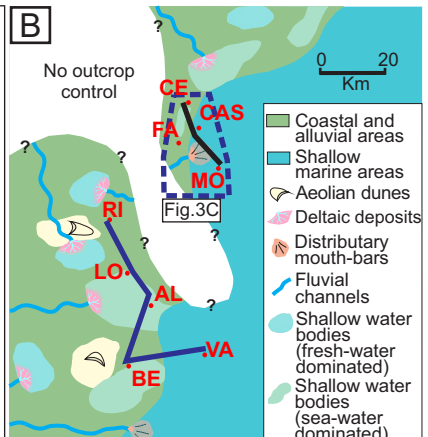
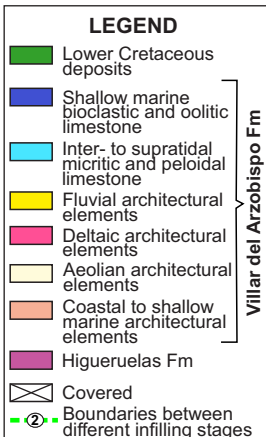
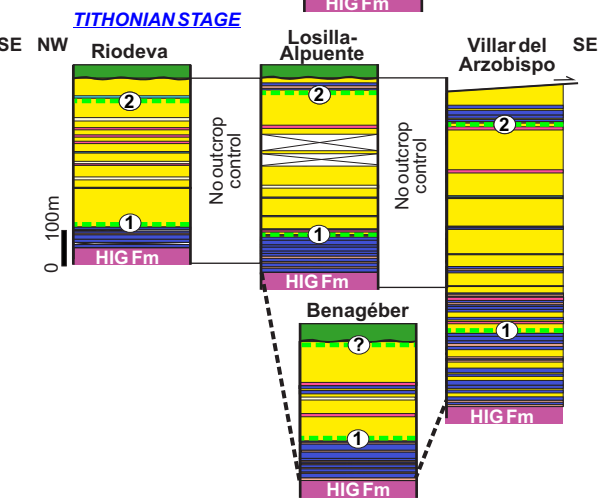
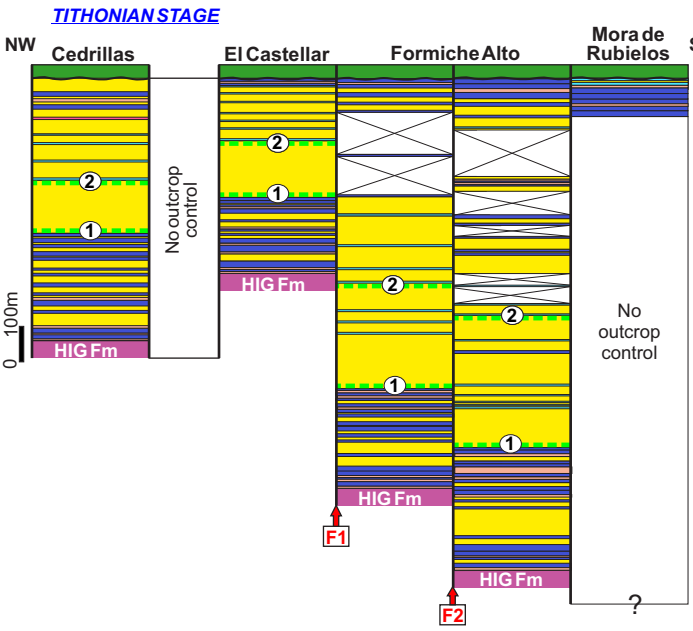
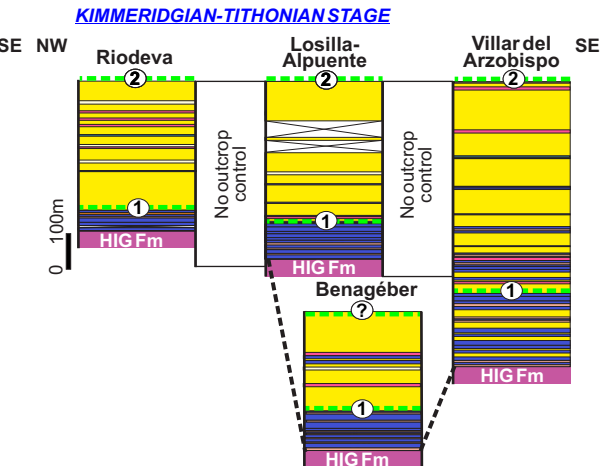
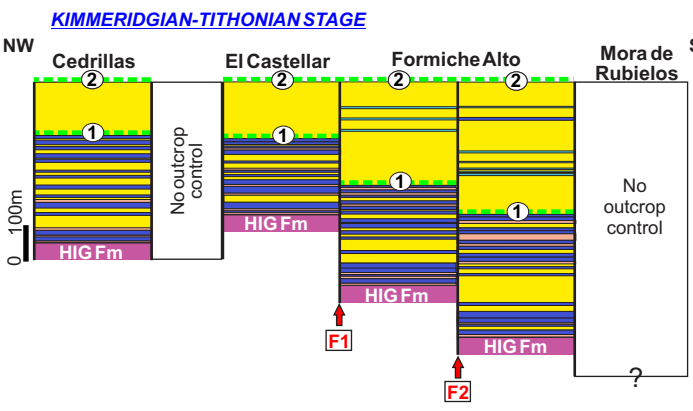
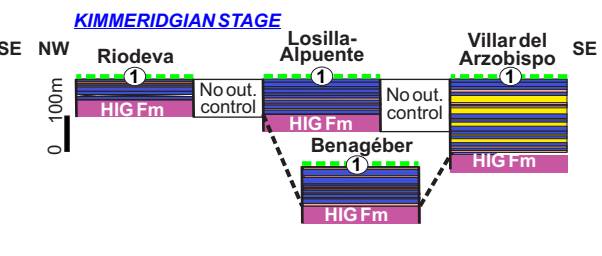
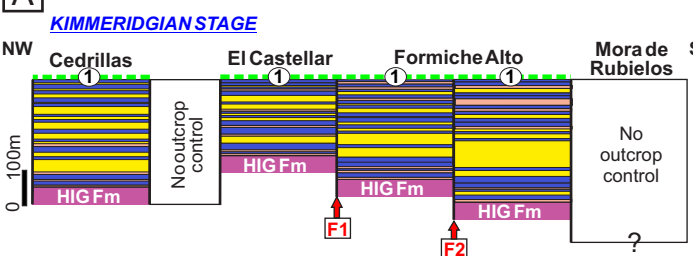


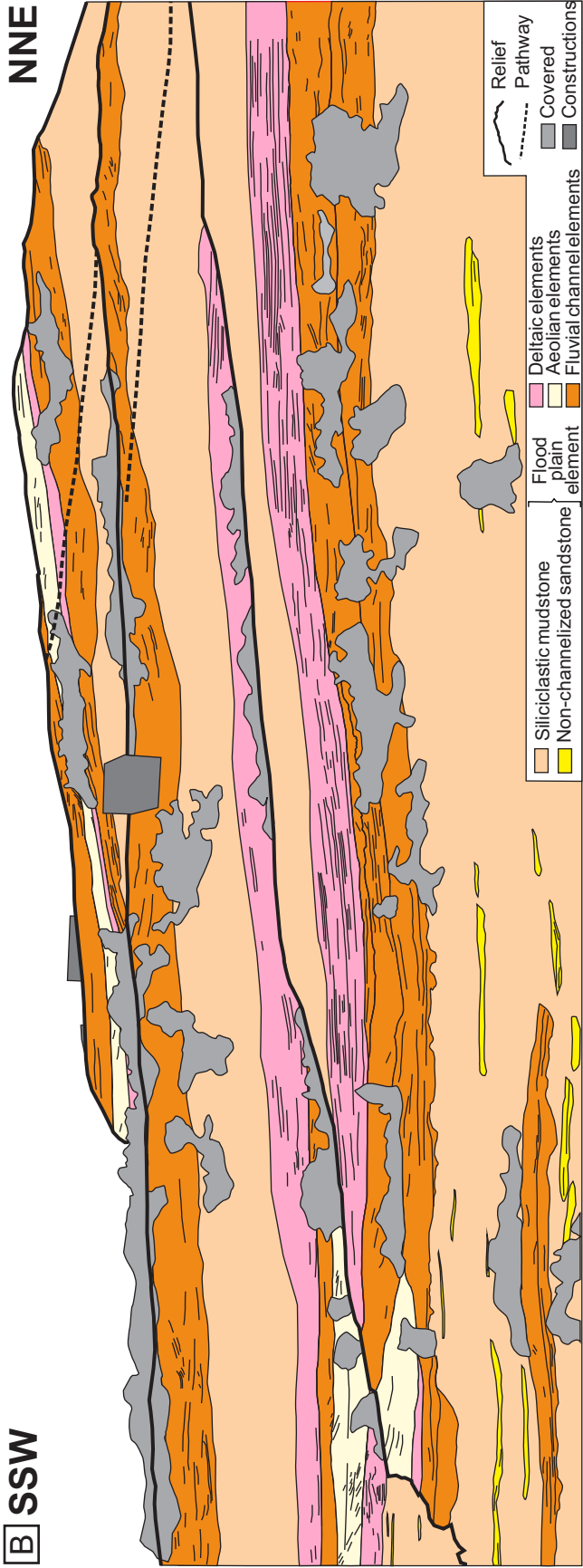
WEST MAESTRAZGO BASIN

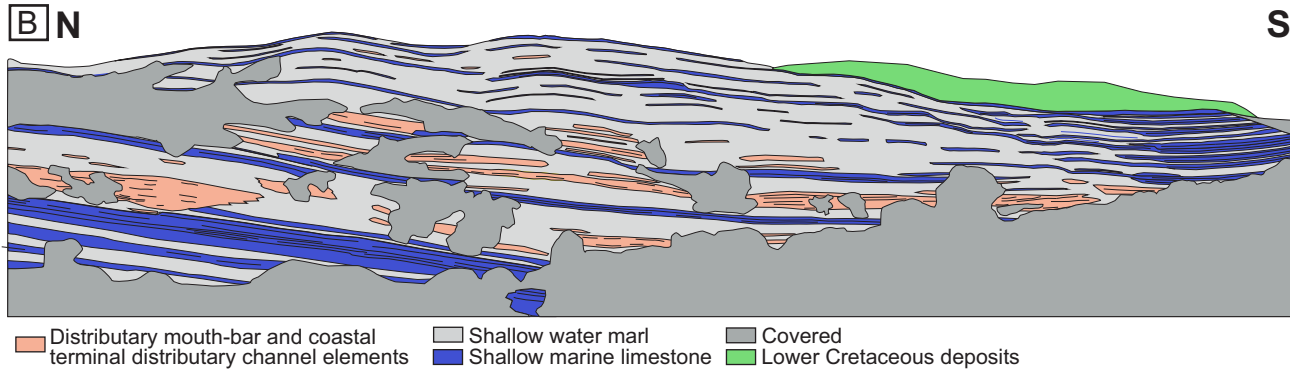


WEST MAESTRAZGO BASIN

SOUTH-IBERIAN BASIN

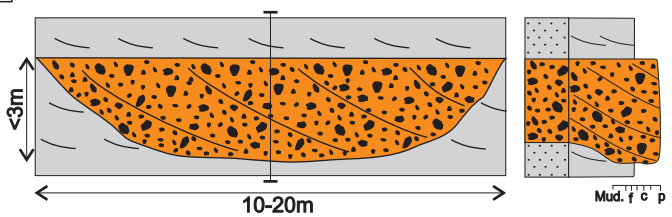




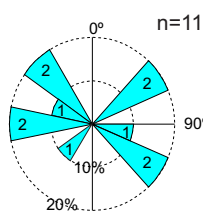


Ephemeral fluvial channel architectural element

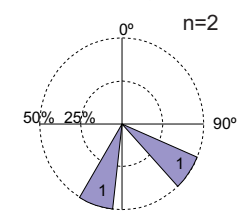
A



South-Iberian Basin



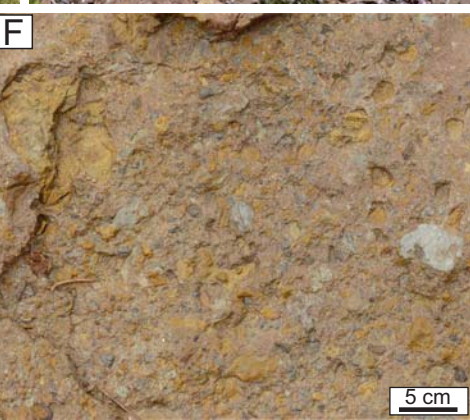
W Maestrazgo Basin



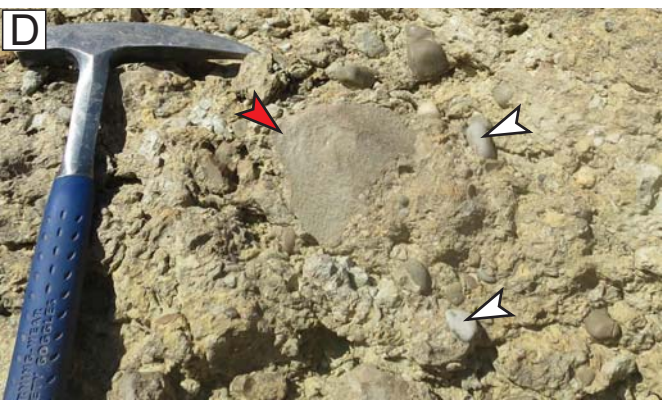
B

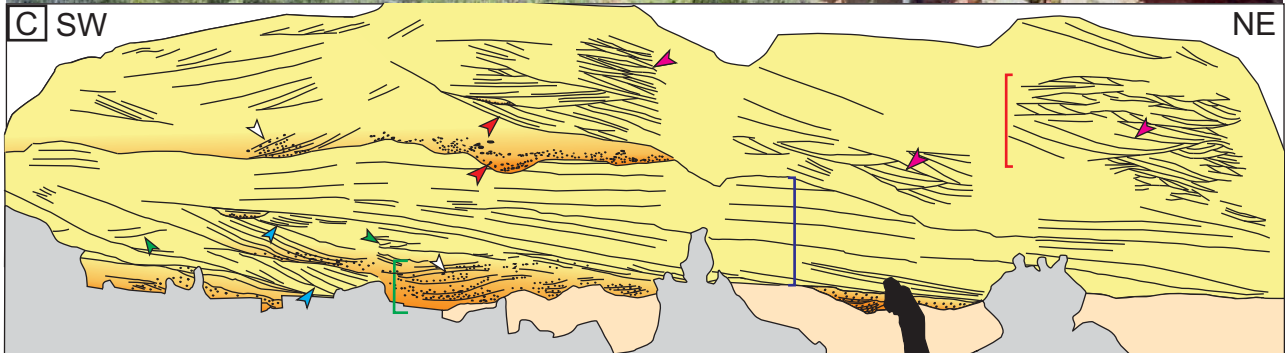
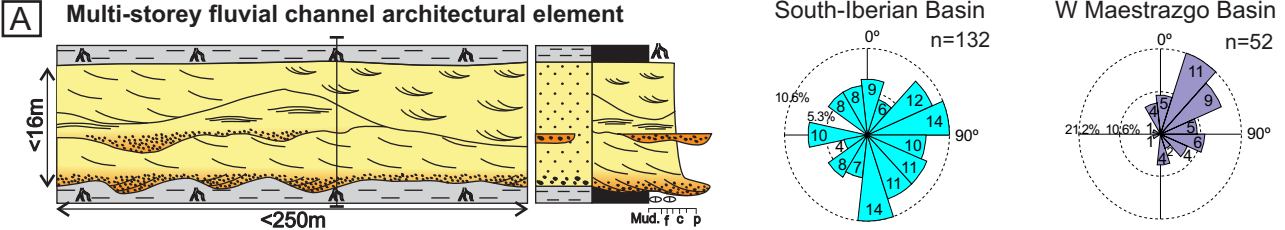


C



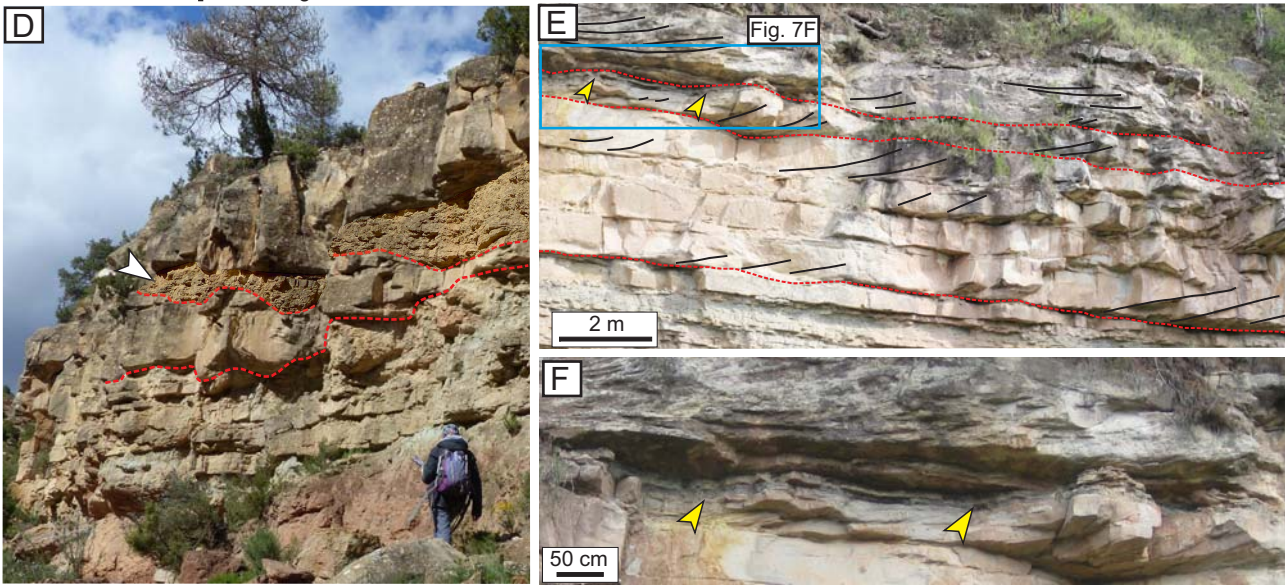
D

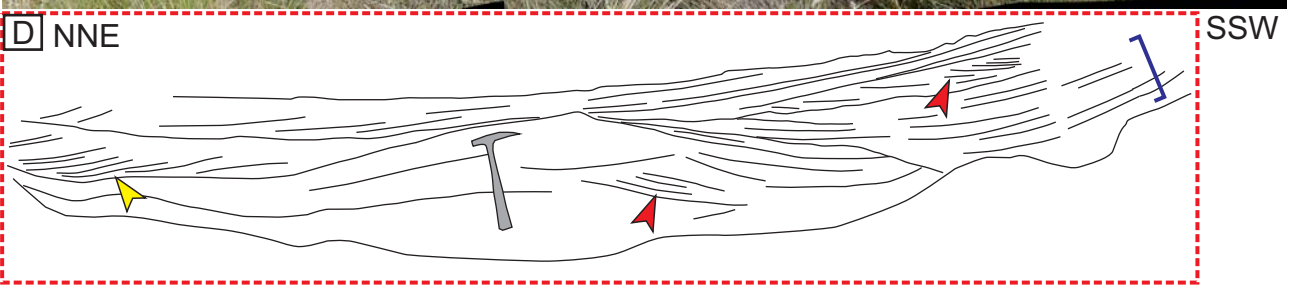
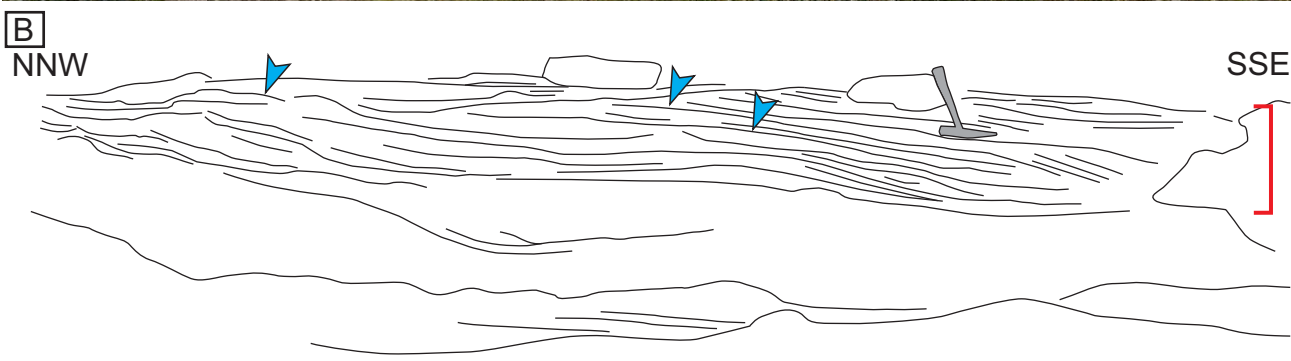




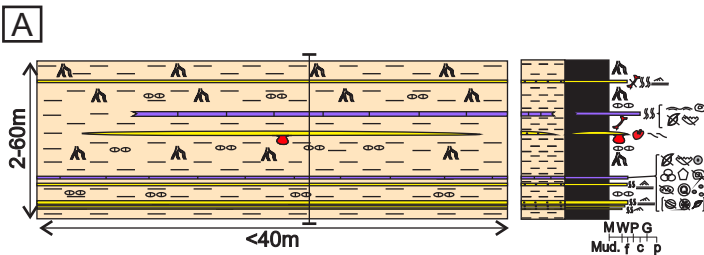
Multi-storey fluvial channel element

- Sandstone
- Conglomerate
- Mud, carbonate and/or sandstone pebbles
- Flood plain element
- Covered
- Person for scale

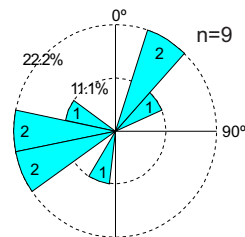




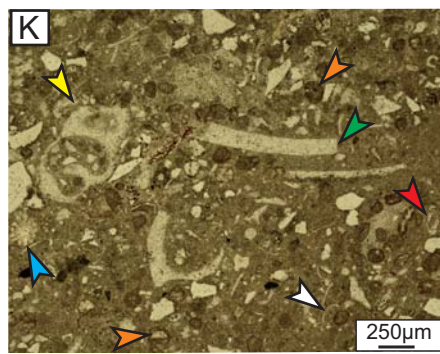
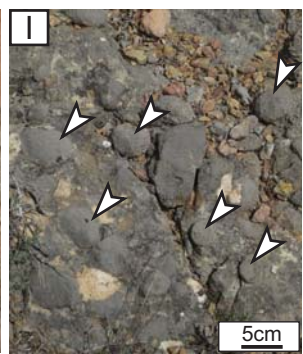
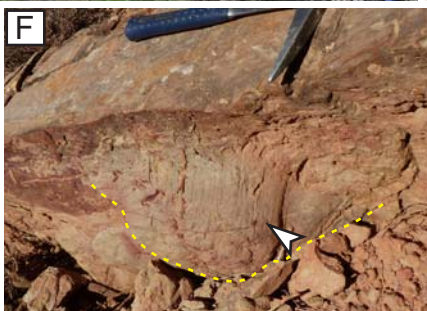
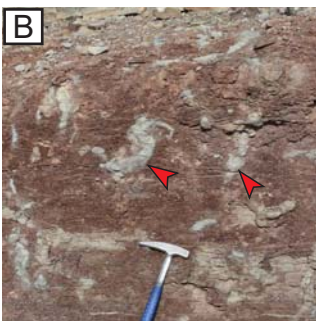
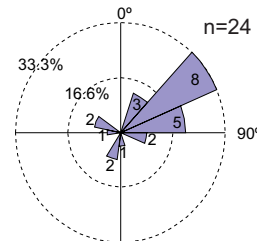
Flood plain architectural element



South-Iberian Basin

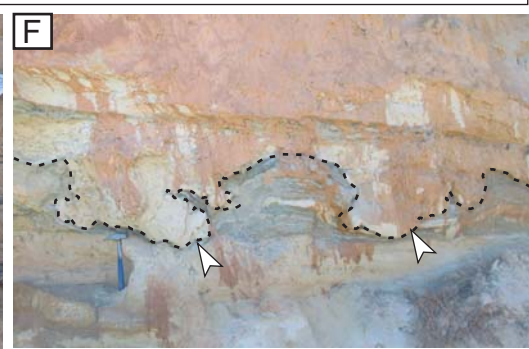
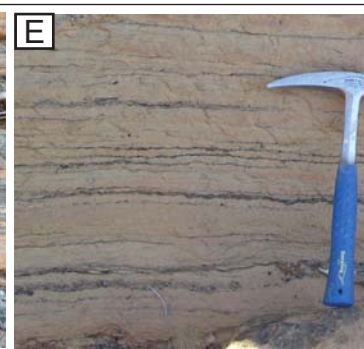
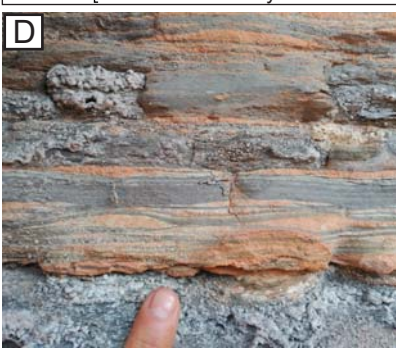
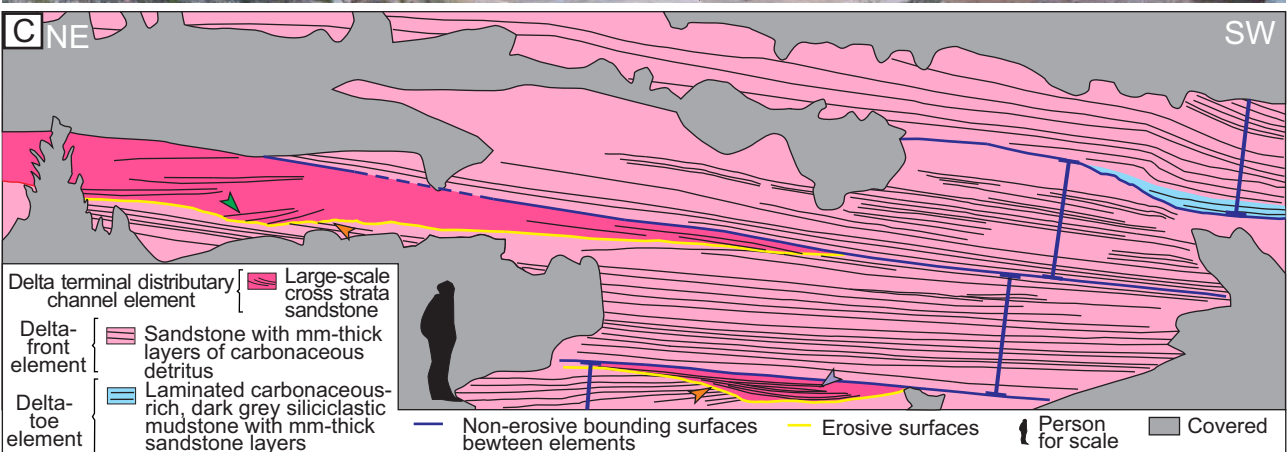
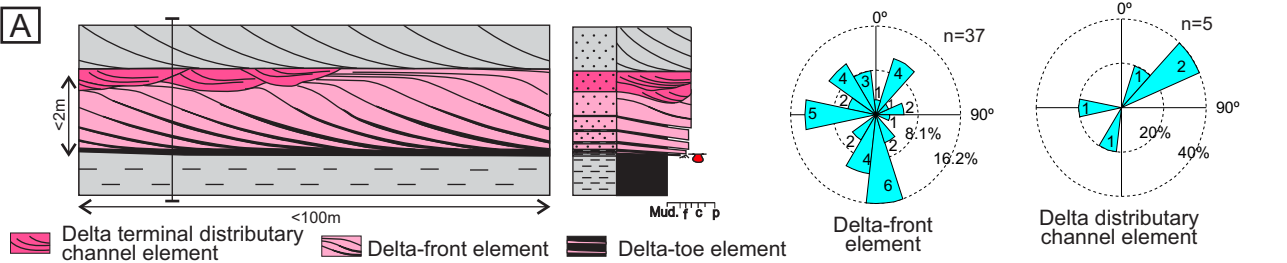


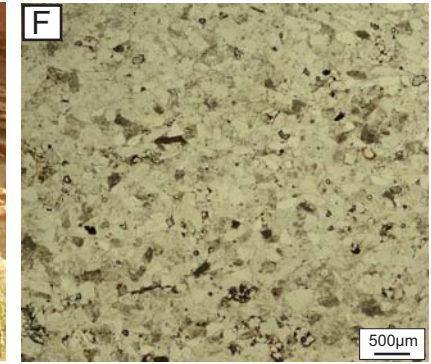
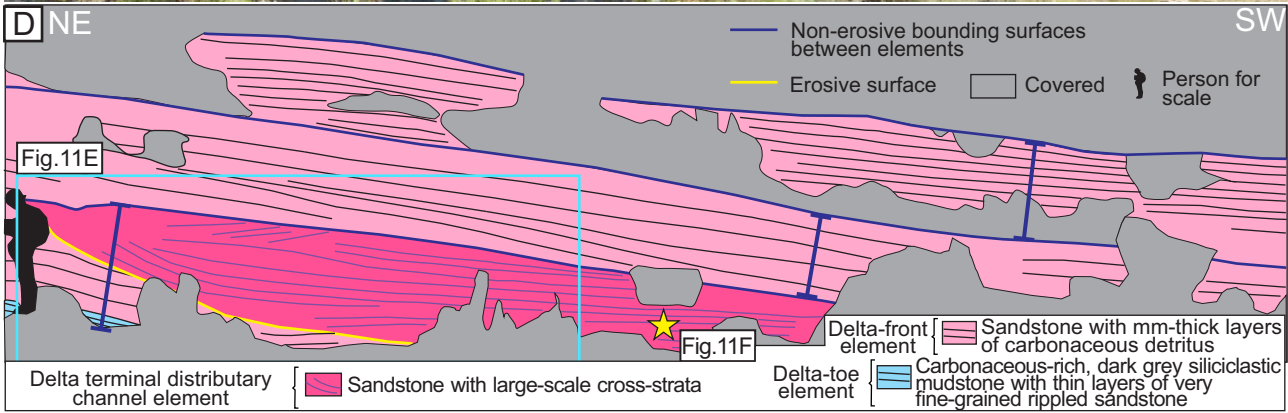
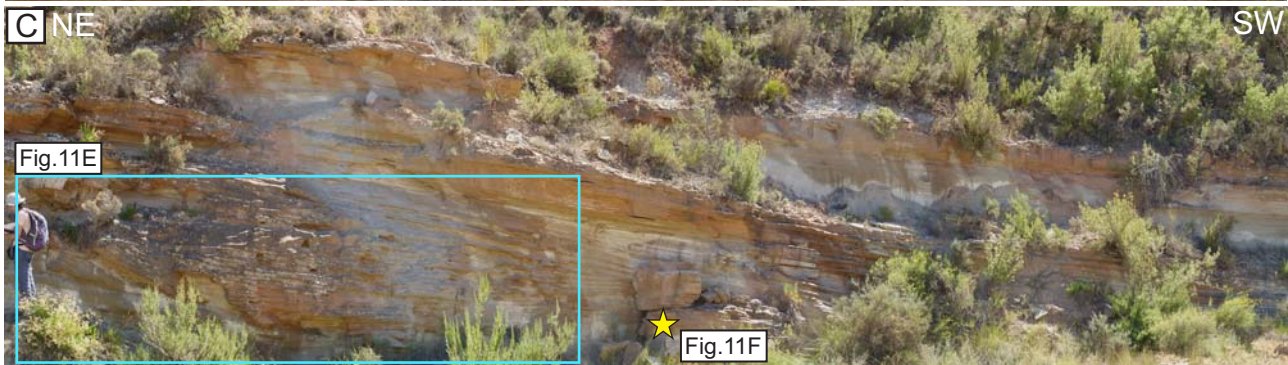
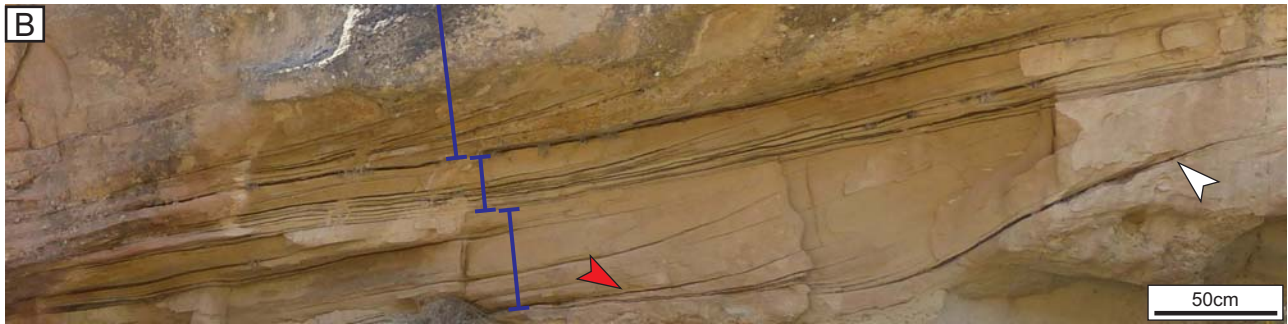
W Maestrazgo Basin



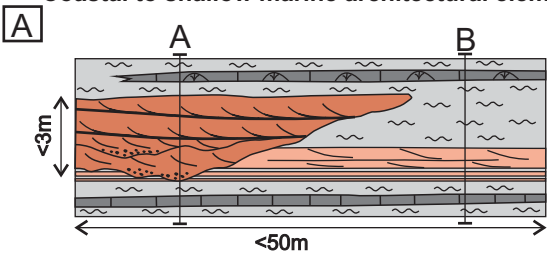
Deltaic architectural elements

South-Iberian Basin

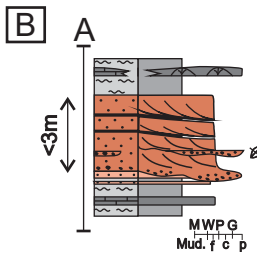




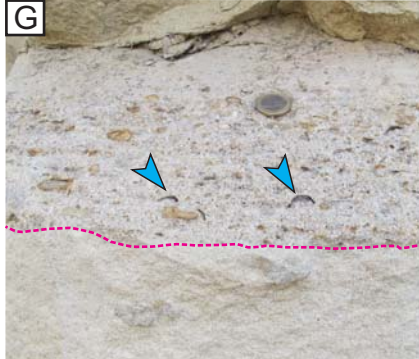
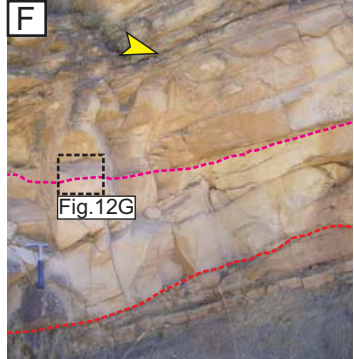
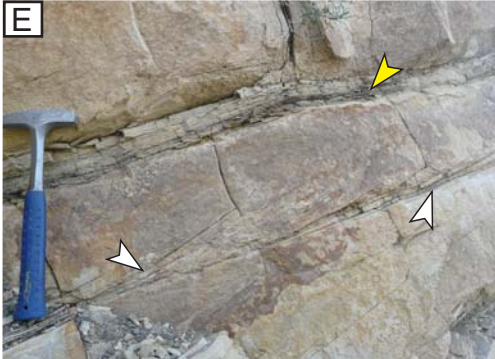
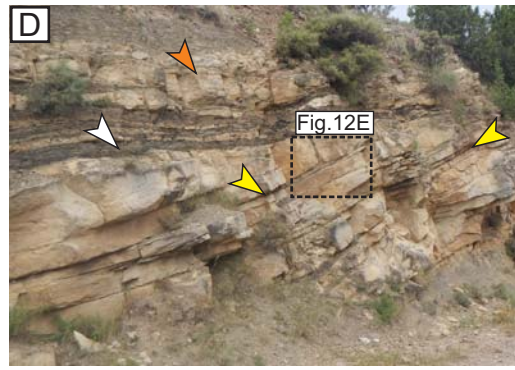
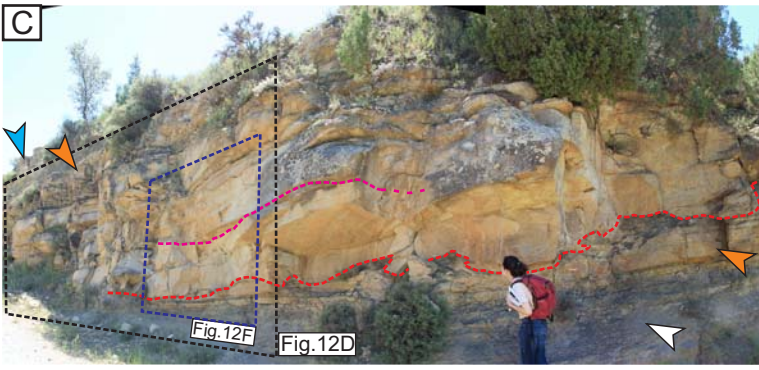
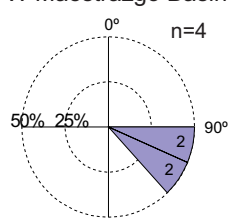
Coastal to shallow marine architectural elements

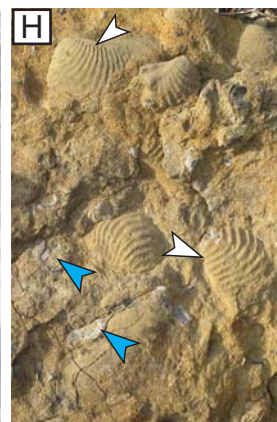
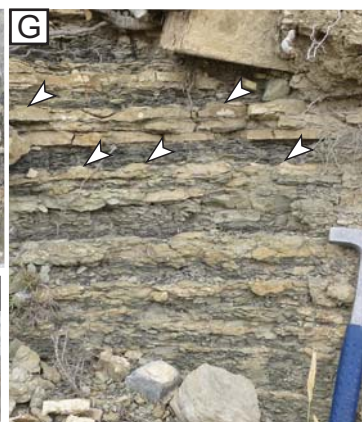
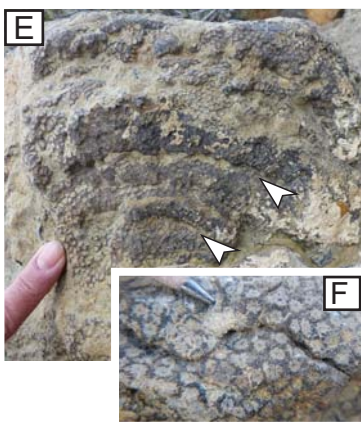
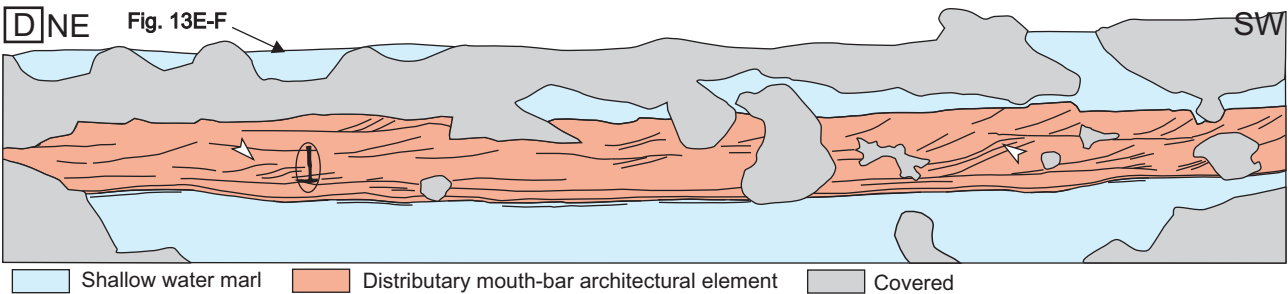
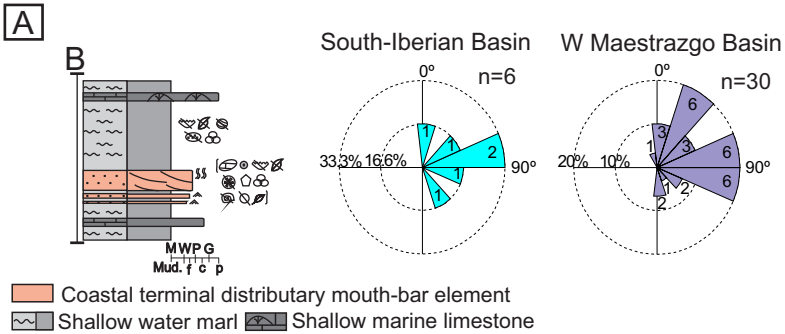


- Coastal terminal distributary channel element
- Distributary mouth-bar element
- Shallow water marl
- Shallow marine limestone



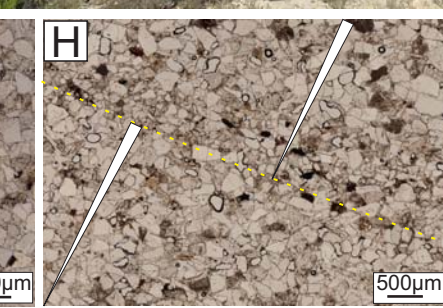
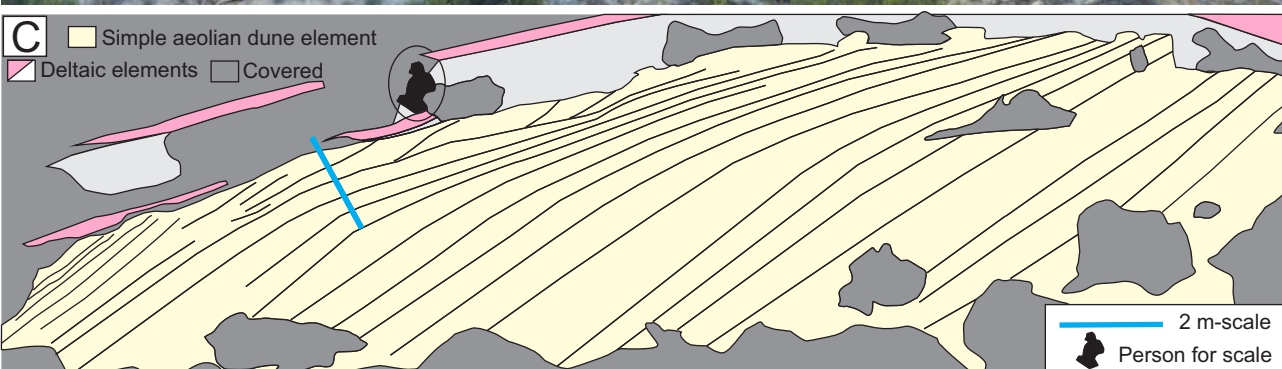
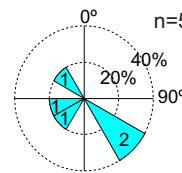
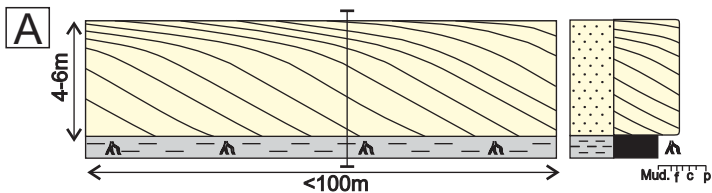
W Maestrazgo Basin





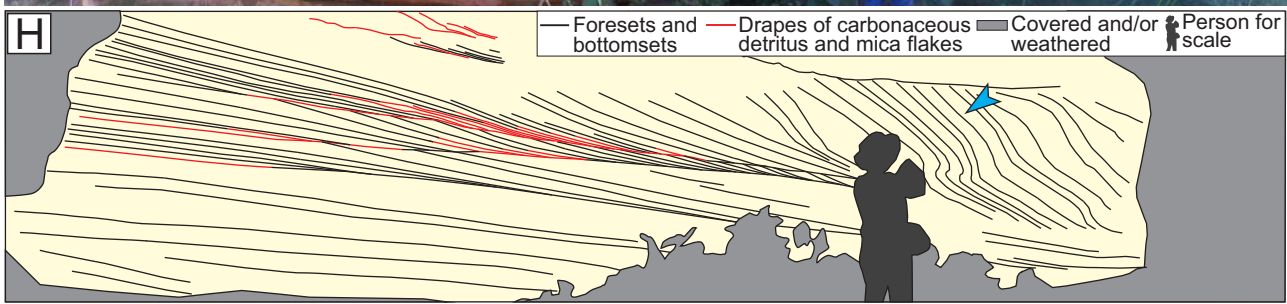
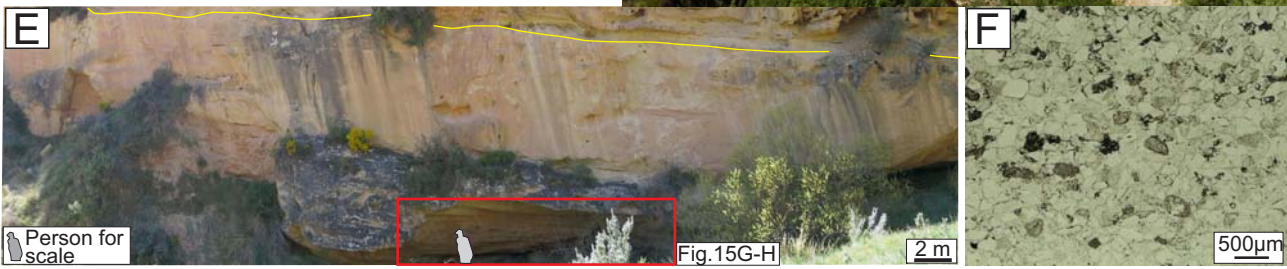
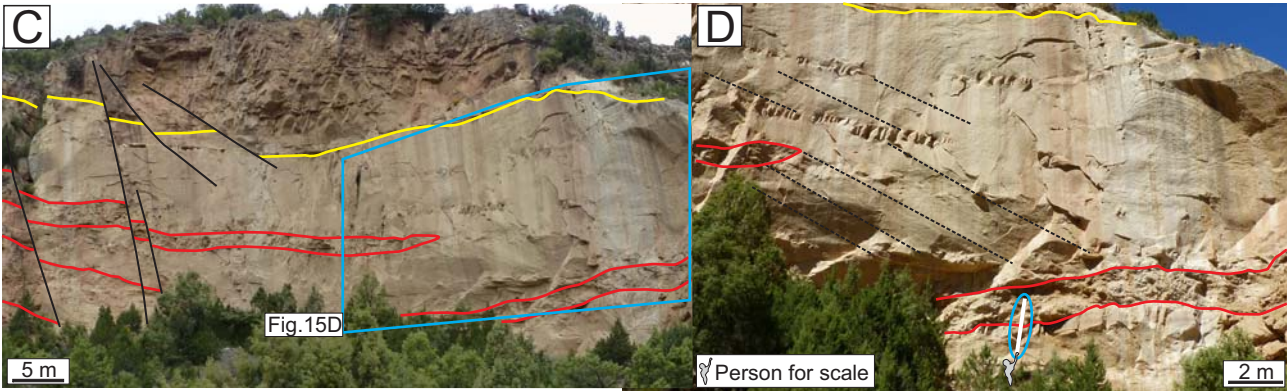
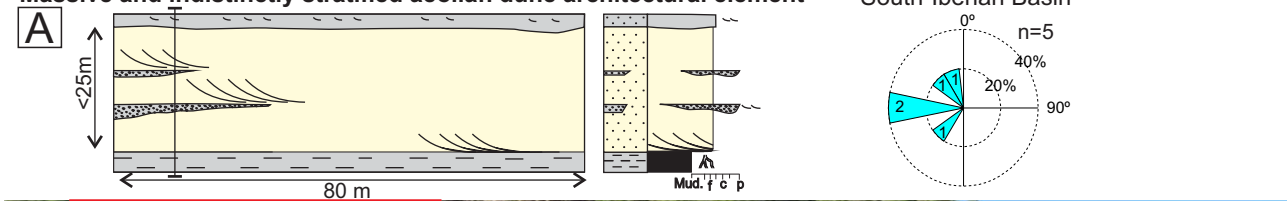
Simple aeolian dune architectural element

South-Iberian Basin

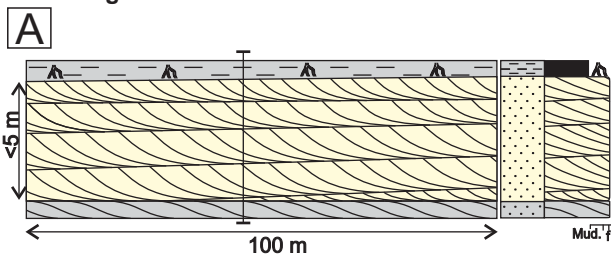


Massive and indistinctly stratified aeolian dune architectural element

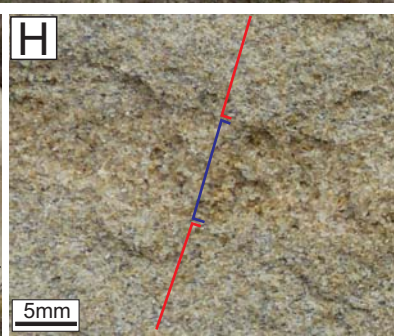
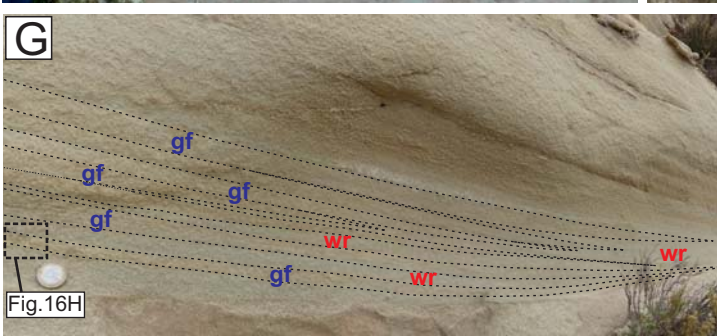
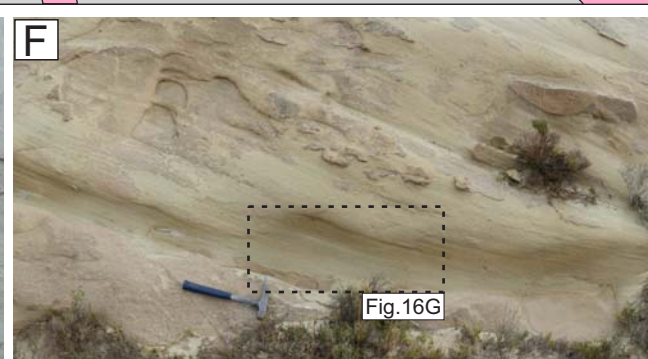
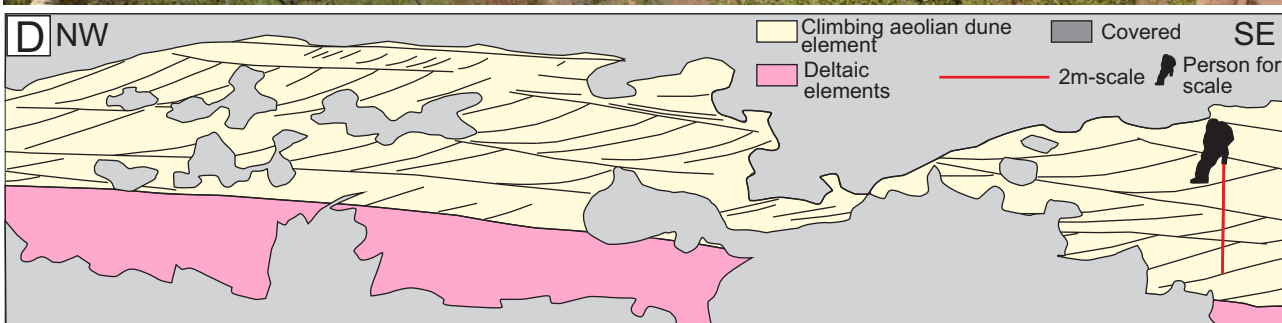
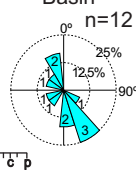
South-Iberian Basin

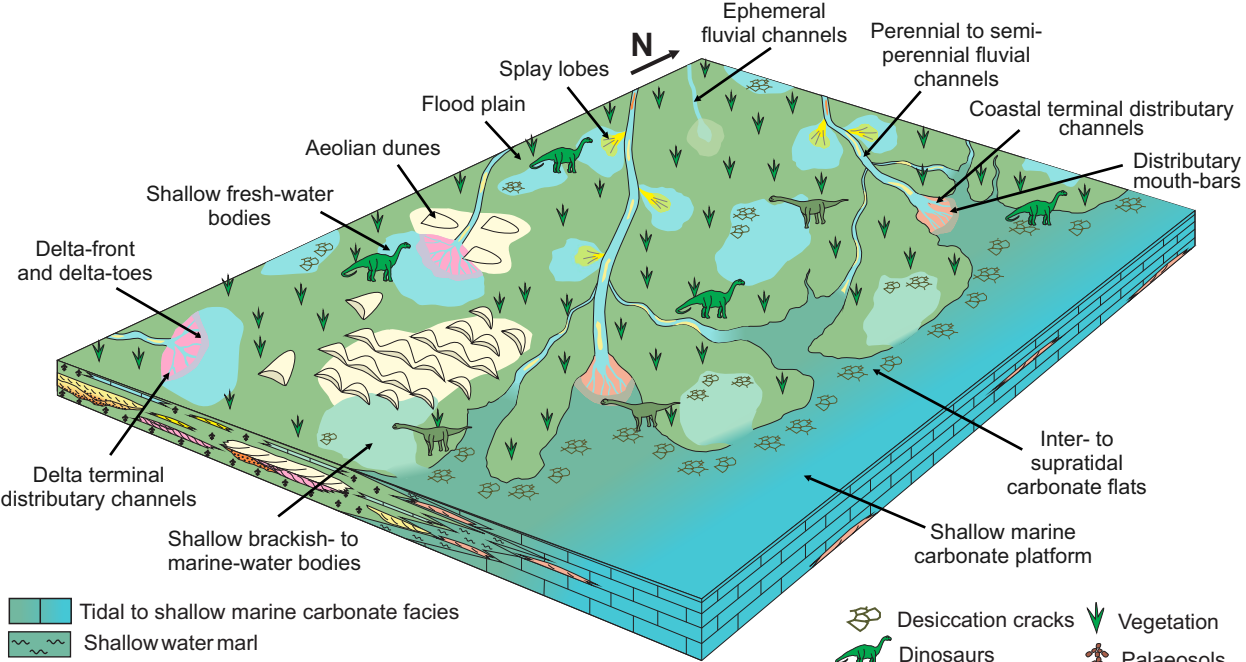


Climbing aeolian dune architectural element



South-Iberian Basin





Tidal to shallow marine carbonate facies
 Shallow water marl

Desiccation cracks
 Vegetation
 Dinosaurs
 Palaeosols

Fluvial elements

- Ephemeral fluvial channel
- Multi-storey fluvial channel
- Siliciclastic mudstone (flood plain deposits)
- Non-channelized sandstone (splay lobe deposits)

Flood plain

- Limestone (shallow water bodies fresh-water dominated)
- Limestone (shallow water bodies sea-water dominated)

Deltaic elements

- Delta terminal distributary channel
- Delta-front and delta-toes

Aeolian elements

- Aeolian dunes

Coastal to shallow marine elements

- Distributary mouth-bar
- Coastal terminal distributary channel

